

RERACKING OF SPENT FUEL POOLS
DIABLO CANYON UNITS 1 AND 2

PACIFIC GAS AND ELECTRIC COMPANY
SAN FRANCISCO, CALIFORNIA 94106

8509260229 850919
PDR/ ADDCK 05000275
P PDR

SEPTEMBER 1985

TABLE OF CONTENTS

<u>Section</u>	<u>Page</u>
1.0 INTRODUCTION	1-1
2.0 GENERAL ARRANGEMENT	2-1
3.0 RACK CONSTRUCTION	3-1
3.1 Fabrication Details	3-1
3.1.1 Region 1	3-1
3.1.2 Region 2	3-4
3.2 Codes, Standards, and Practices for the Spent Fuel Pool Modification	3-5
4.0 NUCLEAR CRITICALITY ANALYSIS	4-1
4.1 Design Bases	4-1
4.2 Summary of Criticality Analyses	4-2
4.2.1 Normal Operating Conditions	4-2
4.2.2 Abnormal and Accident Conditions	4-5
4.3 Reference Fuel Storage Cell	4-7
4.3.1 Reference Fuel Assembly	4-7
4.3.2 Region 1 Storage Cells	4-7
4.3.3 Region 2 Storage Cells	4-7
4.4 Analytical Methodology	4-9
4.4.1 Reference Analytical Methods and Bias	4-9
4.4.2 Fuel Burnup Calculations	4-11
4.4.3 Long-term Decay	4-13
4.4.4 Effect of Axial Burnup Distribution	4-14
4.5 Region 1 Criticality Analysis and Tolerance Variations	4-16
4.5.1 Nominal Design Case	4-16
4.5.2 Boron Loading Variation	4-16
4.5.3 Storage Cell Lattice Pitch Variation	4-17
4.5.4 Stainless Steel Thickness Tolerances	4-18
4.5.5 Fuel Enrichment and Density Variation	4-18
4.5.6 Boraflex Width Tolerance Variation	4-18
4.5.7 Axial Cutback of Boraflex	4-18
4.6 Region 2 Criticality Analysis and Tolerance Variations	4-19
4.6.1 Nominal Design Case	4-19
4.6.2 Storage Cell Lattice Pitch Variations	4-20
4.6.3 Stainless Steel Thickness Tolerance	4-21
4.6.4 Fuel Enrichment and Density Variation	4-21
4.6.5 Eccentric Positioning of Fuel Assembly in Storage Rack	4-21



TABLE OF CONTENTS (Continued)

<u>Section</u>	<u>Page</u>
4.7 Abnormal and Accident Conditions	4-22
4.7.1 Temperature and Water Density Effects	4-22
4.7.2 Dropped Fuel Assembly Accident	4-24
4.7.3 Abnormal Location of a Fuel Assembly	4-24
4.7.4 Lateral Rack Movement	4-25
References to Section 4	4-26
Appendix A Benchmark Calculations	A-1
1. Introduction and Summary	A-2
2. AMPX (NITAWL)-KENO Benchmark Calculations	A-3
3. CASMO-2E Benchmark Calculations	A-5
3.1 General	A-5
3.2 Benchmark Calculations	A-6
References to Appendix A	A-8
5.0 THERMAL-HYDRAULIC CONSIDERATIONS	5-1
5.1 Decay Heat Calculations for the Spent Fuel	5-1
5.1.1 Basis	5-1
5.1.2 Model Description	5-3
5.1.3 Decay Heat Calculation Results	5-7
5.2 Thermal-hydraulic Analyses for Spent Fuel Cooling	5-10
5.2.1 Basis	5-10
5.2.2 Model Description	5-11
5.2.3 Results	5-12
References to Section 5	5-16
6.0 STRUCTURAL ANALYSIS	6-1
6.1 Analysis Outline	6-1
6.2 Fuel Rack-Fuel Assembly Model	6-3
6.2.1 Outline of Model	6-4
6.2.2 Model Description (8 DOF Model)	6-6
6.2.3 Fluid Coupling	6-7
6.2.4 Damping	6-8
6.2.5 Impact	6-9
6.3 Assembly of the Dynamic Model	6-9



TABLE OF CONTENTS (Continued)

<u>Section</u>		<u>Page</u>
6.4	Time Integration of the Equations of Motion	6-13
6.4.1	Time-history Analysis Using 8 DOF Rack Model	6-13
6.4.2	Evaluation of Potential for Inter-rack Impact	6-14
6.5	Structural Acceptance Criteria	6-15
6.6	Material Properties	6-17
6.7	Stress Limits for Various Conditions	6-18
6.7.1	Normal and Upset Conditions (Level A or Level B)	6-18
6.7.2	Level D Service Limits	6-20
6.8	Results	6-21
6.9	Impact Analyses	6-27
6.9.1	Impact Loading Between Fuel Assembly and Cell Wall	6-27
6.9.2	Impacts Between Adjacent Racks	6-27
6.10	Weld Stresses	6-28
6.11	Summary of Mechanical Analyses	6-28
6.12	Evaluation of Spent Fuel Pool Structure	6-30
6.13	Definition of Terms Used in Section 6	6-31
	References to Section 6	6-32
7.0	ENVIRONMENTAL EVALUATION	7-1
7.1	Summary	7-1
7.2	Characteristics of Stored Fuel	7-1
7.3	Related Industry Experience	7-2
7.4	Diablo Canyon Power Plant Experience	7-4
7.5	Spent Fuel Pool Cooling and Cleanup System (FPCC)	7-4
7.6	Fuel Pool Radiation Shielding	7-5
7.6.1	Source Terms	7-5
7.6.2	Radiation Shine Due to Spent Fuel Fuel Storage	7-8



TABLE OF CONTENTS (Continued)

<u>Section</u>	<u>Page</u>
7.6.3 Radiation Shine Due to the Fuel Transfer Operation	7-10
7.7 Radiological Consequences	7-11
7.8 Reracking Operation	7-15
7.9 Conclusions	7-16
References to Section 7	7-18
8.0 IN-SERVICE SURVEILLANCE PROGRAM FOR BORAFLEX NEUTRON ABSORBING MATERIAL	8-1
8.1 Program Intent	8-1
8.2 Description of Specimens	8-1
8.3 Specimen Evaluation	8-2
9.0 COST/BENEFIT ASSESSMENT	9-1
9.1 Specific Needs for Spent Fuel Storage	9-1
9.2 Cost of Spent Fuel Storage	9-2
9.3 Alternatives to Spent Fuel Storage	9-2
9.4 Resource Commitments	9-3
References to Section 9	9-5
10.0 QUALITY ASSURANCE PROGRAM	10-1
10.1 Introduction	10-1
10.2 General	10-1
10.3 System Highlights	10-1
10.4 Summary	10-3



LIST OF TABLES

<u>Table</u>	<u>Page</u>	
1.1a	Diablo Canyon Unit 1 Fuel Assembly Discharge (Tentative Schedule)	1-3
1.1b	Diablo Canyon Unit 2 Fuel Assembly Discharge (Tentative Schedule)	1-4
2.1	Design Data	2-2
2.2	Module Data	2-3
3.1	Boraflex Experience for High Density Racks	3-2
4.1	Summary of Criticality Safety Analyses	4-4
4.2	Reactivity Effects of Abnormal and Accident Conditions	4-5
4.3	Fuel Assembly Design Specifications	4-8
4.4	Comparison of Cold, Clean Reactivities Calculated at 34.5 MWd/kgU Burnup	4-12
4.5	Long-term Changes in Reactivity in Storage Rack (Xenon-Free)	4-15
4.6	Fuel Burnups for Equal Reactivity Values with Fuel of Different Initial Enrichments	4-21
4.7	Effect of Temperature and Voids on Calculated Reactivity of Storage Rack	4-23

Appendix A to Section 4 - Tables

1	Results of 27-GROUP (Scale) AMPX-KENO Calcula- tions of B&W Critical Experiments	A-4
2	Results of CASMO-2E Benchmark (Intercomparison) Calculations	A-7
5.1	List of Cases Analyzed	5-5
5.2	Maximum Pool Bulk Temperature t , Coincident Total Power Q , and Coincident Specific Power for the Hottest Assembly	5-8
5.3	Time (Hrs) to Boiling and Boiling Vaporization Rate From the Instant All Cooling is Lost	5-9



LIST OF TABLES (Continued)

<u>Table</u>		<u>Page</u>
5.4	Maximum Local Pool Water Temperature and Local Fuel Cladding Temperature at Instant of Maximum Pool Bulk Temperature	5-13
5.5	Pool and Maximum Cladding Temperature at the Instant Fuel Assembly Transfer Begins	5-15
6.2.1	Degrees of Freedom	6-7
6.3.1	Numbering System for Gap Elements and Friction Elements	6-11
6.6.1	Rack Material Data	6-17
6.6.2	Support Material Data	6-18
6.8.1	Summary of Results - Rack Type 6x11	6-23
6.8.2	Summary of Results - Rack Type 10x11	6-25
7.1	Photon Energy Production Rates of an Average Spent Fuel Assembly	7-6
7.2	Photon Energy Production Rates of Peak Spent Fuel Assembly	7-7
7.3	Calculated Dose Rates in Areas Adjacent to the Spent Fuel Pool (Unit 1, Typical)	7-9
7.4	Calculated Dose Rate at or Above Pool Water Surface Due to Transfer of a Peak Power Fuel Assembly	7-10
7.5	Decay Heat and Evaporation Rates	7-12
7.6	Atmospheric Dispersion Factors	7-14
7.7	Results of Spent Fuel Pool Boiling Analysis	7-15



LIST OF FIGURES

<u>Figure</u>	<u>Page</u>
2.1a Pool Layout Unit 1	2-4
2.1b Pool Layout Unit 2	2-5
2.2 Typical Rack Elevaton	2-6
3.1 3x3 Typical Array Region 1 (Poisoned Cells)	3-8
3.2 Channel Element (2 for Square Cell)	3-9
3.3 Connecting Element (Gap Channel) (For Adjacent Cells)	3-9
3.4 Composite Box Assembly Region 2 (Poisoned Cells)	3-10
3.5a Typical Cell Elevation Region 1 (Poisoned Cells)	3-11
3.5b Typical Cell Elevation Region 2 (Unpoisoned Cells)	3-12
3.6a Fixed Support	3-13
3.6b Adjustable Support	3-14
3.7 Typical Array Region 2 (Unpoisoned Cells)	3-15
4.1 Acceptable Burnup Domain in Region 2 of Diablo Canyon Spent Fuel Storage Racks	4-28
4.2 Configuration of Region 1 Spent Fuel Storage Cell	4-29
4.3 Configuration of Region 2 Spent Fuel Storage Cell	4-30
4.4 Time-dependent Reactivity of Fuel Assemblies for Fuel of Several Initial Enrichments	4-31
4.5 Effect of Long-term Storage on Reactivity (k) of Spent Fuel Storage Rack	4-32
4.6 Axial Burnup Distribution (Calculated) for Turkey Point Fuel (from HEDL-TME-80-83)	4-33
4.7 Relative Axial Burnup Distribution for H.B. Robinson Fuel (from NUREG/CR-0722)	4-34



LIST OF FIGURES (Continued)

<u>Figure</u>		<u>Page</u>
4.8	Reactivity Effect of Water Spacing Between Fuel Assemblies	4-35
5.1a	Pool Bulk Temperature	5-17
5.1b	Pool Bulk Temperature	5-18
5.1c	Power Discharged	5-19
5.1d	Power Discharged	5-20
5.2a	Pool Bulk Temperature	5-21
5.2b	Pool Bulk Temperature	5-22
5.2c	Power Discharged	5-23
5.2d	Power Discharged	5-24
5.3a	Pool Bulk Temperature; Full Core Discharge	5-25
5.3b	Pool Bulk Temperature; Full Core Discharge	5-26
5.3c	Power Discharged; Full Core Discharge	5-27
5.3d	Power Discharged; Full Core Discharge	5-28
5.4	Idealization of Rack Assembly	5-29
5.5	Thermal Chimney Flow Model	5-30
6.1.1	Hosgri Quake - Horizontal X Direction	6-33
6.1.2	Hosgri Quake - Horizontal Y Direction	6-34
6.1.3	Hosgri Quake - Vertical Direction	6-35
6.1.4	OBE Quake - Horizontal X Direction	6-36
6.1.5	OBE Quake - Horizontal Y Direction	6-37
6.1.6	OBE Quake - Vertical Direction	6-38
6.2.1	Dynamic Model	6-39



LIST OF FIGURES (Continued)

<u>Figure</u>		<u>Page</u>
6.2.2	Gap Elements to Simulate Inter-rack Impacts	6-40
6.2.3	Impact Springs and Fluid Dampers	6-41
6.3.1	Spring Mass Simulation for Two-Dimensional Motion	6-42
8.1	Test Coupon	8-3



1. INTRODUCTION

This report describes the design, fabrication, and safety analysis of high density spent fuel storage racks produced by Joseph Oat Corporation (Oat) for the Diablo Canyon Power Plant Unit 1 and Unit 2. The plant, which is located on the Pacific coastline approximately 12 miles southwest of San Luis Obispo, California, is owned and operated by Pacific Gas and Electric Company (PGandE).

Diablo Canyon is a two-unit pressurized water reactor [(PWR) Westinghouse design] with a net design capacity of 1084 MWe for Unit 1 and 1106 MWe for Unit 2. The reactor core contains 193 fuel assemblies rated to produce 3338 thermal megawatts for Unit 1 and 3411 thermal megawatts for Unit 2. At present, there are no spent fuel assemblies stored in the spent fuel pools. Unit 1 went into commercial operation in May of 1985, with Unit 2 scheduled to go into commercial operation in late 1985.

Each unit is currently licensed for the storage of 270 spent fuel assemblies having a maximum uranium-235 enrichment of 3.5 weight percent. As shown in Tables 1.1a and b, the storage pools would lose full core discharge capability in 1988 (Unit 1) and 1990 (Unit 2). The proposed pool storage densification will equip each pool with 1324 storage locations. Table 1.1 indicates that the proposed reracking of the pool will provide adequate storage with full core discharge capability well into the next century (circa 2007). Tables 1.1a and b are based on a conservatively estimated 18-month fuel cycle. Current trends toward longer cycles, extended burnup, and higher enrichment would further extend the time span of onsite storage.

The proposed racks are free-standing and self-supporting. The principal construction materials are ASTM SA-240, Type 304L for the storage locations and "Boraflex," a patented product of BISCO (a division of Brand, Inc.), as the poison material (Region 1 racks only).



The specifications for design, construction, and quality assurance for the high density spent fuel storage racks were prepared by PGandE. The mechanical design, seismic/structural analysis, thermal-hydraulic analysis, and other related calculations, as well as the fabrication of the hardware, are performed by Oat. PGandE provided the seismic time histories and performed the spent fuel pool structure evaluation. Bechtel Power Corporation performed the radiation shielding analysis and the dose evaluation for a boiling pool. Southern Science, a division of Black & Veatch, is serving as a consultant to Oat in the area of criticality analysis. The analyses performed by Oat in conjunction with Black and Veatch and Bechtel demonstrate that acceptable margins of safety exist with respect to appropriate NRC and ASME acceptance criteria. A cost-benefit comparison of several potential spent fuel disposition alternatives indicates that (1) reracking of the Diablo Canyon pools is the lowest risk and most cost-effective alternative, and (2) that neither the reracking operation nor the increased onsite storage of irradiated material pose an undue hazard to the plant staff or the public.

The following sections provide a synopsis of the design, fabrication, nuclear criticality analysis, thermal/hydraulic analysis, structural analysis, accident analysis, environmental analysis, and cost-benefit appraisal of the high density spent fuel racks. In particular, the integrity of the rack structure under the specified combinations of inertial, seismic, and mechanical loads and thermal gradient per NUREG-0800 is demonstrated.

Also included are descriptions of the rack In-Service Surveillance Program and the Oat Quality Assurance Program. This Quality Assurance Program has been reviewed and found acceptable for engineered fabrication of ASME Section III, Class 1, 2, 3 and MC Components by both ASME and the NRC.



Table 1.1a

DIABLO CANYON UNIT 1 FUEL ASSEMBLY DISCHARGE
(TENTATIVE SCHEDULE)

Refueling Date	Number of Assemblies Discharged	Total Discharged Assemblies in Spent Fuel Pool Following Refueling	Remaining Storage Capability Without Proposed Expansion	Remaining Storage Capability With Proposed Expansion
September 1986	76	76	194	1248
March 1988	76	152	118*	1172
September 1989	76	228	42**	1096
March 1991	76	304		1020
September 1992	76	380		944
March 1994	76	456		868
September 1995	76	532		792
March 1997	76	608		716
September 1998	76	684		640
March 2000	76	760		564
September 2001	76	836		488
March 2003	76	912		412
September 2004	76	988		336
March 2006	76	1064		260
September 2007	76	1140		184*
March 2009	76	1216		108
September 2010	76	1292		32**

* Full core discharge capability lost -- 193 assemblies
 ** Partial core discharge capability lost -- 76 assemblies



Table 1.1b

DIABLO CANYON UNIT 2 FUEL ASSEMBLY DISCHARGE
(TENTATIVE SCHEDULE)

Refueling Date	Number of Assemblies Discharged	Total Discharged Assemblies in Spent Fuel Pool Following Refueling	Remaining Storage Capability Without Proposed Expansion	Remaining Storage Capability With Proposed Expansion
March 1987	76	76	194	1248
September 1988	76	152	118*	1172
March 1990	76	228	42**	1096
September 1991	76	304		1020
March 1993	76	380		944
September 1994	76	456		868
March 1996	76	532		792
September 1997	76	608		716
March 1999	76	684		640
September 2000	76	760		564
March 2002	76	836		488
September 2003	76	912		412
March 2005	76	988		336
September 2006	76	1064		260
March 2008	76	1140		184*
September 2009	76	1216		108
March 2011	76	1292		32**

* Full core discharge capability lost -- 193 assemblies

** Partial core discharge capability lost -- 76 assemblies



2. GENERAL ARRANGEMENT

The high density spent fuel racks consist of individual cells with 8.85-inch by 8.85-inch (nominal) square cross-section, each of which accommodates a single Westinghouse PWR fuel assembly. The cells are arranged in modules of varying sizes. A total of 1324 cells are arranged in 16 distinct modules in two regions. Region 1 is designed for storage of new fuel assemblies with enrichments up to 4.5 weight percent U-235 and spent fuel that has not achieved adequate burnup for Region 2. The Region 2 cells are capable of accommodating fuel assemblies with initial enrichments of 4.5 weight percent U-235 and a minimum burnup of 34,500 MWD/MTU. Figures 2.1a and b show the arrangement of the rack modules in the Diablo Canyon pool for Unit 1 and Unit 2, respectively.

The high density racks are engineered to achieve the dual objective of maximum protection against structural loadings (arising from ground motion, thermal stresses, etc.) and the maximization of available storage locations. In general, a greater width-to-height aspect ratio provides greater margin against rigid body tipping. Hence, the modules are made as large as possible within the constraints of transportation and site handling capabilities.

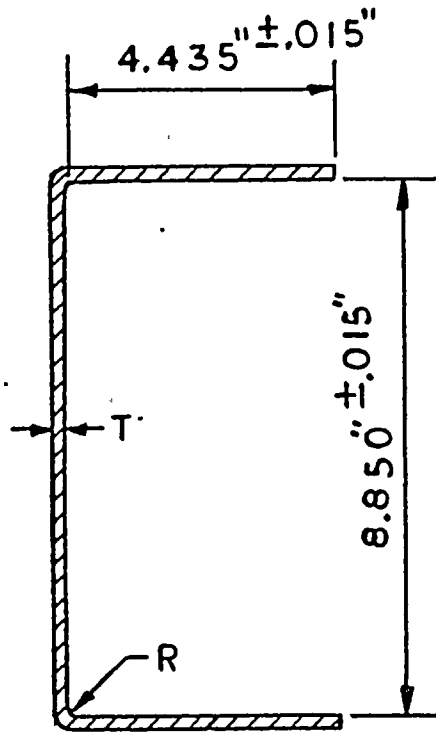
As shown in Figures 2.1a and b, there are 16 discrete modules arranged in the fuel pool. Each rack module is equipped (see Figure 2.2) with girdle bars, 7/8-inch-thick by 3-5/8 inches high or 1-1/16 inches by 3 inches. The nominal gap between adjacent modules is 2-1/4 inches. The modules make surface contact between their contiguous walls at the girdle bar locations and thus maintain a specified gap between them. Table 2.1 gives the relevant design data on each region. The modules in the two regions are of 13 different types. Table 2.2 summarizes the physical data for each module type.



Table 2.1
 DESIGN DATA

Region.	(Cell Pitch) Nominal in.	Min. B-10 Loading	Flux Trap Gap (Nominal) in.
1	10.93	0.012 gm/cm ²	1.786
2	10.93	unpoisoned	1.9





Poisoned Cells :
 T = 0.080" THK.
 R = 0.080"

Unpoisoned Cells:
 T = 0.090" THK.
 R = 0.090"

FIGURE 3.2 Channel Element
 (2 For Sq. Cell)

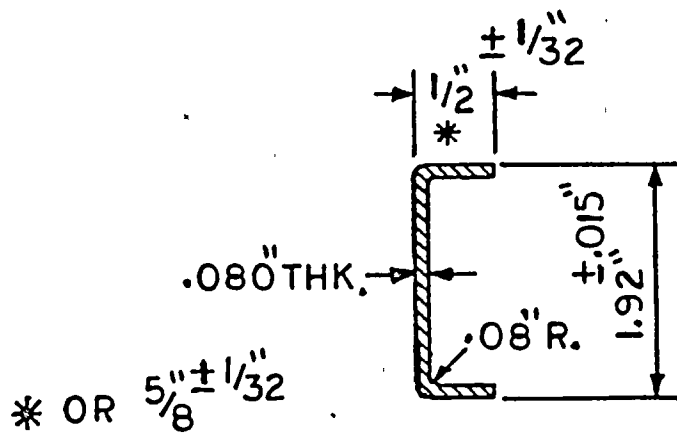


FIGURE 3.3 Connecting Element (Gap Channel)
 (For Adjacent Cells)



Table 2.2
MODULE DATA

Region	Module Type	Quantity Per Unit	Cells per Module	Array Size	Approximate Weight (lb/module)
1	A	2	100	10 x 10	21,500
1	B	1	90	9 x 10	19,500
2	C	1	100	10 x 10	25,500
2	D	3	90	9 x 10	23,000
2	E	1	66	11 x 6	17,000
2	F	1	72	9 x 8	18,500
2	G	1	80	10 x 8	20,500
2	H	1	24 + 10	---	15,000
2	J	1	96	9 x 10 + 6	24,500
2	K	1	54	6 x 9	14,000
2	L	1	81	9 x 9	21,000
2	M	1	110	11 x 10	28,000
2	N	1	81	9 x 9	21,000





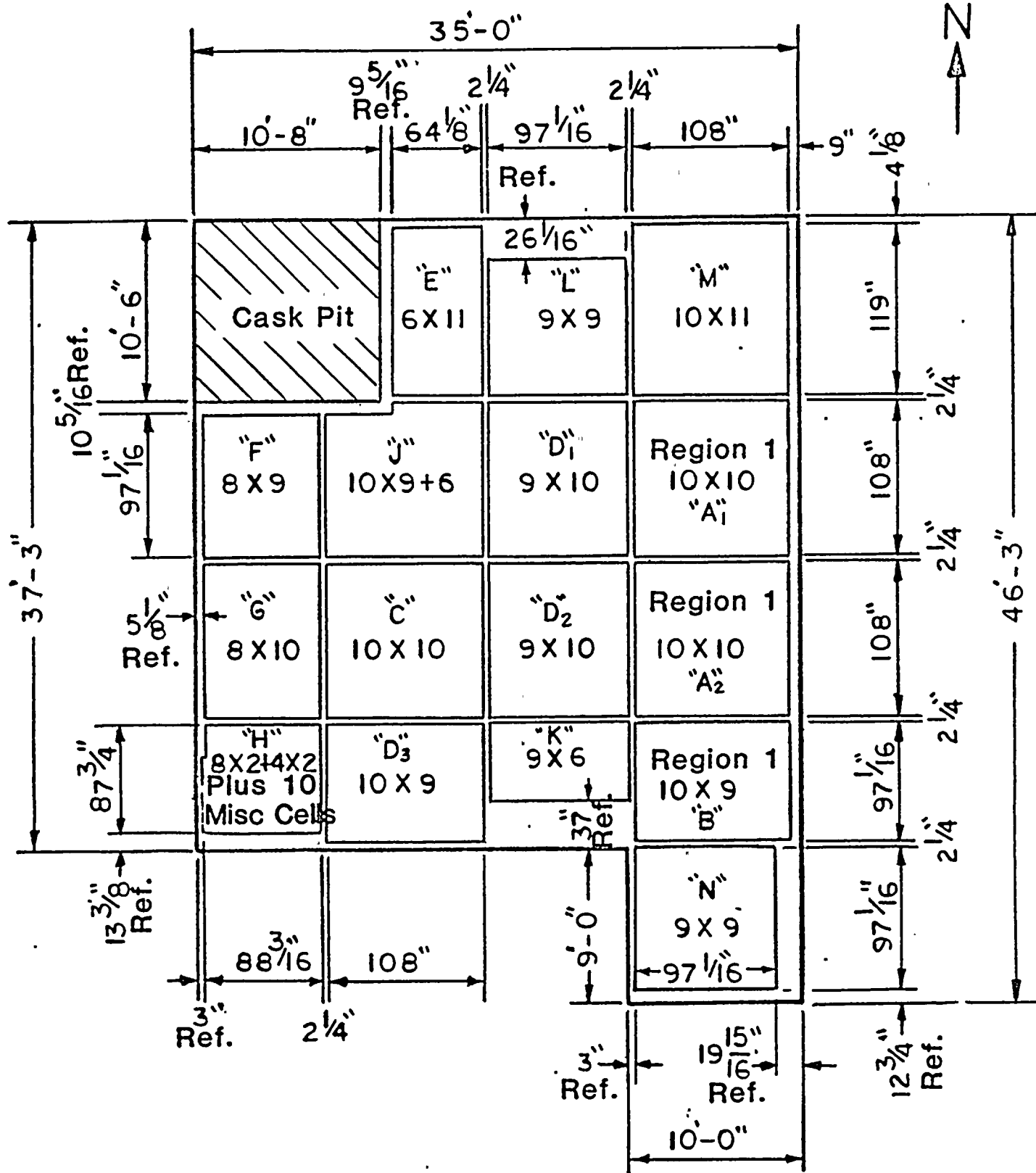


FIGURE 2.1b Pool Layout Unit 2



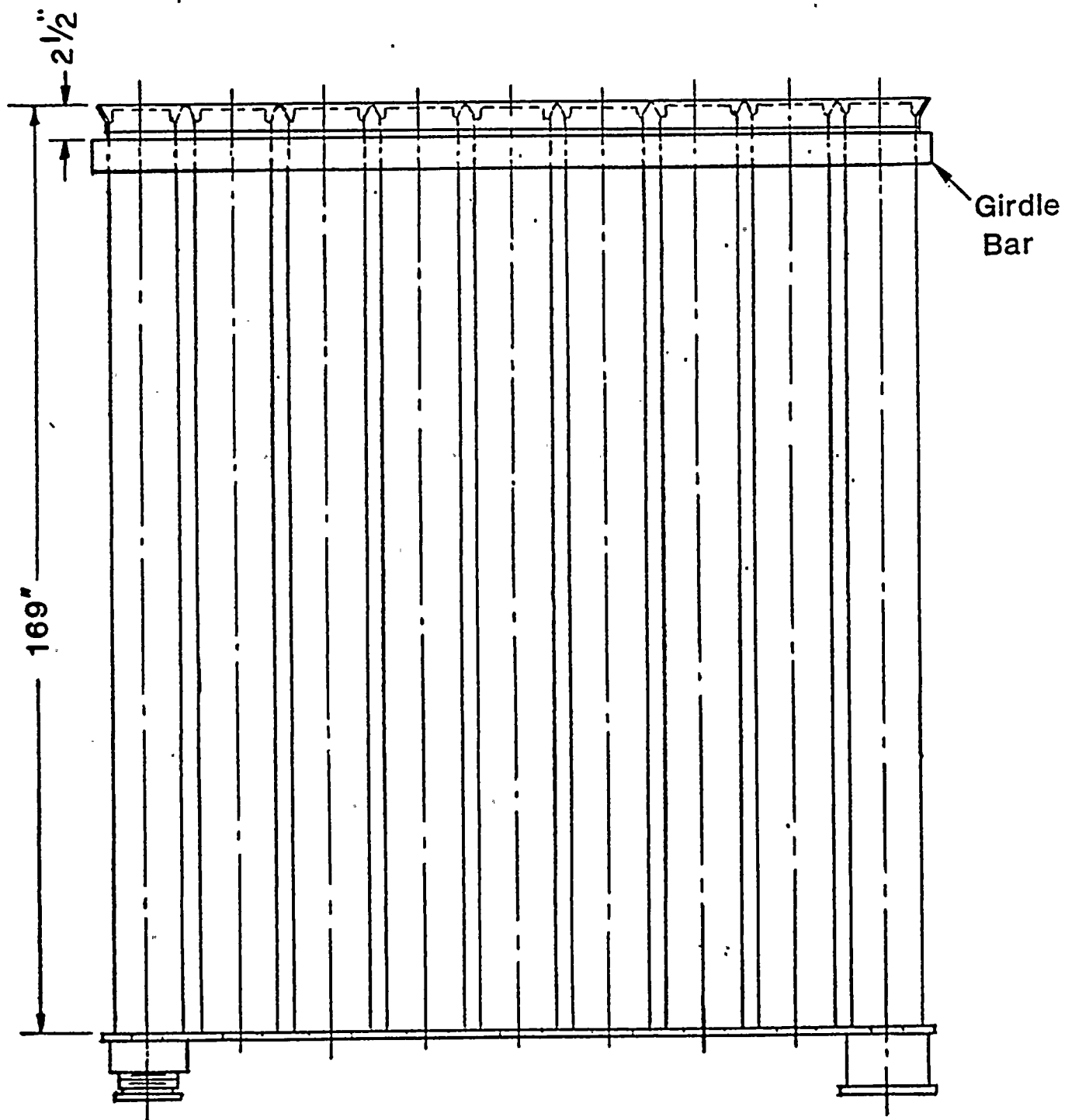


FIGURE 2.2 Typical Rack Elevation



3. RACK CONSTRUCTION

3.1 FABRICATION DETAILS

3.1.1 Region 1

The rack module is fabricated from ASTM A-240-304L austenitic stainless steel sheet and plate material and ASTM A-182, Type F-304L forging material. The weld filler material utilized in body welds is ASME SFA-5.9, Type 308L and 308LSI. Boraflex, a patented brand name product of BISCO (a division of Brand, Inc.) serves as the neutron absorber material. The detailed radiological properties of Boraflex may be found in Section 4. The Boraflex experience list is given in Table 3.1.

A typical module contains storage cells which have an 8.85-inch nominal square cross-sectional opening. This dimension ensures that fuel assemblies with maximum expected axial bow can be inserted and removed from the storage cells without any damage to the fuel assemblies or the rack modules.

Figure 3.1 shows a horizontal cross-section of a 3 x 3 array. The cells provide a smooth and continuous surface for lateral contact with the fuel assembly. The anatomy of the rack modules is best exposed by describing the basic building blocks of the design, namely:

- O Internal square tube
- O Neutron absorber material (Boraflex)
- O Poison sheathing
- O Gap channels
- O Baseplate
- O Support assembly
- O Top lead-in



Table 3.1

BORAFLEX EXPERIENCE FOR HIGH DENSITY RACKS

Site		Plant Type	NRC Docket No.	Licensing Status
Point Beach	1 and 2	PWR	50-226 & 301	Licensed
Nine Mile Point	1	BWR	50-220	Licensed
Oconee	1 and 2	PWR	50-269 & 270	Licensed
Prairie Island	1 and 2	PWR	50-282 & 306	Licensed
Calvert Cliffs	2	PWR	50-318	Licensed
Quad Cities *	1 and 2	BWR	50-254 & 265	Licensed
Watts Bar	1 and 2	PWR	50-390 & 391	Pending
Waterford	3	PWR	50-382	Pending
Fermi *	2	BWR	50-341	Licensed
H. B. Robinson	2	PWR	50-261	Licensed
River Bend	1	BWR	50-458	Licensed
Rancho Seco *	1	PWR	50-312	Licensed
Nine Mile Point	2	BWR	50-410	To be applied for
Shearon Harris	1	PWR	50-400	To be applied for
Millstone	3	PWR	50-423	To be applied for
Grand Gulf *	1	BWR	50-416	Pending
Oyster Creek *		BWR	50-219	Licensed
V. C. Summer *		PWR	50-395	Licensed

* Joseph Oat Corporation-fabricated racks



a. Internal Square Tube

This element provides the lateral bearing surface to the fuel assembly. It is fabricated by joining two formed channels (Fig. 3.2) using a controlled seam welding operation. This element is an 8.85-inch square (nominal) cross-section by 169 inches long.

b. Neutron Absorber Material (Boraflex)

Boraflex is placed on all four sides of a square tube over a length of 139 inches, which covers the active fuel length except the top and bottom 3 inches.

c. Poison Sheathing

Poison sheathing (cover plate), shown in Fig. 3.4, serves to position the poison material in its designated space and to ensure that the poison material will remain in that space for the life of the racks. This is accomplished by spot welding the cover sheet to the square tube along the former's edges at numerous (at least 20) locations. This manner of attachment ensures that the poison material will not sag or laterally displace during fabrication processes and under any subsequent loading condition.

d. Gap Channels

Gap channels, illustrated in Fig. 3.3, position two inner boxes at a predetermined distance to maintain the minimum flux trap gap required between two boxes. The gap channel is welded to the inner box by spot welds. An array of composite box assemblies welded as indicated in Fig. 3.1 form the honeycomb gridwork of cells which harnesses the structural strength of all sheet and plate type members in an efficient manner. The array of composite boxes has overall bending, torsional, and axial rigidities which are an order of magnitude greater than configurations utilizing grid bar type of construction.

e. Baseplate

The baseplate is a 5/8-inch thick plate type member which has 6-inch diameter holes concentrically located with respect to the internal square tube, except at support leg locations, where the hole size is 5 inches in diameter. These holes provide the primary path for coolant flow. Secondary flow paths are available between adjacent cells via the lateral flow holes (1-1/2 inches in diameter) near the root of the honeycomb (Figures 3.5a and 3.5b). The honeycomb is welded to the baseplate with 3/32-inch fillet welds.



f. Support Assembly

Each module has four support legs. One support leg is of fixed height (Fig. 3.6a); the other three are adjustable in length to enable levelling of the rack. The variable height support assembly consists of a flat-footed spindle which rides into an internally-threaded cylindrical member. The cylindrical member is attached to the underside of the baseplate through double fillet and partial penetration welds. The base of the flat-footed spindle sits on the pool floor. Levelling of the rack modules is accomplished by turning the hex sprocket in the spindle using a long arm (approximately 46 feet long) hex head wrench. Fig. 3.6b shows a vertical cross-section of the adjustable support assembly.

The supports elevate the module baseplate approximately 7-1/4 inches (3-1/2 inches for rack H) above the pool floor, thus creating the water plenum for coolant flow. The lateral holes in the cylindrical member provide the coolant entry path leading into the bottom of the storage locations.

g. Top Lead-in

Lead-ins are provided on all four sides of each cell to facilitate fuel assembly insertion. The lead-ins of contiguous walls of adjacent cells are structurally connected at the lead-in. These lead-in joints aid in reducing the lateral deflection of the inner square tube due to the impact of fuel assemblies during the ground motion (postulated seismic motion specified in the FSAR). This type of construction leads to natural venting locations for the inter-cell space where the neutron absorber material is located.

The fabrication of the rack modules is performed under a strict quality assurance system suitable for ASME Section III, Class 1, 2, and 3 manufacturing which has been in place at Oat for over 10 years.

3.1.2 Region 2

The rack modules in Region 2 are fabricated from the same material as that used for Region 1 modules, i.e., ASTM A-240-304L austenitic stainless steel and ASTM A-182, Type F-304L forging material. No neutron absorber material is used.



A typical Region 2 module storage cell also has an 8.85-inch nominal square cross-sectional opening. Figure 3.7 shows a horizontal cross-section of a 3 x 3 array. The rack construction varies from that for Region 1 inasmuch as the stainless steel cover plate and the neutron absorber material are eliminated. Hence, the basic components of this design are as follows:

- O Inner tube
- O Gap channel
- O Baseplate
- O Support assembly
- O Top lead-in

In this construction, two channel elements form the cell of an 8.85-inch nominal square cross-sectional opening. The gap channel positions two inner tubes at a predetermined distance, in addition to functioning as part of the structural support grid work as illustrated in Fig. 3.7.

The baseplate and support assemblies are exactly the same as those described for Region 1. A suitably designed lead-in for fuel assembly insertion is provided on all four sides of each cell, similar to Region 1.

3.2 CODES, STANDARDS, AND PRACTICES FOR THE SPENT FUEL POOL MODIFICATION

The following codes, standards, and practices were used as applicable for the design, construction, and assembly of the spent fuel storage racks and analysis of the pool structure. Additional specific references related to detailed analyses are given at the end of each section and at the beginning of Section 4.



a. Design Codes

- (1) AISC Manual of Steel Construction, 8th Edition, 1980.
- (2) ANSI N210-1976, "Design Objectives for Light Water Reactor Spent Fuel Storage Facilities at Nuclear Power Stations."
- (3) American Society of Mechanical Engineers (ASME), Boiler and Pressure Vessel Code, Section III, 1983 Edition up to and including Summer 1983 Addenda (Subsection NF).
- (4) ASNT-TC-1A June, 1980 American Society for Nondestructive Testing (Recommended Practice for Personnel Qualifications).

b. Material Codes

- (1) American Society for Testing and Materials (ASTM) Standards - A-240.
- (2) American Society of Mechanical Engineers (ASME), Boiler and Pressure Vessel Code, Section II - Parts A and C, 1983 Edition, up to and including Summer 1983 Addenda.

c. Welding Codes

ASME Boiler and Pressure Vessel Code, Section IX - Welding and Brazing Qualifications, 1983 Edition up to and including Summer, 1983 Addenda.

d. Quality Assurance, Cleanliness, Packaging, Shipping, Receiving, Storage, and Handling Requirements

- (1) ANSI N45.2.2 - Packaging, Shipping, Receiving, Storage and Handling of Items for Nuclear Power Plants.
- (2) ANSI 45.2.1 - Cleaning of Fluid Systems and Associated Components during Construction Phase of Nuclear Power Plants.
- (3) ASME Boiler and Pressure Vessel, Section V, Nondestructive Examination, 1983 Edition, including Summer and Winter 1983.
- (4) ANSI - N16.1-75 Nuclear Criticality Safety Operations with Fissionable Materials Outside Reactors.



- (5) ANSI - N16.9-75 Validation of Calculation Methods for Nuclear Criticality Safety.
- (6) ANSI - N45.2.11, 1974 Quality Assurance Requirements for the Design of Nuclear Power Plants.

e. Other References

- (1) NRC Regulatory Guides, Division 1, Regulatory Guides 1.13, 1.29, 1.31, 1.61, 1.71, 1.85, 1.92, 1.124, and 3.41 (revisions as applicable).
- (2) General Design Criteria for Nuclear Power Plants, Code of Federal Regulations, Title 10, Part 50, Appendix A (GDC Nos. 1, 2, 61, 62, and 63).
- (3) NUREG-0800, Standard Review Plan (1981).
- (4) "OT Position for Review and Acceptance of Spent Fuel Storage and Handling Applications," dated April 14, 1978, and the modifications to this document of January 18, 1979.



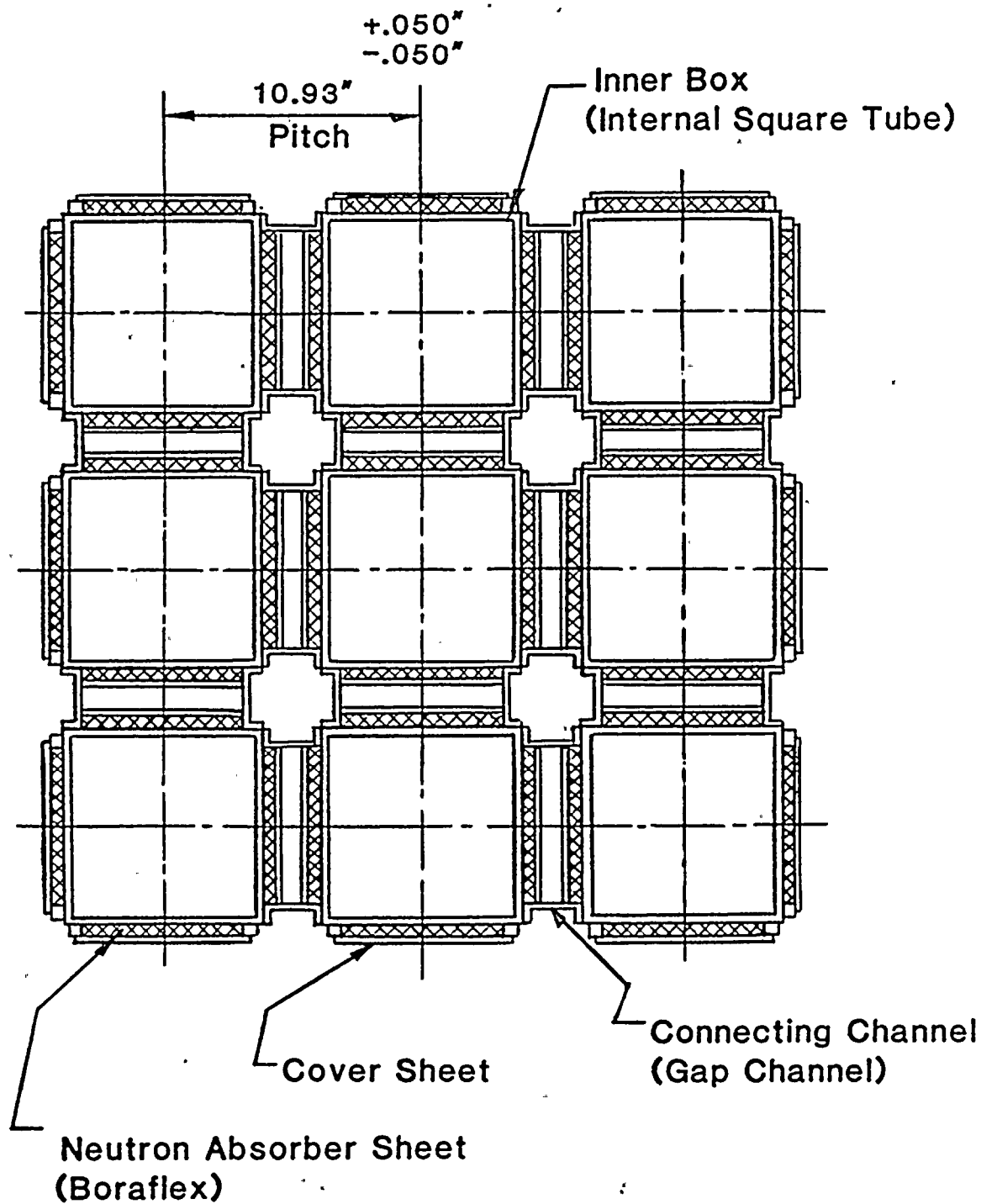


FIGURE 3.1 3 x 3 Typical Array - Region 1 (Poisoned Cells)



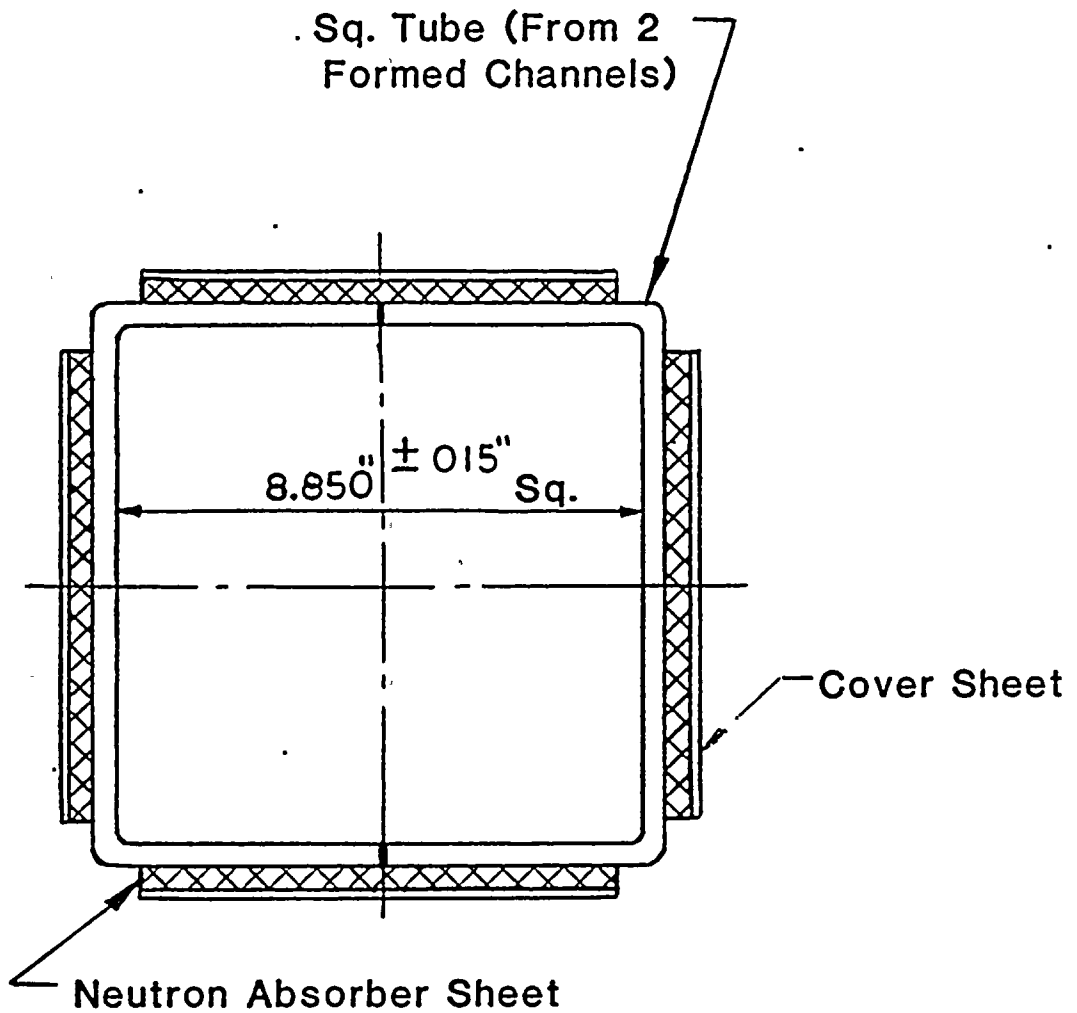


FIGURE 3.4 Composite Box Assembly - Region 1 (Poisoned Cells)



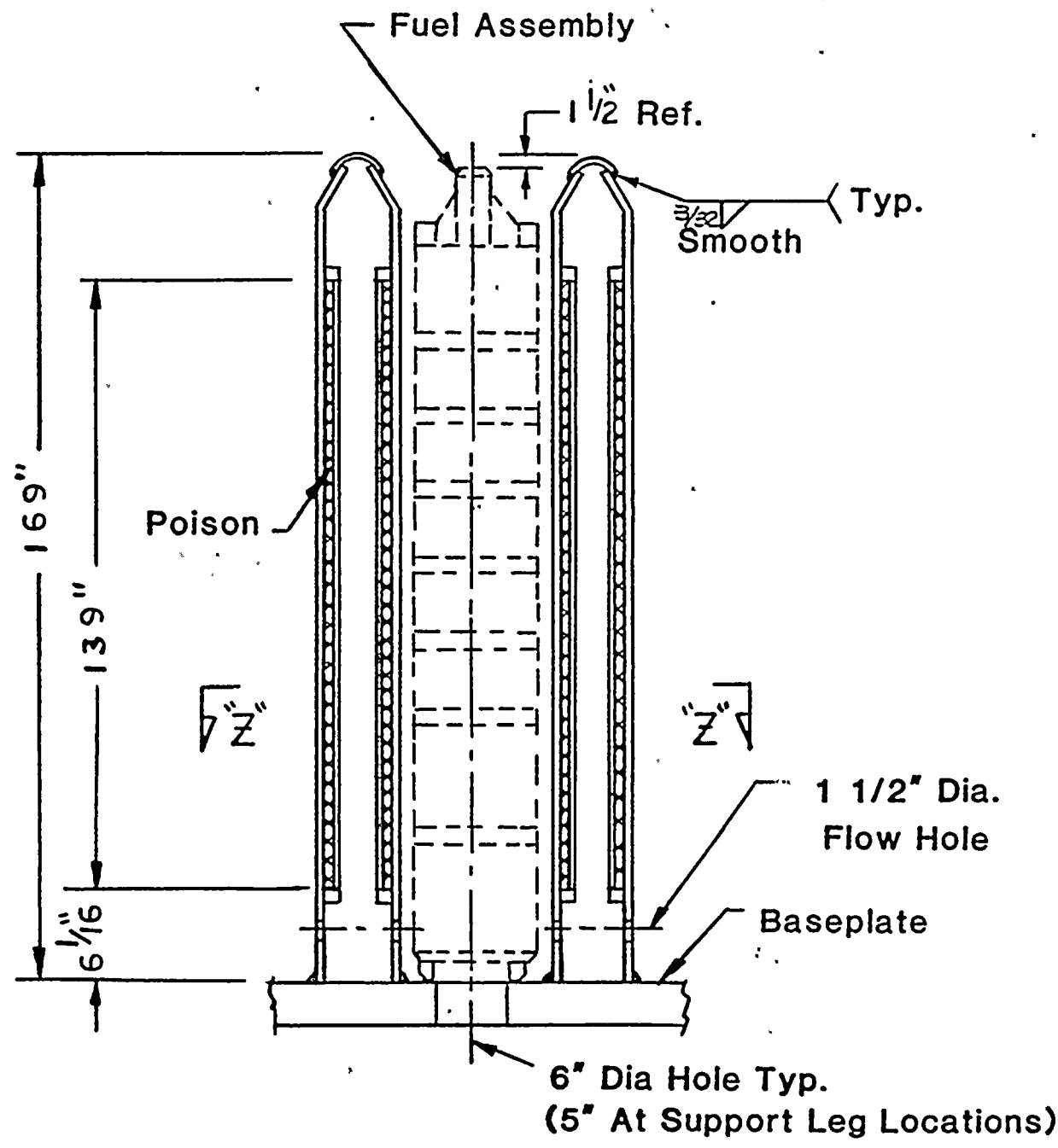
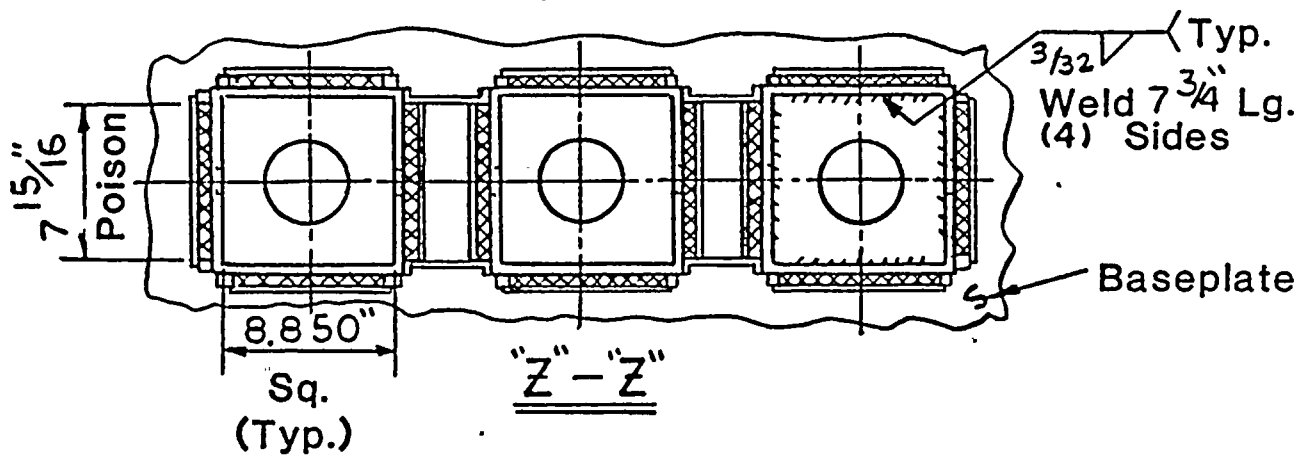


FIGURE 3.5a Typical Cell Elevation - Region 1 (Poisoned Cells)



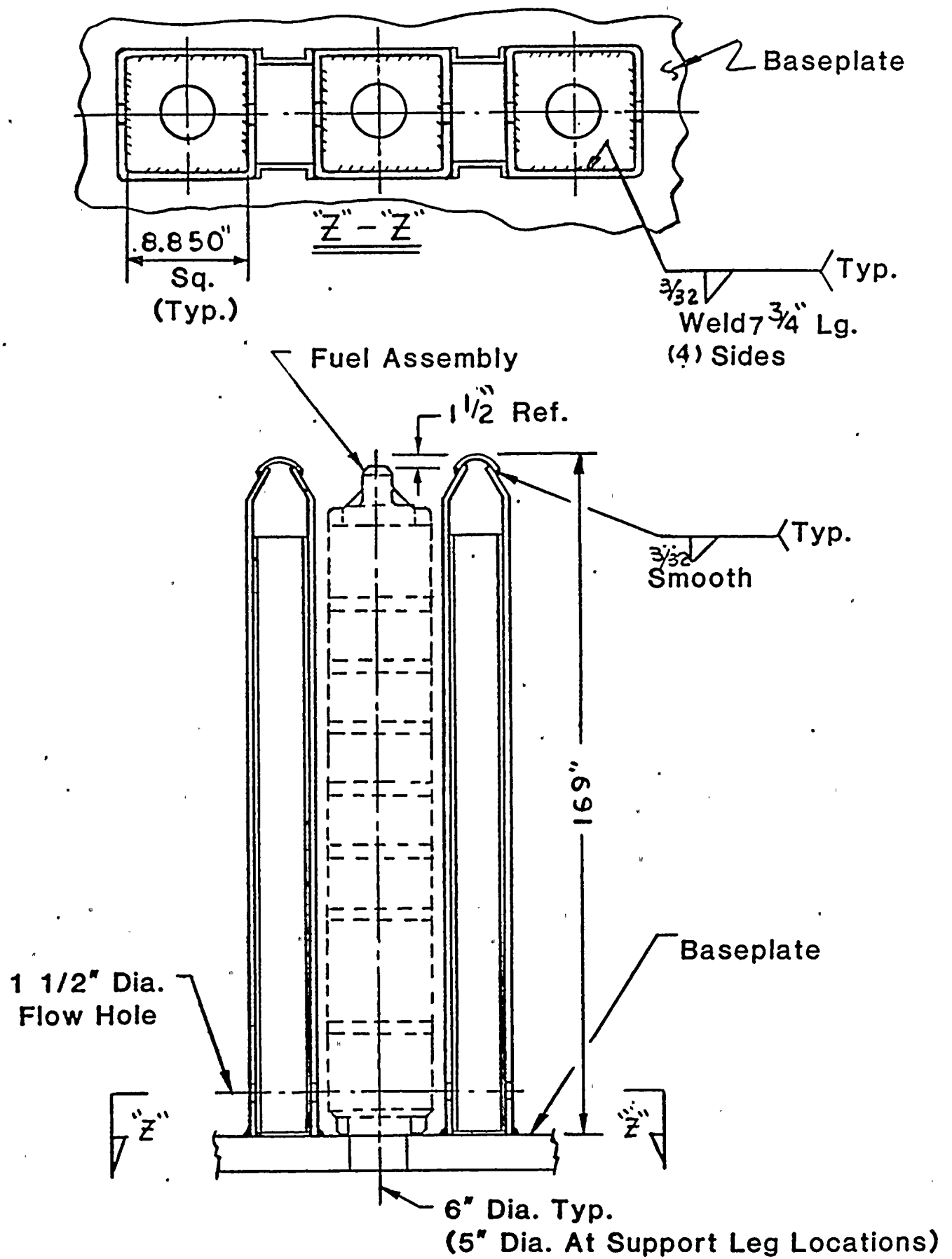


FIGURE 3.5b Typical Cell Elevation - Region 2
(Unpoisoned Cells)



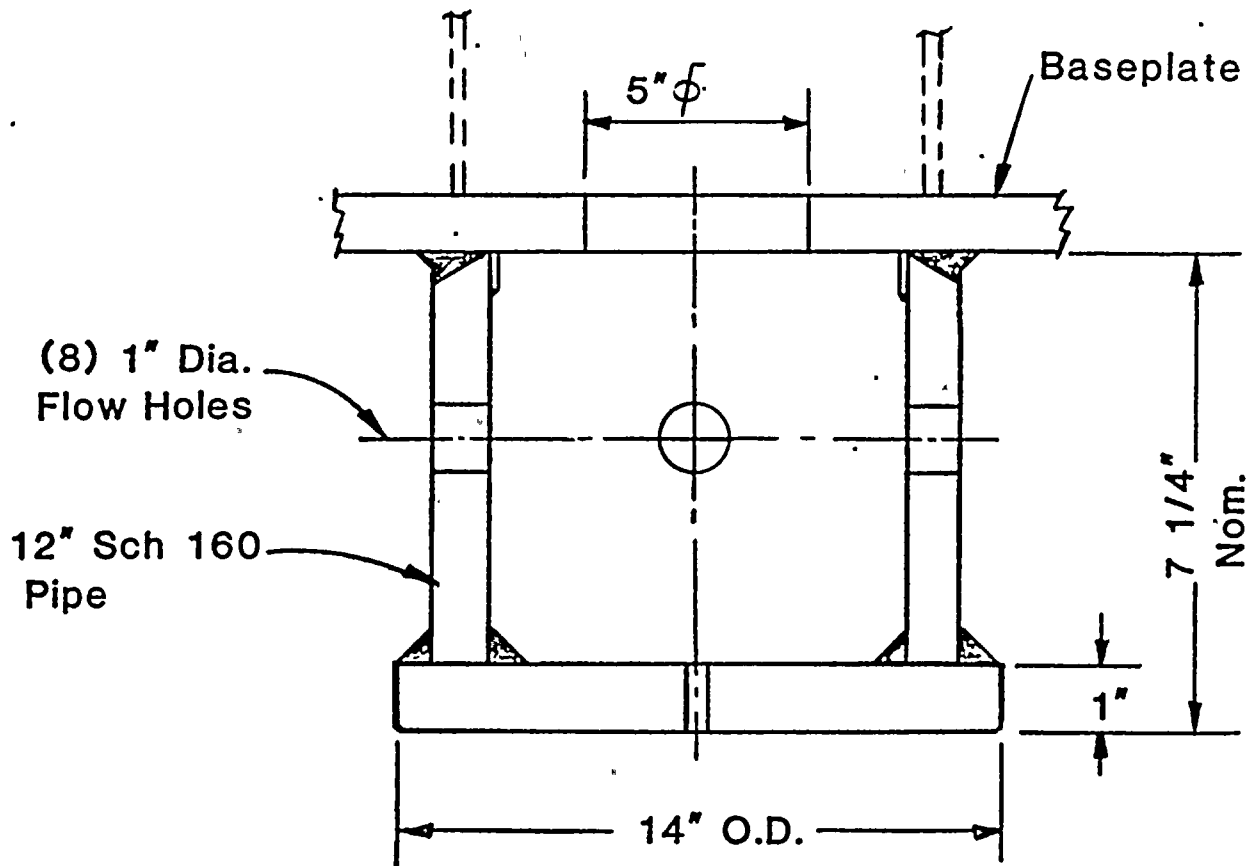


FIGURE 3.6a Fixed Support



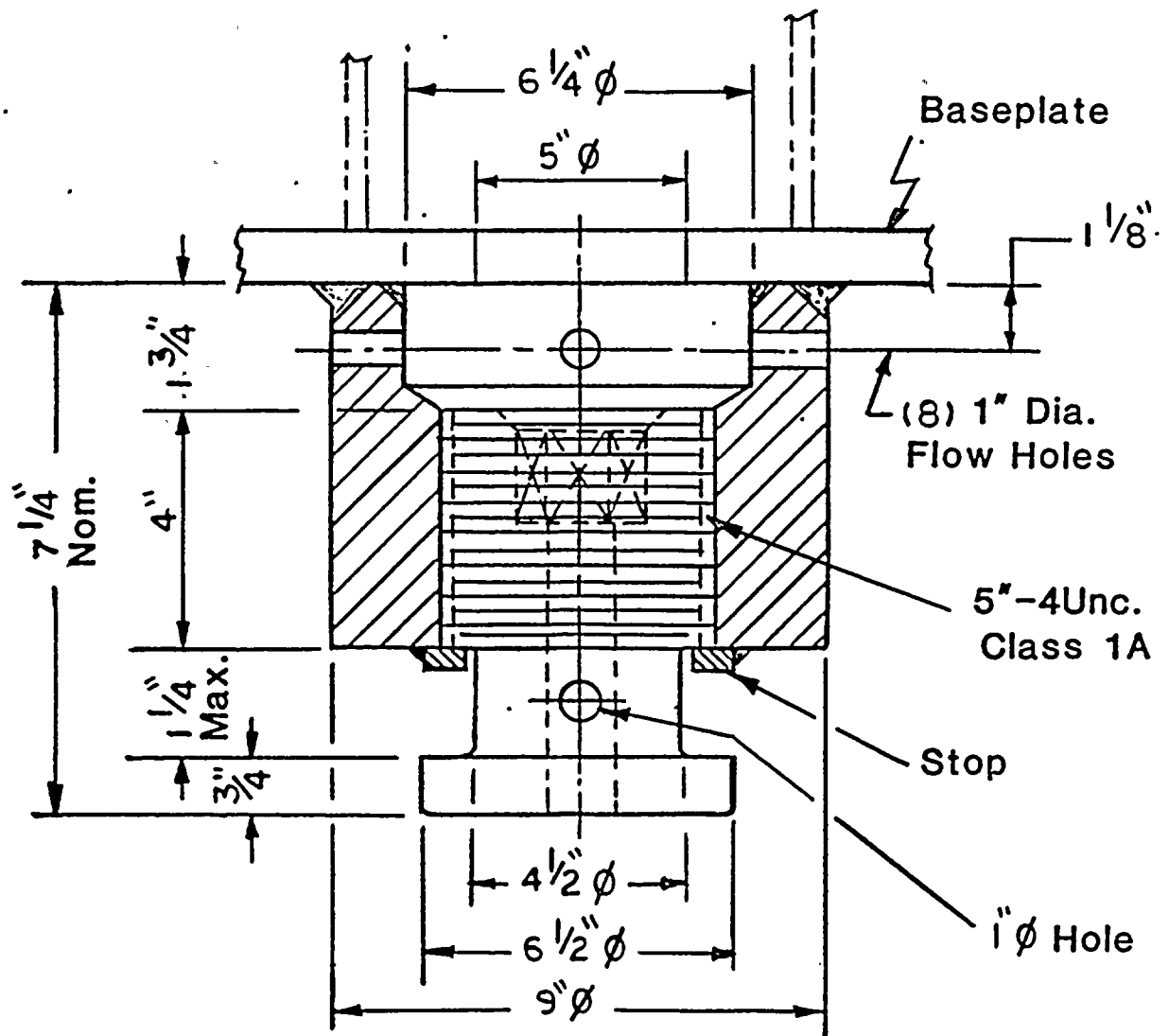


FIGURE 3.6b Adjustable Support



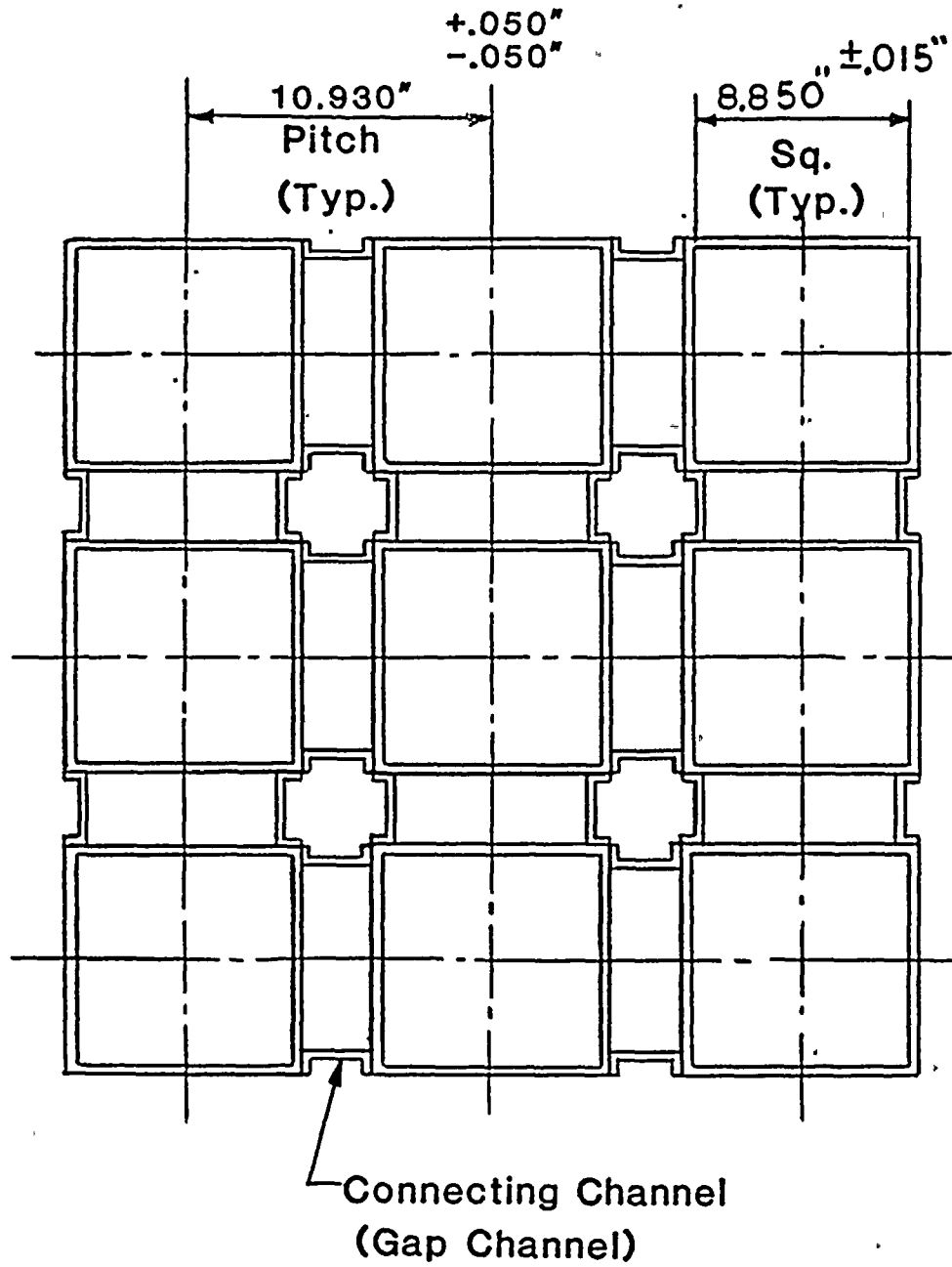


FIGURE 3.7 Typical Array – Region 2
 (Unpoisoned Cells)



4. NUCLEAR CRITICALITY ANALYSIS

4.1 DESIGN BASES

The high density spent fuel storage racks for the Diablo Canyon Power Plant are designed to assure that a k_{eff} equal to or less than 0.95 is maintained with the racks fully loaded with fuel of the highest anticipated reactivity in each of two regions, and flooded with unborated water at a temperature corresponding to the highest reactivity. The maximum calculated reactivity includes a margin for uncertainty in reactivity calculations and in mechanical tolerances, statistically combined, such that the true k_{eff} will be equal to or less than 0.95 with a 95% probability at a 95% confidence level.

Applicable codes, standards, and regulations, or pertinent sections thereof, include the following:

- O General Design Criterion 62, Prevention of Criticality in Fuel Storage and Handling
- O USNRC Standard Review Plan, NUREG-0800, Section 9.1.2, Spent Fuel Storage
- O USNRC letter of April 14, 1978, to all Power Reactor Licensees - OT Position for Review and Acceptance of Spent Fuel Storage and Handling Applications, including modification letter dated January 18, 1979
- O USNRC Regulatory Guide 1.13, Spent Fuel Storage Facility Design Basis, Rev. 2 (proposed), December 1981
- O USNRC Regulatory Guide 3.41, Validation of Computational Method for Nuclear Criticality Safety (and related ANSI N16.9-1975)
- O ANSI/ANS 57.2-1983, Design Requirements for Light Water Reactor Spent Fuel Storage Facilities at Nuclear Power Plants
- O ANSI N210-1976, Design Objectives for Light Water Reactor Spent Fuel Storage Facilities at Nuclear Power Plants
- O ANSI N18.2-1973, Nuclear Safety Criteria for the Design of Stationary Pressurized Water Reactor Plants



To assure the true reactivity will always be less than the calculated reactivity, the following conservative assumptions were made:

- O Moderator is pure, unborated water at a temperature corresponding to the highest reactivity.
- O Lattice of storage racks is assumed infinite in all directions, i.e., no credit is taken for axial or radial neutron leakage (except in the assessment of certain abnormal/accident conditions where leakage is inherent).
- O Neutron absorption in minor structural members is neglected, i.e., spacer grids and gap channels are replaced by water.

The design basis fuel assembly is a 17 x 17 array of fuel rods (Westinghouse design) containing UO_2 at a maximum initial enrichment of 4.5% U-235 by weight, corresponding to 56.77 grams U-235 per axial centimeter of fuel assembly. Two independent regions are provided in the spent fuel storage pool, with separate criteria defining the highest anticipated reactivity in each of the two regions as follows:

- O Region 1 is designed to accommodate new unirradiated fuel with a maximum enrichment of 4.5 wt% U-235, or spent fuel regardless of the discharge fuel burnup.
- O Region 2 is designed to accommodate fuel of 4.5 wt% U-235 initial enrichment which has accumulated a minimum burnup of 34.5 MWd/kgU. Region 2 will also safely accept fuel of lower discharge fuel burnup provided the initial enrichment is correspondingly lower, as depicted in Figure 4.1.

4.2 SUMMARY OF CRITICALITY ANALYSES

4.2.1 Normal Operating Conditions

The criticality analyses of each of the two separate regions of the spent fuel storage pool described above are summarized in Table 4.1 for the anticipated normal storage conditions. The calculated maximum reactivity in Region 2 includes a



0.018 Δk allowance for uncertainty in burnup calculations and provides an additional margin of more than 1% Δk below the limiting value of 0.95. As cooling time increases in long-term storage, decay of Pu-241 results in a significant decrease in reactivity, which will provide an increasing subcriticality margin. Spacing between the two different rack modules is sufficient to preclude adverse nuclear interaction between modules under normal conditions.

Although designed for 4.5% enriched fuel burned to 34.5 MWD/kgU, Region 2 can accommodate fuel of lower discharge fuel burnup provided the initial enrichment is correspondingly lower. Figure 4.1 illustrates, as a function of the initial fuel enrichment, the minimum acceptable burnup which yields the maximum reactivity given in Table 4.1 for Region 2. This curve will be incorporated in the Technical Specifications supplemented with appropriate administrative procedures to assure verified burnup as specified in draft Regulatory Guide 1.13, Revision 2.

In Region 2, the design basis temperature for the fuel storage pool water of 65°C is above the maximum of 64°C (147.3°F) conservatively estimated in Section 5, Thermal-Hydraulic Considerations, for partial core discharge refueling operations. For the maximum heat load conditions of a full core discharge, the spent fuel pool water is estimated to increase to a bulk temperature of 78.6°C (173.4°F). At this temperature, the reactivity of Region 2 would increase to 0.941 (maximum including uncertainties) in the absence of soluble poison. Administrative procedures will also be employed to confirm and assure the presence of soluble poison in the pool water during fuel handling operations, as a further margin of safety and as a precaution in the event of abnormal or accident conditions discussed in Section 4.2.2.



Table 4.1

SUMMARY OF CRITICALITY SAFETY ANALYSES

	Region 1	Region 2
Minimum acceptable burnup @ 4.5% initial enrichment	0	34.5 MWd/kgU
Temperature assumed for analysis	0°C	65°C
Reference k_{∞} (nominal)	0.9104	0.9119
Computational bias	0.0013	0.0013
Uncertainties		
Bias	± 0.0018	± 0.0018
B-10 concentration	∓ 0.0013	NA
Boraflex thickness	∓ 0.0064	NA
Boraflex width	∓ 0.0006	NA
Inner box dimension	± 0.0008	∓ 0.0002
Water gap thickness	∓ 0.0029	∓ 0.0041
SS thickness	± 0.0018	∓ 0.0028
Fuel enrichment	± 0.0011	± 0.0011
Fuel density	± 0.0029	± 0.0029
Eccentric assembly position	<u>$+0.0010$</u>	<u>$+0.0020$</u>
Statistical combination	± 0.0083	± 0.0064
Allowance for burnup uncertainty	NA	$+0.0183$
Total	0.9117 ± 0.0083	0.9315 ± 0.0064
Maximum reactivity	0.920	0.938



4.2.2 Abnormal and Accident Conditions

Although credit for the soluble poison normally present in the spent fuel pool water is permitted under abnormal or accident conditions*, most abnormal or accident conditions will not result in exceeding the limiting reactivity (k_{eff} of 0.95) even in the absence of soluble poison. The effects on reactivity of credible abnormal and accident conditions are summarized in Table 4.2 below. Of these abnormal/accident conditions, only two have the potential for a more than negligible positive reactivity effect.

Table 4.2

REACTIVITY EFFECTS OF ABNORMAL AND ACCIDENT CONDITIONS

Accident/Abnormal Conditions	Reactivity Effect
Temperature increase	Negative in Region 1 Positive in Region 2
Void (boiling)	Negative in both regions
Assembly dropped on top of rack	Negligible
Lateral rack module movement	Negligible
Misplacement of a fuel assembly	Positive

* Double contingency principle of ANSI N16.1-1975, as specified in the April 14, 1978 NRC letter (Section 1.2).



Calculations of temperature effects (Section 4.7.1) indicates that a temperature of 114°C (237°F, approximately the temperature of boiling at the submerged depth of the racks) could be tolerated without exceeding the limiting value for reactivity (k_{eff} of 0.95). The negative void coefficient of reactivity and increased leakage would reduce reactivity in the event of boiling. Administrative procedures to assure the presence of soluble poison during fuel handling operations provide further assurance that the reactivity will always remain below the limiting value for any temperature.

For the abnormal condition involving the misplacement of a new fuel assembly (either into a Region 2 storage cell or outside and adjacent to a rack module), credit for the soluble poison present in the fuel pool water is taken to ensure a k_{∞} of less than 0.95. Administrative procedures to assure the presence of soluble poison during fuel handling operations will preclude the possibility of the simultaneous occurrence of these two independent accident conditions (assembly misplacement and loss of soluble poison). With the nominal concentration of soluble poison present (2000 ppm boron), the maximum reactivity, k_{∞} , is less than 0.85 and is less than the limiting value for reactivity (k_{eff} of 0.95) with 1200 ppm boron even if Region 2 were to be fully loaded with fresh fuel of 4.5% enrichment.



4.3 REFERENCE FUEL STORAGE CELL

4.3.1 Reference Fuel Assembly

The reference design basis fuel assembly, illustrated in Fig. 4.2, is a 17 x 17 array of fuel rods with 25 rods replaced by 24 control rod guide tubes and 1 instrument thimble. Table 4.3 summarizes the fuel assembly design specifications and the expected range of significant variations.

4.3.2 Region 1 Storage Cells

The nominal spent fuel storage cell used for the criticality analyses of Region 1 storage cells is shown in Fig. 4.2. The rack is composed of Boraflex absorber material sandwiched between a 0.080-inch inner stainless steel box and a 0.020-inch outer stainless steel coverplate (0.125-inch coverplate for module periphery cell walls). The fuel assemblies are centrally located in each storage cell on a nominal lattice spacing of 10.930 ± 0.050 inches. Stainless steel gap channels connect one storage cell box to another in a rigid structure and define an outer water space between boxes. This outer water space constitutes a flux-trap between the two Boraflex absorber plates that are essentially opaque (black) to thermal neutrons. The Boraflex absorber has a thickness of 0.047 ± 0.007 inch and a nominal B-10 areal density of 0.0148 gram per cm^2 .

4.3.3 Region 2 Storage Cells

Region 2 storage cells, designed for fuel of 4.5 wt% U-235 initial enrichment burned to 34.5 MWd/kgU, are unpoisoned, other than that of the 0.090-inch-thick stainless steel plates forming the walls of the storage cell. These cells, shown in Fig. 4.3, are located on a lattice spacing of 10.929 ± 0.051 inches defining a 1.899 ± 0.051 -inch water gap between the steel walls.



Table 4.3

FUEL ASSEMBLY DESIGN SPECIFICATIONS

Fuel Rod Data

Outside diameter, in.	0.374
Cladding thickness, in.	0.0225
Cladding material	Zircaloy-4
Pellet diameter, in.	0.3225
UO ₂ pellet density, % TD	95 ± 2
UO ₂ stack density, g/cm ³	10.286 ± 0.217
Enrichment, wt% U-235	4.5 ± 0.02

Fuel Assembly Data

Number of fuel rods	264 (17 x 17 array)
Fuel rod pitch, in.	0.496
Control rod guide tube	
Number	24
Outside diameter, in.	0.482
Thickness, in.	0.016
Material	Zircaloy-4
Instrument thimble	
Number	1
Outside diameter, in.	0.482
Thickness, in.	0.016
Material	Zircaloy-4

U-235 loading (@ 4.5% enrichment) g/axial cm of assembly	56.77 ± 1.19
---	--------------



4.4 ANALYTICAL METHODOLOGY

4.4.1 Reference Analytical Methods and Bias

Criticality analyses of the high density spent fuel storage racks were performed with the AMPX-KENO (Refs. 1 and 2) computer package, using both the 27-group SCALE and the 123-group GAM-THERMOS cross-section sets with the NITAWL subroutine for U-238 resonance shielding effects (Nordheim integral treatment). AMPX-KENO has been extensively benchmarked against a number of critical experiments (Refs. 3 through 7), including those most representative of spent fuel storage racks (Refs. 4 and 6). (See Appendix A for benchmark calculations with the 27-group SCALE cross-section library.)

In the geometric model used in KENO, each fuel rod and its cladding were described explicitly. For two-dimensional X-Y analysis, a zero current (white albedo) boundary condition was applied in the axial direction and at the centerline through the outer water space (flux-trap) on all four sides of the cell, effectively creating an infinite array of storage cells. The AMPX-KENO Monte Carlo calculations inherently include a statistical uncertainty due to the random nature of neutron tracking. To minimize the statistical uncertainty of the KENO-calculated reactivity, a total of 50,000 neutron histories is normally accumulated for each calculation, in 100 generations of 500 neutrons each.

Results of benchmark calculations (Ref. 6) with the 123-group cross-section set on a series of appropriate critical experiments indicate a calculational bias of 0, with an uncertainty of ± 0.003 (95% probability at a 95% confidence level). Similar benchmark calculations (Appendix A) with the 27-group SCALE (Ref. 7) cross-section set yielded a calculational bias of 0.0106 ± 0.0048 (95%/95%). AMPX-KENO calculations with the SCALE cross-section



set, however, do not exhibit a trend toward under-prediction with large water gaps that has been identified for the 123-group cross-section set (Ref. 6).

The CASMO-2E computer code, a two-dimensional, multigroup transport theory code for fuel assemblies (Ref. 8), has also been benchmarked (see Appendix A) and is used both as a primary method of analysis and as a means of evaluating small reactivity increments associated with manufacturing tolerances. CASMO-2E benchmarking resulted in a calculational bias of 0.0013 ± 0.0018 (95%/95%). In fuel rack analyses, the higher, hence more conservative, of the reactivity values (including uncertainties) calculated by either CASMO-2E or AMPX-KENO was used for the reference storage cell infinite multiplication factor. In tracking long-term reactivity effects in spent fuel (Region 2 of fuel storage rack), CASMO-2E calculations indicate a small rise (+0.0033 Δk) from decay of short-lived fission products prior to the more pronounced reduction in reactivity due primarily to Pu-241 decay. This small rise has been added to the allowance for uncertainty in CASMO-2E burnup calculations resulting in a net burnup uncertainty of 0.0183 for Region 2 calculations.

A third independent method of analysis, utilizing diffusion/blackness theory, was also used for additional confidence in results of the primary calculational methods, although no reliance for criticality safety is placed on the reactivity value from the diffusion/blackness theory technique. This technique, however, is used for auxiliary calculations of small incremental reactivity effects (e.g., axial cutback or mechanical tolerances) that would otherwise be lost in normal KENO statistical variations, or would be inconsistent with CASMO-2E geometry limitations.

Cross-sections for the diffusion/blackness theory calculations were derived from CASMO-2E or calculated by the NULIF computer



code (Ref. 9) supplemented by a blackness theory routine that effectively imposes a transport theory boundary condition at the surface of the Boraflex neutron absorber. Two different spatial diffusion theory codes, PFQ07 (Ref. 10) in two dimensions and SNEID* in one dimension, were used to calculate reactivities. The two-dimensional PDQ07 code was used to describe the actual storage cell geometry, with NULIF cell-homogenized constants representing each fuel rod and its associated water moderator. SNEID is a one-dimensional model, in cylindrical or slab geometry, used for the calculation of axial cutback reactivity effects and in the study of abnormal occurrences.

4.4.2 Fuel Burnup Calculations

Fuel burnup calculations in the hot operating condition were performed primarily with the CASMO-2E code. The CASMO-2E results were independently confirmed by calculations with the NULIF code (Ref. 9). Figure 4.4 compares the results of the two independent methods of burnup analysis under hot reactor operating conditions. Agreement is good (within 0.008 Δk) although reactivities calculated by CASMO-2E are somewhat higher (more conservative), probably due to differences in treatment of temperature effects and resonance capture. For additional information, burnup-dependent reactivities extracted from a CHEETAH-P (Ref. 11) and an EPRI-CELL (Ref. 12) calculation for a comparable reactor system with essentially the same core nuclear properties are also shown on Fig. 4.4.

* SNEID is a one-dimensional diffusion theory routine developed by Black & Veatch and verified by comparison with PDQ07 one-dimensional calculations.



In addition to depletion calculations under hot-operating conditions, reactivity comparisons under conditions more representative of fuel to be stored in the racks (cold, xenon-free) are also significant in storage rack criticality analyses. Table 4.4 below compares the cold, xenon-free reactivities calculated at 65°C by CASMO-2E and NULIF/PDQ07.

Table 4.4
COMPARISON OF COLD, CLEAN REACTIVITIES CALCULATED
AT 34.5 MWd/kgU BURNUP

Calculational Method	k_{∞} Xe-free @65°C and 34.5 MWd/kgU	
	Fuel Assembly	In Region 2 Cell
CASMO-2E	1.1465	0.9119*
NULIF/PDQ07	1.1471	0.9140

* Maximum CASMO-2E value is 0.915 with bias and uncertainty (Appendix A) added.

No definitive method exists for determining the uncertainty in burnup-dependent reactivity calculations. All of the codes discussed above have been used with accuracy to follow reactivity changes in operating reactors. CASMO-2E has been extensively benchmarked (Appendix A and Ref. 13) against cold, clean, critical experiments (including plutonium-bearing fuel), Monte Carlo calculations, reactor operations, and heavy-element concentrations in irradiated fuel. In particular, the analyses (Ref. 13) of 11 critical experiments with plutonium-bearing fuel showed an average k_{eff} of 1.002 ± 0.011 (95%/95%), showing adequate treatment of the plutonium nuclides.



With fuel of 34.5 MWd/kgU burnup, the total reactivity worth of the fission products (excluding Xe) is estimated to be 8.4% Δk (by differential NULIF/PDQ07 calculations). Assuming the fission product reactivity worth is accurate to $\pm 5\%$, the uncertainty in k_{∞} would be $\pm 0.004 \Delta k$. Statistically combined with the uncertainty derived from the analysis of Pu-bearing critical experiments, the total uncertainty becomes ± 0.0117 . Long-term decay calculations with CASMO-2E (cold, xenon-free) indicate a very small rise in reactivity (0.0033 Δk) immediately after shutdown (see Section 4.4.3), which has been added to the uncertainty in burnup calculations. In addition, due to the possible existence of a small positive reactivity increment from the axial distribution in burnup (see Section 4.4.4), the uncertainty was increased to 0.018 Δk in Region 2 (34.5 MWd/kgU fuel) and treated as an additive term for the present evaluation, rather than being combined statistically with other uncertainties. This is believed to be a conservative estimate, particularly in view of the substantial reactivity decrease with aged fuel as discussed in Section 4.4.3. Although the uncertainty at lower burnups associated with fuel of lower initial enrichment would normally be expected to be less, this refinement has not been made and the same uncertainty (0.018 Δk) has been assigned to the Region 2 storage cells independent of initial enrichment.

4.4.3 Long-term Decay

Since the fuel racks in Region 2 are intended to contain spent fuel for long periods of time, calculations were made using CASMO-2E* to follow the long-term changes in reactivity of

* CASMO-2E tracks the decay and burnup dependence of 22 separate fission products in 12 chains accounting for more than 90% of the total fission product absorption. (The remainder is accommodated by two pseudo-fission products.)



spent fuel over a 30-year period. Early in the decay period (with xenon removed), decay of short-lived radionuclides results in a small (0.0033 Δk extrapolated) increase in reactivity, although for longer storage periods the decay of Pu-241 (13-year half life) substantially reduces reactivity. These effects are illustrated in Fig. 4.5 and listed in Table 4.5. The reference design criticality calculations do not take credit for this long-term reduction in reactivity, other than to indicate an increasing subcriticality margin in Region 2 of the spent fuel storage pool.

Table 4.5
LONG-TERM CHANGES IN REACTIVITY IN STORAGE RACK
(XENON-FREE)

Storage Time, years	Δk from Shutdown (Xenon-free)		
	2.5%E @11.53 MWd/kgU	3.6%E @24.76 MWd/kgU	4.5%E @34.5 MWd/kgU
0.5	+0.0028	+0.0027	+0.0028
1.0	+0.0024	+0.0019	+0.0018
4.0	-0.0001	-0.0039	-0.0050
10.0	-0.0050	-0.0143	-0.0181
30.0	-0.0148	-0.0348	-0.0434

4.4.4 Effect of Axial Burnup Distribution

Initially, fuel loaded into the reactor will burn with a slightly skewed cosine power distribution. As burnup progresses, the burnup distribution will tend to flatten, becoming more highly burned in the central regions than in the upper and lower ends. This effect may be clearly seen in the curves compiled in



Reference 14. At high burnup, the more reactive fuel near the ends of the fuel assembly (less than average burned) occurs in regions of lower reactivity worth due to neutron leakage. Consequently, it is expected that distributed burnup fuel assemblies would exhibit a slightly lower reactivity than that calculated for the average burnup. As burnup progresses, the distribution, to some extent, tends to be self-regulating as controlled by the axial power distribution, precluding the existence of large regions of significantly reduced burnup (unless isolated individual assemblies may be locally perturbed by the long-term insertion of control rods).

To investigate the potential reactivity effect of the axial burnup distribution in spent fuel, the calculated burnup distribution in Turkey Point fuel (cycle 4, average burnup of 29 MWd/kgU), as given in Reference 15, was used as a basis for evaluation (see Fig. 4.6). In one-dimensional diffusion theory calculations (CASMO-2E-derived, homogenized diffusion constants for fuel of different burnups in Region 2 cells), the distributed enrichment case showed a lower reactivity ($-0.013 \Delta k$) than the reference reactivity for the average burnup.

A second and more conservative estimate was made using the experimentally derived burnup (see Fig. 4.7) in a fuel assembly (Ref. 16) removed from the H.B. Robinson reactor (similar to the Diablo Canyon Power Plant). With this distribution, the axially distributed burnup case exhibited a slightly higher reactivity ($+0.0033 \Delta k$) than the uniform average burnup case. Although this may be unique to the particular Robinson fuel assembly, or to experimental uncertainty in determining the actual fuel burnup, the results indicate the possibility of a small positive reactivity effect due to the axial distribution in burnup. This potential for a positive reactivity effect was considered in establishing a reactivity uncertainty ($0.0183 \Delta k$), as discussed in Section 4.4.2 above and listed in the summary, Table 4.1.



4.5 REGION 1 CRITICALITY ANALYSIS AND TOLERANCE VARIATIONS

4.5.1 Nominal Design Case

Under normal conditions, with nominal dimensions, the k_{∞} values calculated by the four methods of analysis are as follows:

<u>Analytical Method</u>	<u>Bias-corrected k_{∞}</u>	<u>Maximum k_{∞} (95%/95%)</u>
CASMO-2E	0.9117 \pm 0.0018	0.9135
27-group AMPX-KENO	0.9011 \pm 0.0075	0.9086
123-group AMPX-KENO	0.9059 \pm 0.0071	0.9130
Diffusion-blackness theory	0.9078	0.9078

The AMPX-KENO calculations include a one-sided tolerance factor (Ref. 17) of 1.799 corresponding to 95% probability at a 95% confidence level. For the nominal design case, the CASMO-2E calculation yields the highest (most conservative) reactivity and is, therefore, used as the reference reactivity.

4.5.2 Boron Loading Variation

The Boraflex absorber plates used in Region 1 storage cells are nominally 0.047-inch thick, with a B-10 areal density of 0.0148 g/cm². Independent manufacturing tolerance limits are ± 0.007 inch thick and ± 0.0007 g/cm² in B-10 content. This assures that at any point where the minimum boron loading (0.0141 gram B-10/cm²) and minimum Boraflex thickness (0.040 inch) may coincide, the boron areal density will not be less than 0.012 gram B-10/cm². Differential CASMO-2E calculations indicate that these tolerance limits result in an incremental reactivity



uncertainty of $\pm 0.0013 \Delta k$ for boron content and ± 0.0064 for Boraflex thickness variations.

4.5.3 Storage Cell Lattice Pitch Variation

The design storage cell lattice spacing between fuel assemblies in Region 1 is 10.93 ± 0.050 inches. A decrease in storage cell lattice spacing may or may not increase reactivity depending upon other dimensional changes that may be associated with the decrease in lattice spacing. Decreasing lattice spacing by decreasing the outer (flux-trap) water thickness increases reactivity. However, increasing the inner water thickness (between the fuel and the inner stainless steel box) results in a small increase in reactivity. The reactivity effect of the outer (flux-trap) water thickness, however, is more significant. Both of these effects have been evaluated for independent design tolerances.

The inner stainless steel box dimension, 8.850 ± 0.032 inches, defines the inner water thickness between the fuel and the inside of the box. For a tolerance limit of ± 0.031 inch, the uncertainty in reactivity is $\pm 0.0008 \Delta k$ as determined by differential CASMO-2E calculations, with k_{∞} increasing as the inner stainless steel box dimension (and derivative lattice spacing) increases.

The design outer (flux-trap) water thickness is 1.786 ± 0.050 inches, which results in an uncertainty of $\pm 0.0029 \Delta k$ due to the tolerance in flux-trap water thickness, assuming the water thickness is simultaneously reduced on all four sides. Since the manufacturing tolerances on each of the four sides are statistically independent, the actual reactivity uncertainties would be less than ± 0.0029 , although the more conservative value has been used in the criticality evaluation.



4.5.4 Stainless Steel Thickness Tolerances

The nominal stainless steel thickness in Region 1 is 0.080 inch for the inner stainless steel box and 0.020 inch for the Boraflex coverplate (0.125 inch on module boundary). The maximum positive reactivity effect of the expected stainless steel thickness tolerance variations, statistically combined, was calculated (CASMO-2E) to be $\pm 0.0018 \Delta k$.

4.5.5 Fuel Enrichment and Density Variation

The design maximum enrichment is 4.50 ± 0.02 wt% U-235. Calculations of the sensitivity to small enrichment variations by CASMO-2E yielded a coefficient of $0.0053 \Delta k$ per 0.1 wt% U-235 at the design enrichment. For a tolerance on U-235 enrichment of ± 0.02 in wt%, the uncertainty on k_{∞} is $\pm 0.0011 \Delta k$.

Calculations were made with the UO_2 fuel density increased to a maximum value of 97% theoretical density (TD). For the mid-range value (95% TD) used for the reference design calculations, the uncertainty in reactivity is $\pm 0.0029 \Delta k$ over the range of UO_2 densities expected.

4.5.6 Boraflex Width Tolerance Variation

The reference storage cell design for Region 1 (Fig. 4.2) uses a Boraflex blade width of 7.9375 ± 0.0625 inches. A positive increment in reactivity occurs for a decrease in Boraflex absorber width. For a reduction in width of the maximum tolerance, 0.0625 inch, the calculated positive reactivity increment is $+0.0006 \Delta k$.

4.5.7 Axial Cutback of Boraflex

The axial length of the Boraflex poison material is less than the active fuel length by 3 inches at the top and at the bottom



of the Region 1 storage rack modules. To account for the reactivity effect of this axial cutback, one-dimensional (slab) diffusion theory calculations were made using flux-weighted homogenized diffusion theory constants edited from PDQ07 calculations of the array of storage cells, with and without Boraflex present. In the one-dimensional calculations, an infinite (30 cm) water reflector was used above and below the fuel assembly, with the lengths of the unpoisoned "cutback" regions, top and bottom, varied in a series of parametric calculations. Results of these calculations showed that the k_{eff} remains less than the reference k_{∞} of the reference central storage cell region, until the axial cutback exceeds 4 inches top and bottom. Thus, the actual axial neutron leakage more than compensates for the 3-inch design cutback and the reference infinite multiplication factor (k_{∞}) remains a conservative overestimate of the true reactivity.

4.6 REGION 2 CRITICALITY ANALYSIS AND TOLERANCE VARIATIONS

4.6.1 Nominal Design Case

CASMO-2E calculations in Region 2, with fuel burned to 34.5 MWD/kgU in the reference design storage cell at a reference temperature of 65°C, yielded a k_{∞} of 0.9119. Iterative CASMO-2E calculations with fresh fuel of varying enrichments resulted in an enrichment of 1.743 wt% U-235 yielding the same k_{∞} value. AMPX-KENO calculations were then made on fresh fuel of 1.743% enrichment, yielding bias-corrected k_{∞} values of 0.9064 ± 0.0050 (95% probability at a 95% confidence level) and 0.8929 ± 0.0050 , respectively, for the 27-group and 123-group calculations. Compared to AMPX-KENO, the CASMO-2E calculation yields the highest (most conservative) k_{∞} value (0.9119) and is, therefore, taken as the reference reactivity in the Region 2 storage cells. The 123-group AMPX-KENO calculation is known (Ref. 6) to underpredict reactivity when large water gaps are present.



Subsequently, iterative burnup and storage cell calculations were made with CASMO-2E for fuel of varying initial enrichments (4.3%, 3.6%, 3.0%, and 2.5%), in each case searching for the burnup which gave the same k_{∞} as the reference fuel at 34.5 MWd/kgU. These converged burnup values are those shown in Fig. 4.1 and listed in Table 4.6. At the design basis burnup (34.5 MWd/kgU), the sensitivity to burnup is calculated to be $-0.0066 \Delta k$ per MWd/kgU.

The reference temperature for Region 2 was taken as 65°C. However, for a full core discharge, the maximum temperature is conservatively projected (Section 5, Table 5.2, p. 5-8) to increase to 78.6°C (173.4°F). At this temperature, the maximum reactivity including uncertainties is calculated to be 0.941 (see data in Section 4.7.1) in the absence of soluble poison. Thus, the spent fuel racks can safely accept a full core discharge without exceeding the limiting k_{eff} value of 0.95.

4.6.2 Storage Cell Lattice Pitch Variations

The design storage cell lattice spacing between fuel assemblies in Region 2 is 10.929 ± 0.051 inches. In unpoisoned racks, increasing the lattice spacing reduces the reactivity, regardless of whether the increase is in the inner or the outer (flux-trap) water thickness. However, the reactivity uncertainty of the tolerances on the stainless steel box inside dimension and on the lattice pitch has been independently evaluated.

The inner stainless steel box dimension, 8.850 ± 0.032 inches, defines the inner water thickness between the fuel and the inside of the box. For the tolerance limit of ± 0.032 inch, the uncertainty in reactivity at the reference pitch is $\pm 0.0002 \Delta k$ as determined by differential CASMO-2E calculations.



Table 4.6

FUEL BURNUPS FOR EQUAL REACTIVITY VALUES WITH FUEL OF DIFFERENT INITIAL ENRICHMENTS

Initial Enrichment	Burnup for k_{∞} of 0.9119
4.5 (reference design)	34.5
4:3	32.467
3.6	24.755
3.0	17.673
2.5	11.534
1.743	0

The outer water thickness is nominally 1.899 inches, and the manufacturing tolerance of ± 0.051 inch directly affects the lattice pitch. For the stated tolerance, the uncertainty in reactivity is $\pm 0.0041 \Delta k$.

4.6.3 Stainless Steel Thickness Tolerance

The nominal thickness of the stainless steel box wall is 0.090 inch with a tolerance limit of ± 0.005 inch, resulting in an uncertainty in reactivity of $\pm 0.0028 \Delta k$. Increasing the stainless steel box wall thickness reduces reactivity.

4.6.4 Fuel Enrichment and Density Variation

Uncertainties in reactivity due to tolerances on fuel enrichment and UO_2 density in Region 2 are assumed to be the same as those determined for Region 1.

4.6.5 Eccentric Positioning of Fuel Assembly in Storage Rack

The fuel assembly is normally located in the center of the storage rack cell with bottom fittings and spacers that mechanically limit lateral movement of the fuel assemblies. Nevertheless, calculations were made with the fuel assemblies



moved into the corner of the storage rack cell (four-assembly cluster at closest approach). In Regions 1 and 2, these calculations indicated that the reactivity increase slightly, as determined by PDQ07 calculations with diffusion coefficients* generated by NULIF and a blackness theory routine. The calculated positive reactivity increments were 0.0010 in Region 1 and 0.0020 in Region 2.

4.7 ABNORMAL AND ACCIDENT CONDITIONS

4.7.1 Temperature and Water Density Effects

The temperature coefficient of reactivity in Region 1 is negative and a temperature of 0°C, with a water density of 1.0, was assumed for the reference design, which assures that the true reactivity will always be lower, regardless of temperature. In Region 2, the temperature coefficient of reactivity is positive in the temperature range to which the racks are routinely exposed. For this reason, a design basis temperature of 65°C was assumed for the criticality evaluation in Region 2, being slightly above the highest temperature (64°C) expected during partial core discharge refueling operations. Temperatures above 65°C can result from full core discharge or accident conditions, although the soluble poison actually present would assure that the reactivity is maintained less than the limiting value.

Temperature effects on reactivity have been calculated and the results are shown in Table 4.7. Introducing voids in the water internal to the storage cell (to simulate boiling) decreased

* This calculational approach was necessary since the reactivity effects are too small to be calculated by KENO, and CASMO-2E geometry is not readily amenable to eccentric positioning of a fuel assembly.



Table 4.7

EFFECT OF TEMPERATURE AND VOIDS ON CALCULATED
REACTIVITY OF STORAGE RACK

Case	Incremental Reactivity Change, Δk	
	Region 1	Region 2
0°C	Reference	
20°C	-0.0028	-0.0114
40°C	-0.0074	-0.0069
65°C		Reference
80°C	-0.0174	(+0.0034)*
90°C		+0.0056
120°C	-0.0304	+0.0137
120°C + 20% void	-0.0951	-0.0061

* Interpolated

reactivity, as shown in the table. Voids due to boiling will not occur in the outer (flux-trap) water region.

With soluble poison present, the temperature coefficients of reactivity would be expected to differ from those inferred from the data in Table 4.7. However, the reactivities would also be substantially lower at all temperatures with soluble boron present, and the data in Table 4.7 are pertinent to the higher-reactivity unborated case.

The data in Table 4.7 may be used to infer a temperature of 114°C (237°F) at which the reactivity, without credit for soluble poison, has increased to the 0.95 k_{∞} design limit. Local boiling, with a negative coefficient of reactivity, will begin near the top of the fuel at a temperature of approximately 116°C (240°F). Thus, it is concluded that credible temperature increases will not result in exceeding the reactivity limit in the absence of soluble poison, and the soluble poison actually present provides further assurance of a low reactivity for all temperatures and heat load conditions.



4.7.2 Dropped Fuel Assembly Accident

To investigate the possible reactivity effect of a postulated fuel assembly drop accident, calculations were made for unpoisoned assemblies separated only by water. Figure 4.8 shows the results of these calculations. From these data, the reactivity (k_{∞}) will be less than 0.95 for any water gap spacing greater than ~5 inches in the absence of any absorber material, other than water, between assemblies. For a drop on top of the rack, the fuel assembly will come to rest horizontally on top of the rack with a minimum separation distance of >12 inches. Maximum expected deformation under seismic or accident conditions will not reduce the minimum spacing between fuel assemblies to less than 12 inches. Consequently, fuel assembly drop accidents will not result in an increase in reactivity above that calculated for the infinite nominal design storage rack. Furthermore, soluble boron in the pool water would substantially reduce the reactivity and assure that the true reactivity is always less than the limiting value for any conceivable fuel handling accident.

4.7.3 Abnormal Location of a Fuel Assembly

For the abnormal condition of a misplaced fuel assembly, credit for the soluble poison present in the fuel pool water is taken to ensure a k_{∞} of less than 0.95. This includes the cases where either a fresh unirradiated fuel assembly of 4.5% enrichment is positioned outside of and adjacent to a storage rack module, or an assembly with less than the required burnup (including a fresh unirradiated assembly) is loaded into a Region 2 storage cell. Soluble poison (approximately 2000 ppm boron) is present in the spent fuel pool water (for which credit is permitted under these conditions) and would maintain the reactivity substantially less than the design limitation. Administrative procedures are used to confirm and assure the continued presence of soluble poison in



the spent fuel pool water to assure the limiting reactivity ($k_{\text{eff}} = 0.95$) will not be exceeded. Strict administrative controls will assure that fuel assemblies are not inadvertently loaded into the wrong regions of the fuel racks.

4.7.4 Lateral Rack Movement

Lateral motion of the rack modules under seismic conditions could potentially alter the spacing between rack modules. However, the bottom plate and upper girdle bar assembly limit lateral movement to a minimum flux-trap water gap spacing of 1.75 inches. Lift-off during a seismic event is not sufficient for the support plate of one module to ride up and over that of an adjacent module. At a minimum water gap spacing of 1.75 inches between modules, the reactivity (k_{eff}) remains less than 0.95 even in the absence of soluble poison. In addition, the presence of soluble poison provides further assurance that the reactivity is always less than the design limitation.



REFERENCES TO SECTION 4.

1. Green, Lucious, Petrie, Ford, White, Wright, "PSR-63/AMPX-1 (code package), AMPX Modular Code System for Generating Coupled Multigroup Neutron-Gamma Libraries from ENDF/B," ORNL-TM-3706, Oak Ridge National Laboratory, March 1976.
2. L. M. Petrie and N. F. Cross, "KENO-IV, An Improved Monte Carlo Criticality Program," ORNL-4938, Oak Ridge National Laboratory, November 1975.
3. S. R. Bierman et al., "Critical Separation Between Subcritical Clusters of 4.29 wt% U²³⁵ Enriched UO₂ Rods in Water with Fixed Neutron Poisons," NUREG/CR-0073, Battelle Pacific Northwest Laboratories, May 1978, with errata sheet issued by the USNRC, August 14, 1979.
4. M. N. Baldwin et al., "Critical Experiments Supporting Close Proximity Water Storage of Power Reactor Fuel," BAW-1484-7, The Babcock & Wilcox Company, July 1979.
5. R. M. Westfall and J. R. Knight, "Scale System Cross-section Validation with Shipping-cask Critical Experiments," ANS Transactions, Vol. 33, p. 368, November 1979.
6. S. E. Turner and M.K. Gurley, "Evaluation of AMPX-KENO Benchmark Calculations for High Density Spent Fuel Storage Racks," Nuclear Science and Engineering, 80(2): 230-237, February 1982.
- 7.a. R. M. Westfall et al., "SCALE: A Modular Code System for Performing Standardized Computer Analyses for Licensing Evaluation," NUREG/CR-0200, 1979.
b. A. M. Hathout, R. M. Westfall, and H. L. Dodds, "Validation of Three Cross-section Libraries Used with the SCALE System for Criticality Safety Analysis," NUREG/CR-1917, June 1981.
- 8.a. A. Ahlin and M. Edenius, "CASMO - A Fast Transport Theory Depletion Code for LWR Analysis," ANS Transactions, Vol. 26, p. 604, 1977.
b. "CASMO-2E Nuclear Fuel Assembly Analysis, Application Users Manual," Rev. A, Control Data Corporation, 1982.
- 9.a. W. A. Wittkopf, "NULIF - Neutron Spectrum Generator, Few-Group Constant Generator and Fuel Depletion Code," BAW-426, The Babcock & Wilcox Company, August 1976.



REFERENCES TO SECTION 4 (Continued)

- b. J. J. Woods et al., "Comparison of Core Physics Calculations with Measurements," BAW-10120P, The Babcock & Wilcox Company, March 1978.
- 10. W. R. Cadwell, "PDQ-7 Reference Manual," WAPD-TM-678, Bettis Atomic Power Laboratory, January 1967.
- 11.a. "NAI Modified LEOPARD, Rev. 2," NAI Report 71-13 (Proprietary), Nuclear Associates International Corporation, December 10, 1973.
- b. "CHEETAH-P Report Module Within the LEAHS Nuclear Fuel Management and Analysis Package," Publication No. 84004100 (Proprietary), Nuclear Associates International Corporation, July 1974.
- 12. W. J. Eich, "Advanced Recycle Methodology Program, CEM-3," Electric Power Research Institute, 1976.
- 13.a. E. E. Pilat, "Methods for the Analysis of Boiling Water Reactors (Lattice Physics)," YAEC-1232, Yankee Atomic Electric Company, December 1980.
- b. M. Edenius et al., "CASMO Benchmark Report," Studsvik/RF-78/6293, Aktiebolaget Atomenergi, March 1978.
- 14. H. Richings, "Some Notes on PWR (W) Power Distribution Probabilities for LOCA Probabilistic Analyses," NRC Memorandum to P.S. Check, dated July 5, 1977.
- 15. R. B. Davis, "Pre-test Nondestructive Examination Data Summary Report on Turkey Point Spent Fuel Assemblies D01, D04, and D06 for the CLIMAX - Spent Fuel Test," HEDL-TME-80-83, Hanford Engineering Development Laboratory, January 1981.
- 16. R. A. Lorenz et al., "Fission Product Release from Highly Irradiated LWR Fuel," NUREG/CR-0722, February 1980.
- 17. M. G. Natrella, Experimental Statistics, National Bureau of Standards, Handbook 91, August 1963.



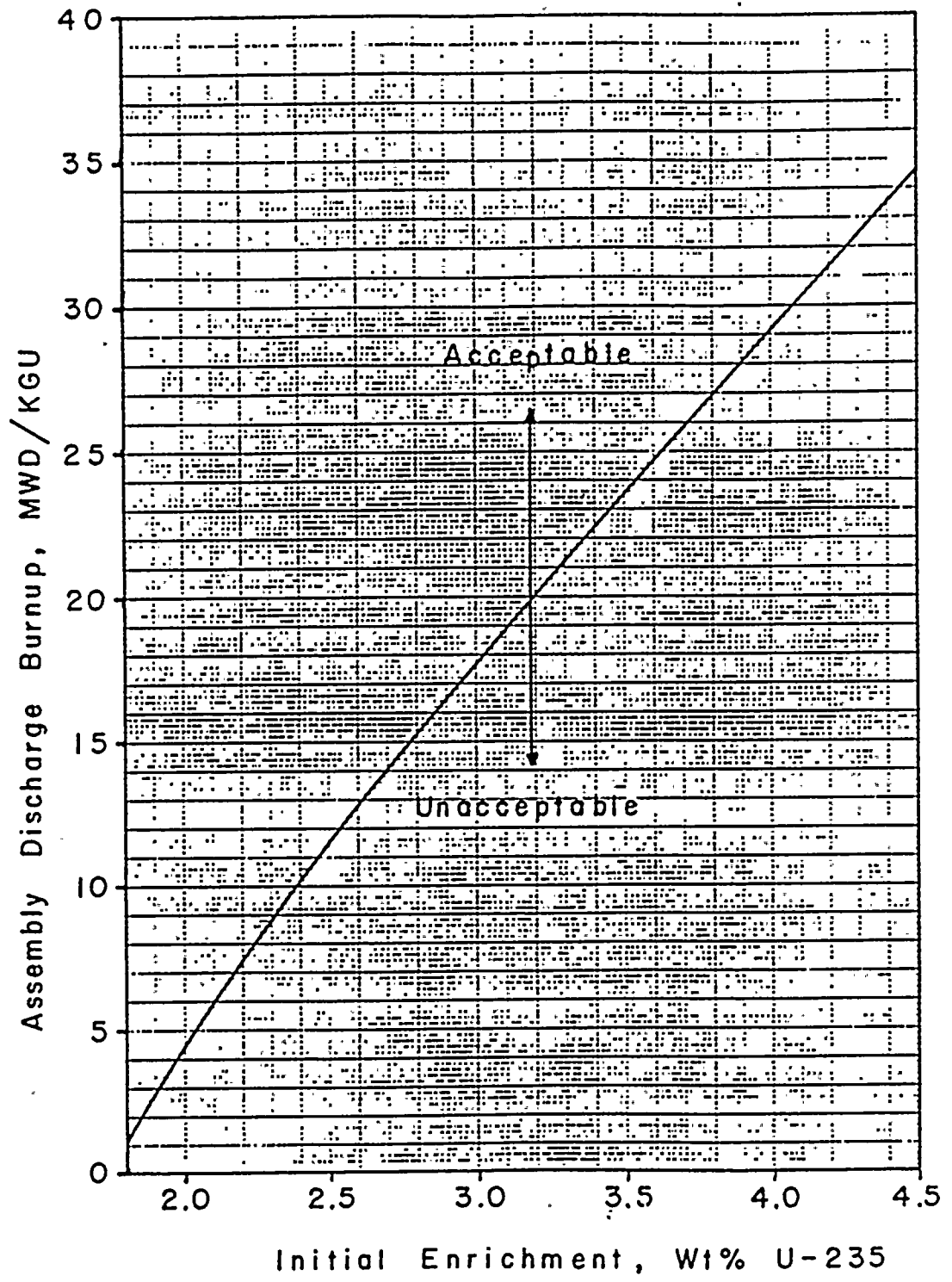


FIGURE 4.1 Acceptable Burnup Domain In Region 2 Of Diablo Canyon Spent Fuel Storage Racks



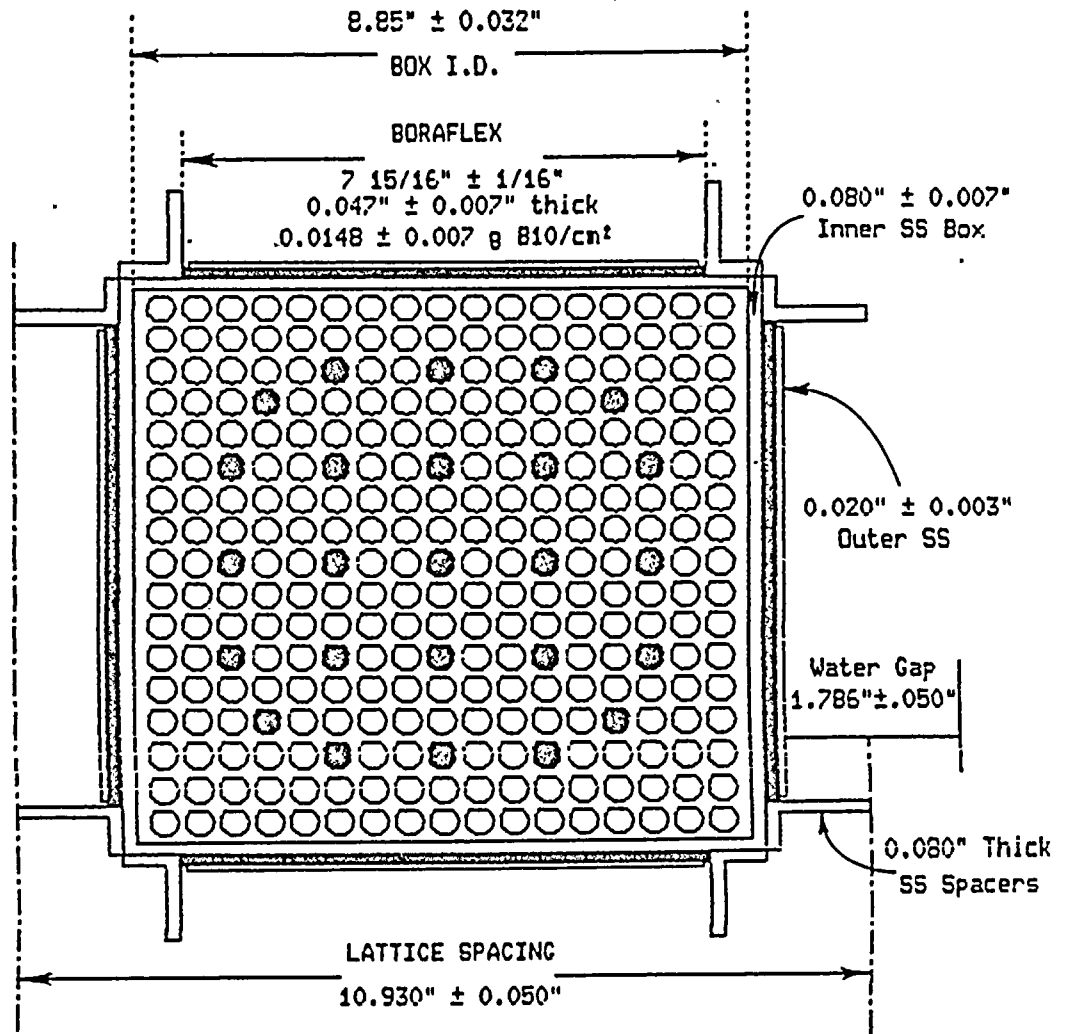


FIGURE 4.2 Configuration Of Region 1 Spent Fuel Storage Cell



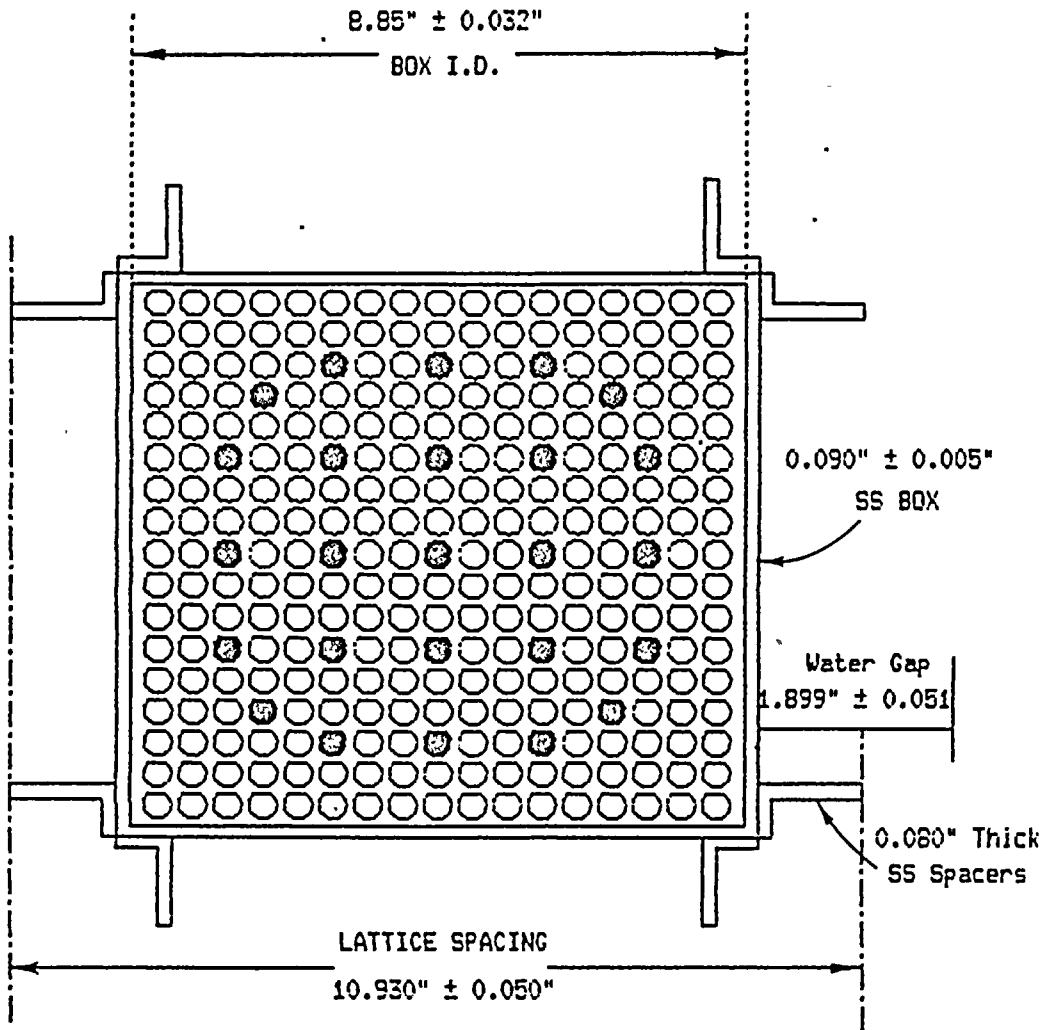


FIGURE 4.3 Configuration Of Region 2 Spent Fuel Storage Cell



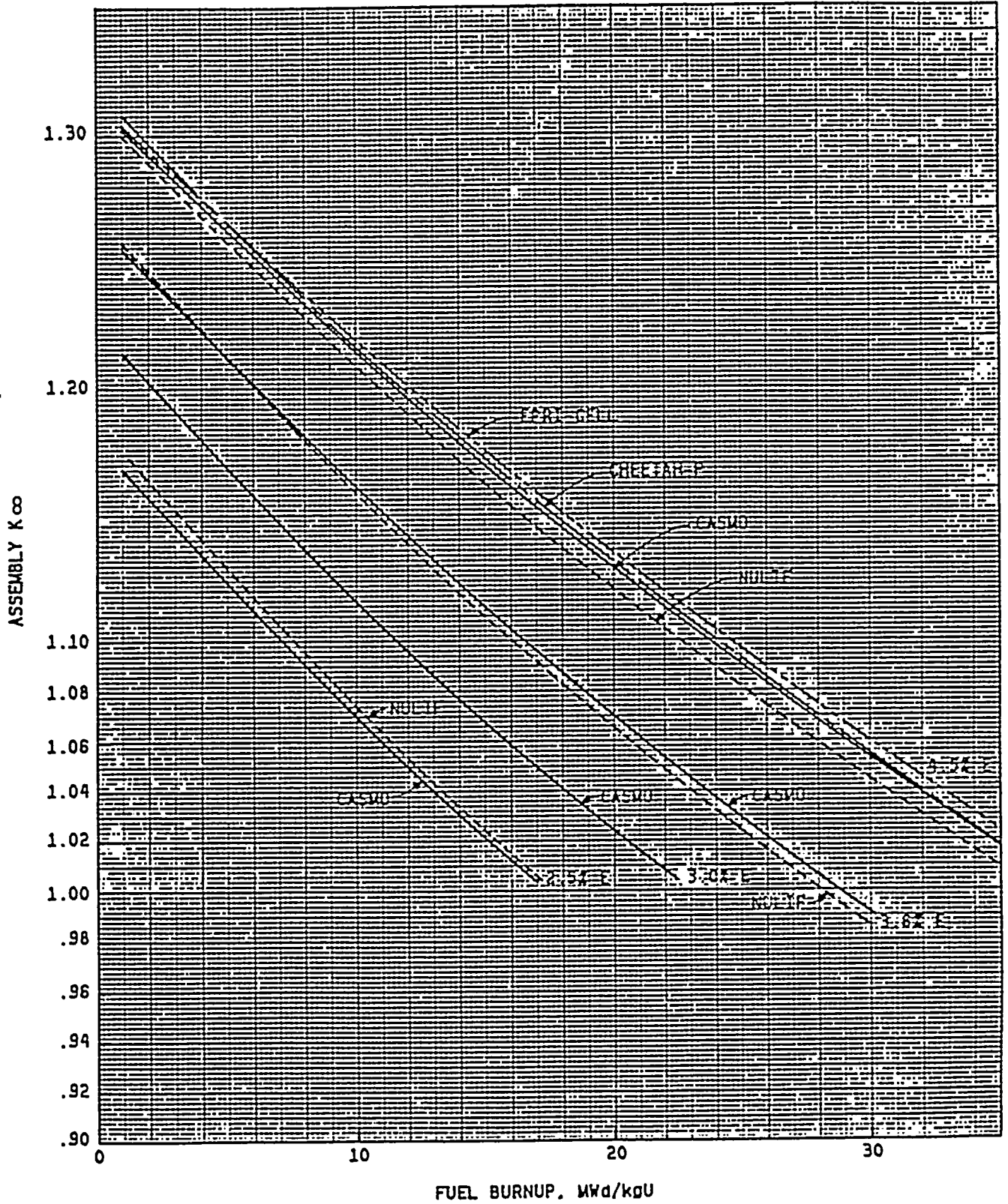


FIGURE 4.4 Time-dependent Reactivity Of Fuel Assemblies For Fuel Of Several Initial Enrichments



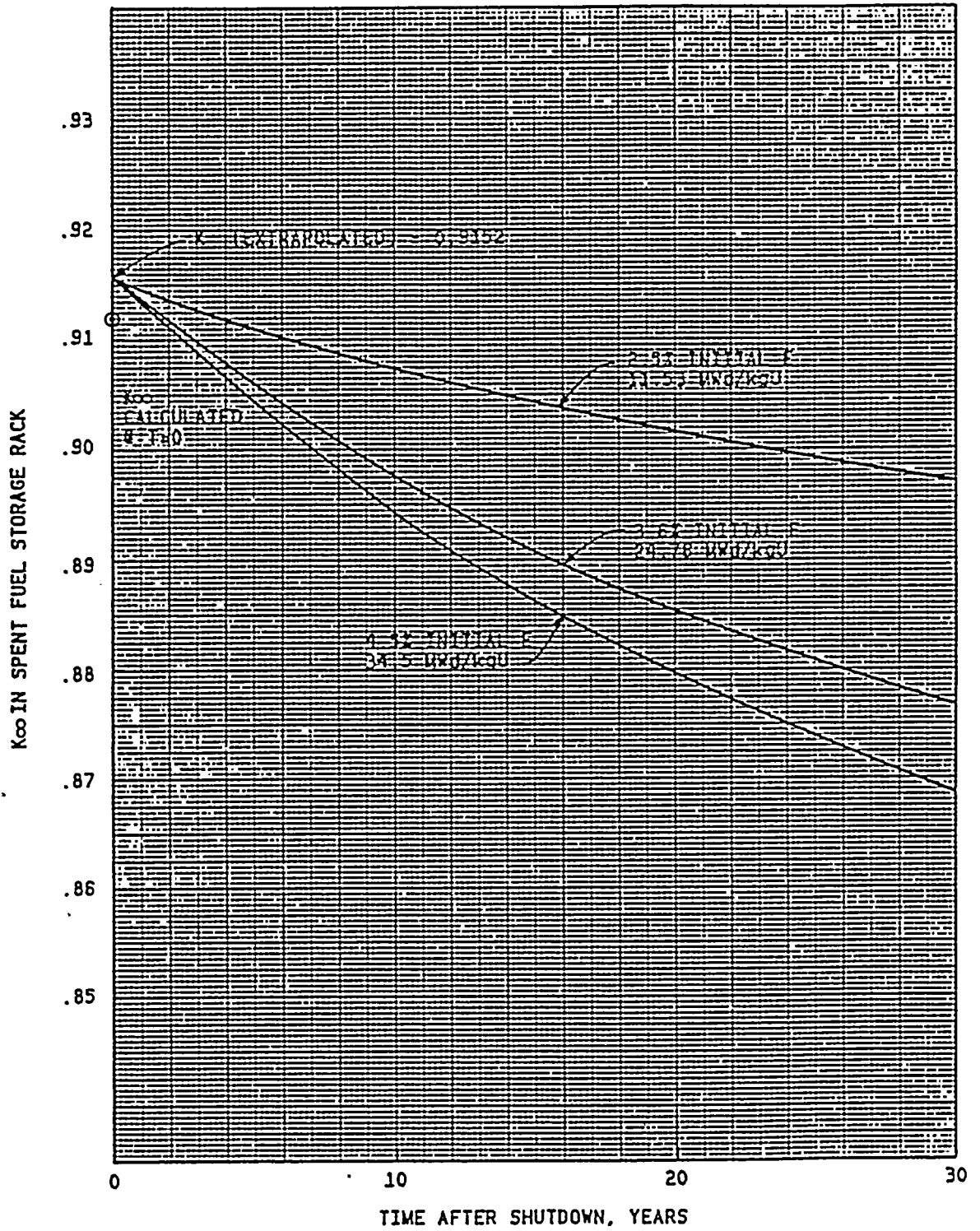


FIGURE 4.5 Effect Of Long-term Storage On Reactivity (k_{∞}) Of Spent Fuel Storage Rack



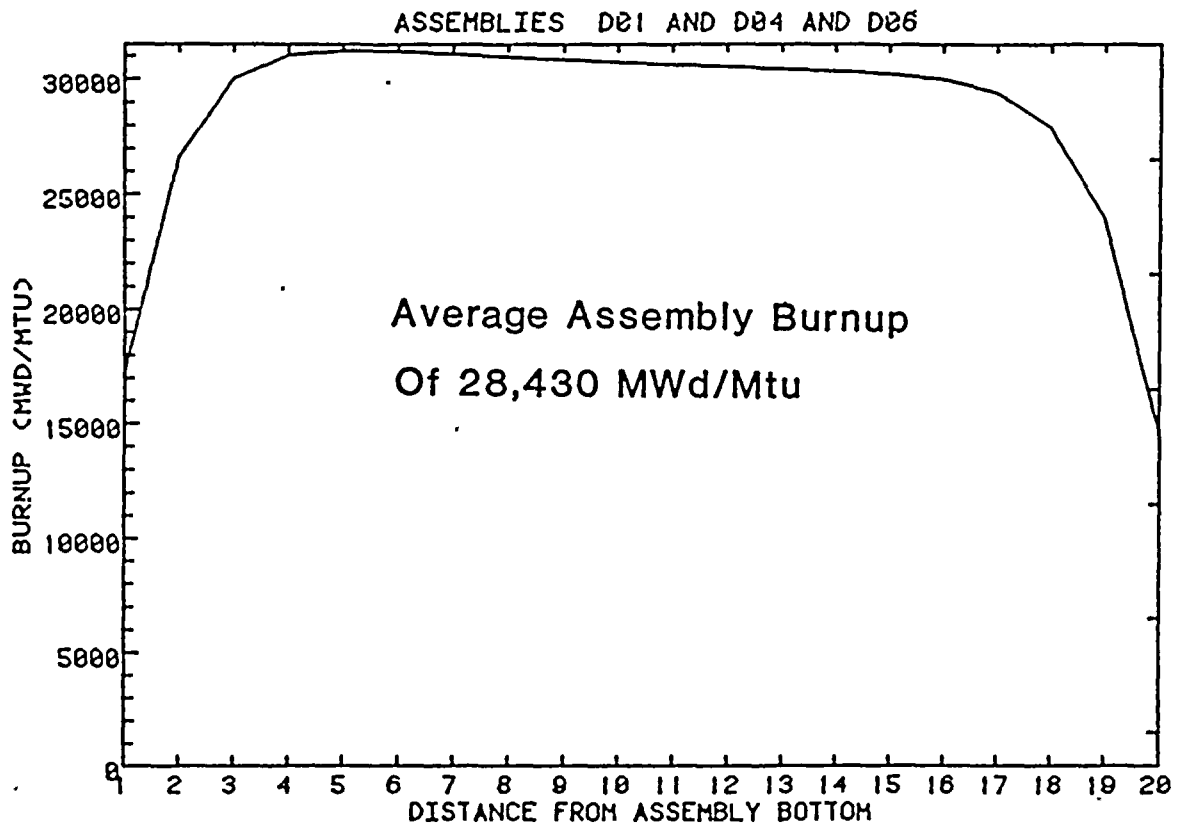


FIGURE 4.6 Axial Burnup Distribution (calculated) For Turkey Point Fuel (From HEDL-TME-80-83)



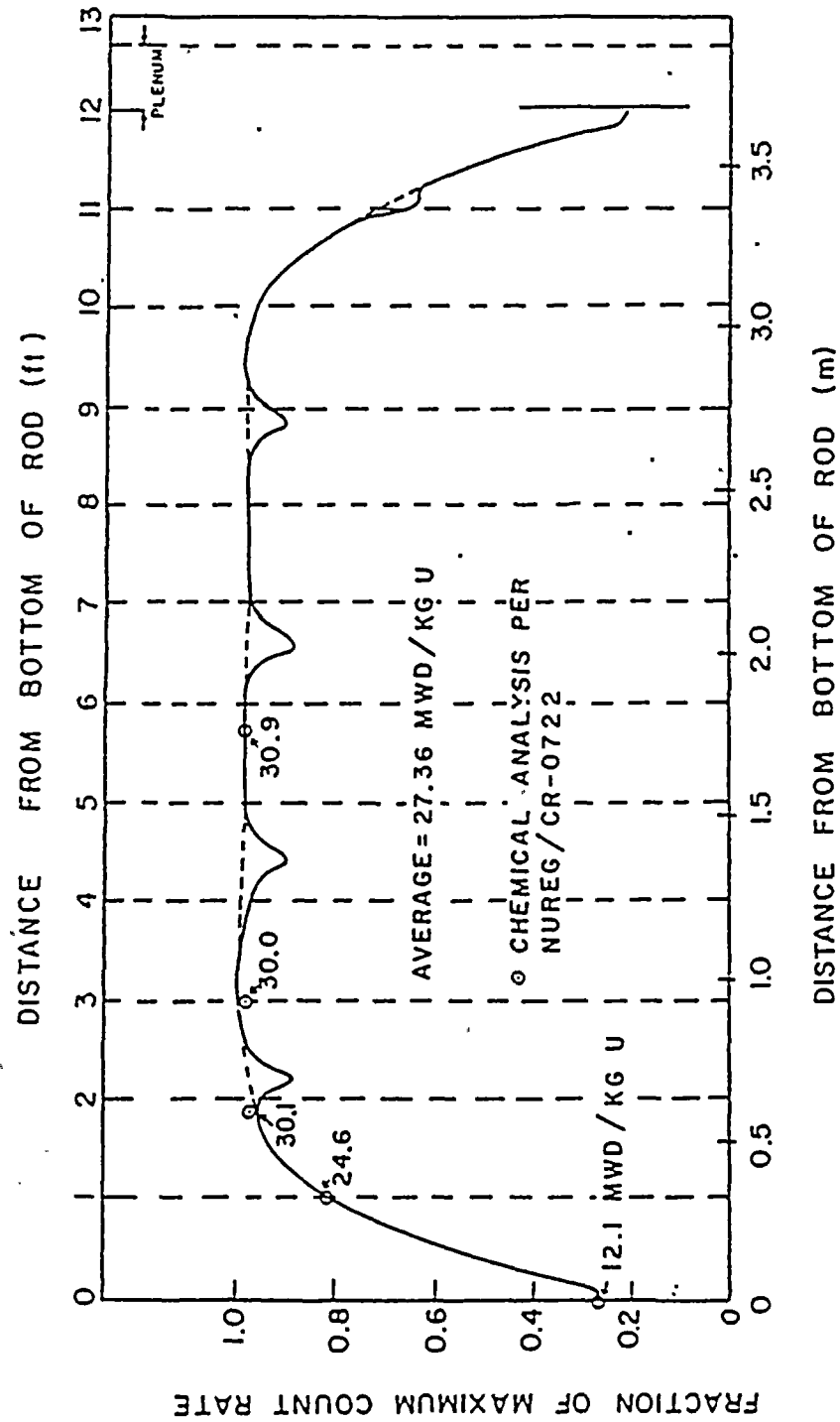


FIGURE 4.7 Relative Axial Burnup Distribution From H. B. Robinson Fuel
(From NUREG/CR-0722)



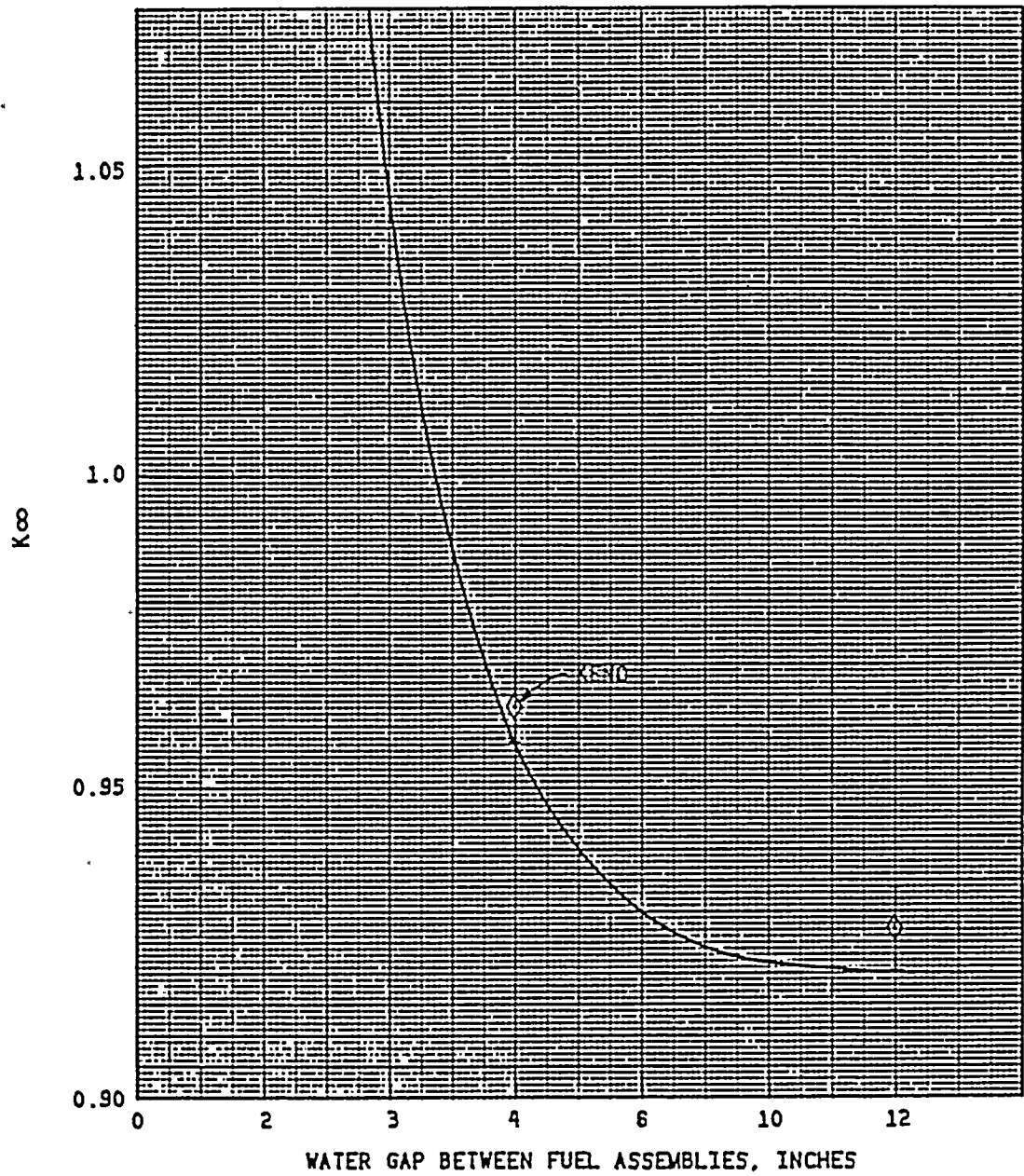


FIGURE 4.8 Reactivity Effect Of Water Spacing Between Fuel Assemblies



APPENDIX A

BENCHMARK CALCULATIONS



1. INTRODUCTION AND SUMMARY

The objective of this benchmarking study is to verify both the AMPX (NITAWL)-KENO (Ref. 1) methodology with the 27-group SCALE cross-section library (Ref. 2) and the CASMO-2E code (Ref. 3) for use in criticality calculations of high density spent fuel storage racks. Both calculational methods are based on transport theory and have been benchmarked against critical experiments that simulate typical spent fuel storage rack designs as realistically as possible. Results of these benchmark calculations with both methodologies are consistent with corresponding calculations reported in the literature and with the requirements of Regulatory Guide-3.41,* Rev. 1, May 1977.

Results of these benchmark calculations show that the 27-group (SCALE) AMPX-KENO calculations consistently underpredict the critical eigenvalue by $0.0106 \pm 0.0048 \Delta k$ (with a 95% probability at a 95% confidence level) for critical experiments selected to be representative of realistic spent fuel storage rack configurations and poison worths. Similar calculations by Westinghouse suggest a bias of 0.012 ± 0.0023 , and the results of ORNL analyses of 54 relatively "clean" critical experiments show a bias of 0.0100 ± 0.0013 .

Similar calculations with CASMO-2E for clean critical experiments resulted in a bias of 0.0013 ± 0.0018 (95%/95%). CASMO-2E and AMPX-KENO intercomparison calculations of infinite arrays of poisoned cell configurations show very good agreement and suggest that a bias of 0.0013 ± 0.0018 is the reasonably expected bias and uncertainty for CASMO-2E calculations.

* Validation of Calculational Methods for Nuclear Criticality Safety. (See also ANSI N16.9-1975.)



The benchmark calculations reported here indicate that either the 27-group (SCALE) AMPX-KENO or CASMO-2E calculations are acceptable for criticality analysis of high density spent fuel storage racks. The preferred methodology, however, is to perform independent calculations with both code packages and to utilize the higher, more conservative value for the reference design infinite multiplication factor.

2. AMPX (NITAWL)-KENO BENCHMARK CALCULATIONS

Analysis of a series of Babcock & Wilcox (B&W) critical experiments (Ref. 4), which include some with absorber plates typical of a spent fuel rack, is summarized in Table 1 as calculated with AMPX-KENO using the 27-group SCALE cross-section library and the Nordheim resonance integral treatment in NITAWL. The mean (and standard deviation of the mean) for these calculations is 0.9894 ± 0.0019 . With a one-sided tolerance factor ($K = 2.502$), corresponding to 95% probability at a 95% confidence level (Ref. 5), the calculational bias is $+0.0106$ with an uncertainty of ± 0.0048 .

Similar calculational deviations reported by Westinghouse (Ref. 6) are also shown in Table 1 and suggest a bias of 0.012 ± 0.0023 (95%/95%). In addition, ORNL (Ref. 7) has analyzed some 54 critical experiments using the same methodology, obtaining a mean bias of 0.0100 ± 0.0013 (95%/95%). These published results are in good agreement with the results obtained in the present analysis and lend further credence to the validity of the 27-group AMPX-KENO calculational model for use in criticality analysis of high density spent fuel storage racks. Variance analysis of the data in Table 1 suggests the possibility that an unknown factor may be causing a slightly larger variance than might be expected from the Monte Carlo statistics alone. However, such a factor, if one truly exists, is too small to be resolved on the basis of critical-experiment data presently



Table 1

RESULTS OF 27-GROUP (SCALE) AMPX-KENO CALCULATIONS
OF B&W CRITICAL EXPERIMENTS

Experiment Number	Calculated k_{eff}	σ	Westinghouse Calculated-meas. k_{eff}
I	0.9889	± 0.0049	-0.008
II	1.0040	± 0.0037	-0.012
III	0.9985	± 0.0046	-0.008
IX	0.9924	± 0.0046	-0.016
X	0.9907	± 0.0039	-0.008
XI	0.9989	± 0.0044	+0.002
XII	0.9932	± 0.0046	-0.013
XIII	0.9890	± 0.0054	-0.007
XIV	0.9830	± 0.0038	-0.013
XV	0.9852	± 0.0044	-0.016
XVI	0.9875	± 0.0042	-0.015
XVII	0.9811	± 0.0041	-0.015
XVIII	0.9784	± 0.0050	-0.015
XIX	0.9888	± 0.0033	-0.016
XX	0.9922	± 0.0048	-0.011
XXI	<u>0.9783</u>	<u>± 0.0039</u>	<u>-0.017</u>
Mean	0.9894	$\pm 0.0011^*$	-0.0120 ± 0.0010
Bias	0.0106	$\pm 0.0019^{**}$	0.0120 ± 0.0010
Bias (95%/95%)	0.0106	± 0.0048	0.0120 ± 0.0023
Maximum bias	0.0154		0.0143

* Calculated from individual standard deviations

** Calculated from k_{eff} values



available. No trends in k_{eff} with intra-assembly water gap, with absorber plate reactivity worth or with soluble poison concentration, were identified.*

3. CASMO-2E BENCHMARK CALCULATIONS

3.1 General

The CASMO-2E code is a multigroup transport theory code utilizing transmission probabilities to accomplish two-dimensional calculations of reactivity and depletion for BWR and PWR fuel assemblies. As such, CASMO-2E is well-suited to the criticality analysis of spent fuel storage racks, since general practice is to treat the racks as an infinite medium of storage cells, neglecting leakage effects.

CASMO-2E is closely analogous to the EPRI-CPM code (Ref. 9) and has been extensively benchmarked against hot and cold critical experiments by Studsvik Energiteknik (Ref. 3). Reported analyses of 26 critical experiments indicate a mean k_{eff} of 1.000 ± 0.0037 (1σ). Yankee Atomic (Ref. 10) has also reported results of extensive benchmark calculations with CASMO-2E. Their analysis of 54 Strawbridge and Barry critical experiments (Ref. 11) using the reported value for buckling indicates a mean of 0.9987 ± 0.0009 (1σ), or a bias of 0.0013 ± 0.0018 (with 95% probability at a 95% confidence level). Calculations were repeated for seven of the Strawbridge and Barry experiments selected at random, yielding a mean k_{eff} of 0.9987 ± 0.0021 (1σ), thereby confirming that the cross-section library and analytical methodology being used for the present calculations are the same as those used in the Yankee analyses. Thus, the

* Significantly large trends in k_{eff} with water gap and with absorber plate reactivity worth have been reported (Ref. 8) for AMPX-KENO calculations with the 123-group GAM-THERMOS library.



expected bias for CASMO-2E in the analysis of "clean" critical experiments is 0.0013 ± 0.0018 (95%/95%).

3.2 Benchmark Calculations

CASMO-2E benchmark calculations have also been made for the B&W series of critical experiments with absorber plates, simulating high density spent fuel storage racks. However, CASMO-2E, as an assembly code, cannot directly represent an entire core configuration* without introducing uncertainty due to reflector constants and the appropriateness of their spectral weighting. For this reason, the poisoned cell configurations of the central assembly, as calculated by CASMO-2E, were benchmarked against corresponding calculations with the 27-group (SCALE) AMPX-KENO code package. Results of this comparison are shown in Table 2. Since the differences are well within the normal KENO statistical variation, these calculations confirm the validity of CASMO-2E calculations for the typical high density poisoned spent fuel rack configurations. The differences shown in Table 2 are also consistent with a bias of 0.0013 ± 0.0018 , determined in Section 3.1, as the expected bias and uncertainty of CASMO-2E calculations.

* Yankee has attempted such calculations (Ref. 10) using CASMO-2E generated constants in a two-dimensional, four-group PDQ model, obtaining a mean k_{eff} of 1.005 for 11 poisoned cases and 1.009 for 5 unpoisoned cases. Thus, Yankee benchmark calculations suggest that CASMO-2E tends to slightly overpredict reactivity.



Table 2

RESULTS OF CASMO-2E BENCHMARK (INTERCOMPARISON) CALCULATIONS

B&W Experiment No. *	k_{∞} *		Δk
	AMPX-KENO **	CASMO-2E	
XIX	1.1203 ± 0.0032	1.1193	0.0010
XVII	1.1149 ± 0.0039	1.1129	0.0020
XV	1.1059 ± 0.0038	1.1052	0.0007
Interpolated ***	1.1024 ± 0.0042	1.1011	0.0013
XIV	1.0983 ± 0.0041	1.0979	0.0004
XIII	1.0992 ± 0.0034	1.0979	<u>0.0013</u>
Mean	± 0.0038		0.0011
Uncertainty			± 0.0006
BWR fuel rack	0.9212 ± 0.0027	0.9218	- 0.006

* Infinite array of central assemblies of 9-assembly B&W critical configuration (Ref. 4)

** k_{∞} from AMPX-KENO corrected for bias of 0.0106 Δk

*** Interpolated from Fig. 28 of Reference 4 for soluble boron concentration at critical condition



REFERENCES TO APPENDIX A

- 1.a. Green, Lucious, Petrie, Ford, White, Wright, "PSR-63/AMPX-1 (code package), AMPX Modular Code System for Generating Coupled Multigroup Neutron-Gamma Libraries from ENDF/B," ORNL-TM-3706, Oak Ridge National Laboratory, March 1976.
- b. L.M. Petrie and N. F. Cross, "KENO-IV, An Improved Monte Carlo Criticality Program," ORNL-4938, Oak Ridge National Laboratory, November 1975.
- 2.a. R. M. Westfall et al., "SCALE: A Modular Code System for Performing Standardized Computer Analyses for Licensing Evaluation," NUREG/CR-0200, 1979.
- b. W. E. Ford, III et al., "A 218-Neutron Group Masta Cross-section Library for Criticality Safety Studies," ORNL/TM-4, 1976.
- 3.a. A. Ahlin, M. Edenius, H. Haggblom, "CASMO - A Fuel Assembly Burnup Program," AE-RF-76-4158, Studsvik report (proprietary).
- b. A. Ahlin and M. Edenius, "CASMO - A Fast Transport Theory Depletion Code for LWR Analysis," ANS Transactions, Vol. 26, p. 604, 1977.
- c. M. Edenius et al., "CASMO Benchmark Report," Studsvik/RF-78-6293, Aktiebolaget Atomenergi, March 1978.
- d. "CASMO-2E Nuclear Fuel Assembly Analysis, Application Users Manual," Rev. A, Control Data Corporation, 1982.
4. M. N. Baldwin et al., "Critical Experiments Supporting Close Proximity Water Storage of Power Reactor Fuel," BAW-1484-7, The Babcock & Wilcox Company, July 1979.
5. M. G. Natrella, Experimental Statistics, National Bureau of Standards, Handbook 91, August 1963.
6. B. F. Cooney et al., "Comparisons of Experiments and Calculations for LWR Storage Geometries," Westinghouse NES, ANS Transactions, Vol. 39, p. 531, November 1981.
7. R. M. Westfall and J. R. Knight, "Scale System Cross-section Validation with Shipping-cask Critical Experiments," ANS Transactions, Vol. 33, p. 368, November 1979.



REFERENCES TO APPENDIX A (Continued)

8. S. E. Turner and M. K. Gurley, "Evaluation of AMPX-KENO Benchmark Calculations for High Density Spent Fuel Storage Racks," Nuclear Science and Engineering, 80(2): 230-237, February 1982.
9. "The EPRI-CPM Data Library," ARMP Computer Code Manuals, Part II, Chapter 4, CCM3, Electric Power Research Institute, November 1975.
10. E.E. Pilat, "Methods for the Analysis of Boiling Water Reactors (Lattice Physics)," YAEC-1232, Yankee Atomic Electric Co., December 1980.
11. L. E. Strawbridge and R. F. Barry, "Criticality Calculations for Uniform, Water-moderated Lattices," NSE 23, 58, September 1965.



5. THERMAL-HYDRAULIC CONSIDERATIONS

A primary objective in the design of the high density fuel racks is to ensure adequate cooling of the fuel assembly cladding. In the following, a brief synopsis of the design basis, the method of analysis, and computed results are given. Similar analysis has been used in previous licensing reports on high density spent fuel racks for Fermi II (Docket 50-341), Quad Cities I and II (Dockets 50-254 and 50-265), Rancho Seco (Docket 50-312), Grand Gulf Unit 1 (Docket 50-416), Oyster Creek (Docket 50-219), and Virgil C. Summer (Docket 50-395).

5.1 DECAY HEAT CALCULATIONS FOR THE SPENT FUEL

This report section covers requirement III.1.5(2) of the NRC's "OT Position for Review and Acceptance of Spent Fuel Storage and Handling Applications" issued on April 14, 1978. This requirement states that calculations for the amount of thermal energy removed by the spent fuel cooling system shall be made in accordance with Branch Technical Position APCS 9-2, "Residual Decay Energy for Light Water Reactors for Long Term Cooling" (Ref. 1). The calculations contained herein have been made in accordance with this requirement.

5.1.1 Basis

The Diablo Canyon Power Plant Unit 1 and Unit 2 reactors are rated at 3338 and 3411 megawatts thermal (MWt), respectively. For analysis purposes, the Unit 2 power rating is used. The core contains 193 fuel assemblies. Thus, the average operating power per fuel assembly, P_0 , is 17.6736 MW. The fuel discharge can be made in one of the following two modes:

- O Partial core discharge - Mode i
- O Full core discharge - Mode ii



The average fuel batch size is 76 fuel assemblies (18-month cycle). The fuel transfer begins after 100 hours of decay time in the reactor (time after shutdown). It is assumed that the time period of discharge of this batch is 19 hours (four assemblies transferred to the pool per hour). An alternate average batch size of 96 fuel assemblies (24-month cycle) discharge is also considered. For this latter case, the fuel transfer is assumed to take 24 hours and the decay time before transfer begins is 100 hours. The cooling system consists of a Seismic Category I spent fuel cooling circuit. The bulk temperature analysis assumes a 95°F coolant inlet temperature to the spent fuel pool heat exchanger for these refueling cases.

Mode ii corresponds to a full core discharge (193 assemblies). Full core offload condition implies that the reactor core has no remaining fuel. It is assumed that the total time period for the discharge of one full core is 48 hours (after 100 hours of shutdown time in the reactor). The discharge rate to the pool is assumed to be continuous and uniform. The bulk temperature analysis assumes an 85°F coolant inlet temperature to the fuel pool cooler, which takes into account the reduced heat load to the component cooling water system during this mode.

The fuel assemblies are removed from the reactor after a maximum postulated time of 4.5 years of cumulative operating time. Since the decay heat load is a monotonically increasing function of the cumulative reactor operating time, τ_0 , it is conservatively assumed that every fuel assembly discharged has had the maximum postulated τ_0 of 4.5 years for the batch size of 76. For the alternate average batch size of 96, the assumed cumulative operating time is 4 years.

The water inventory in the reactor cavity cooled by the residual heat removal (RHR) heat exchanger exchanges heat with the fuel pool water mass through the refueling canal. This source of



heat removal is neglected in the analysis. Thus, the results obtained for both modes i and ii are conservative.

The spent fuel pool cooling system consists of one pump and heat exchanger per unit as described in Chapter 9.1 of the Diablo Canyon FSAR Update (Ref. 2).

The following list identifies all relevant performance data for the spent fuel pool heat exchanger:

O	Type	Tube and shell
O	Quantity	1
O	Performance data	
	- Heat transferred	11.95×10^6 Btu/hr
	<u>Tube Side</u>	
	- Fluid flow	1.14×10^6 lb/hr
	- Pool water inlet temperature	120°F
	- Outlet temperature	109.5°F
	<u>Shell Side</u>	
	- Fluid flow	1.49×10^6 lb/hr
	- Coolant inlet temperature	95°F (mode i)*
	- Outlet temperature	103°F
	- Fouling factor	0.0005

The above data enables complete characterization of the thermal performance of the fuel pool heat exchanger.

5.1.2 Model Description

Reference 1 is utilized to compute the heat dissipation requirements in the pool. The total decay power consists of fission products decay and heavy element decay. Total decay power P for a fuel assembly is given as a linear function of P_0 and

* For full core discharge, mode ii coolant inlet temperature is 85°F.



as an exponential function of τ_0 and τ_s :

$$P = P_0 f(\tau_0, \tau_s) \quad (5.1-1)$$

where:

P = total decay power per fuel assembly, linear function of P_0

P_0 = average operating power per fuel assembly

τ_0 = cumulative exposure time of the fuel assembly in the reactor

τ_s = time elapsed since reactor shutdown

The uncertainty factor K (Ref. 1), which occurs in the functional relationship $f(\tau_0, \tau_s)$ is set equal to 0.1 for $\tau_s > 10^7$ seconds in the interest of conservatism. Furthermore, the operating power P_0 is taken equal to the rated power, even though the reactor may be operating at less than its rated power during much of the exposure period for the batch of fuel assemblies. Finally, the computations and results reported here are based on the discharge taking place when the inventory of fuel in the pool will be at its maximum resulting in an upper bound on the computed decay heat rate.

Having determined the heat dissipation rate, the next task is to evaluate the time-temperature history of the pool water. Table 5.1 identifies the loading cases examined. The pool bulk temperature time-history is determined using the first law of thermodynamics (conservation of energy).

A number of simplifying assumptions are made which render the analysis conservative, principally:

- 0 The cooling water temperature in the fuel pool cooler is based on the maximum postulated values given in the FSAR (Ref. 2) for mode i refueling case, and a conservatively high value for the full core discharge cases, which takes into account the lower plant heat load after the core is removed from the reactor.



Table 5.1

LIST OF CASES ANALYZED

Case No.	Condition	No. of Fuel Assemblies Discharged, N	Total Time to Transfer Fuel Into the Pool t_h , hrs	Decay Time Before Transfer Begins, hrs
1	76 fuel discharge*	76	19	100
2	Half core discharge**	96	24	100
3	Full core* discharge	193	48	100

* Discharge is assumed to be into a pool containing fuel from 15 previous discharges of 76 assemblies each at 18-month intervals.

** Discharge is assumed to be into a pool containing fuel from 12 previous discharges of 96 assemblies each at 24-month intervals.



- O The heat exchangers are assumed to have maximum fouling. Thus, the temperature effectiveness, S , for the heat exchanger utilized in the analysis is the lowest postulated value: $S = 0.32$ for fuel pool cooler. S is calculated from heat exchanger technical data sheets. No heat loss is assumed to take place through the concrete floor.
- O No credit is taken for the improvement in the film coefficients of the heat exchanger as the operating temperature rises. Thus, the film coefficient used in the computations are lower bounds.
- O No credit is taken for heat loss by evaporation of the pool water.
- O No credit is taken for heat loss to pool walls and pool floor slab.

The basic energy conservation relationship for the pool heat exchanger system yields:

$$C_t \frac{dt}{d\tau} = Q_1 - Q_2 \quad (5.1-2)$$

where:

C_t = Thermal capacitance of stored water in the pool

t = Temperature of pool water at time, τ

Q_1 = Heat generation rate due to stored fuel assemblies in the pool; Q_1 is a known function of time, τ from the preceding section.

Q_2 = Heat removed in the fuel pool cooler

The pool has a total water inventory of 47,640 cubic feet when all racks are in place in the pool and every storage location is occupied.



5.1.3 Decay Heat Calculation Results

The calculations were performed for the pool, disregarding the additional thermal capacity and cooling system available in the transfer channel, and the reactor cavity.

For a specified coolant inlet temperature and flow rate, the quantity Q_2 is shown to be a linear function of τ in a recent paper by Singh (Ref. 3). As stated earlier, Q_1 is an exponential function of τ . Thus, Equation 5.1-2 can be integrated to determine t directly as a function of τ . The results are plotted in Figures 5.1 through 5.3. The results show that the pool water never approaches the boiling point under the most adverse conditions. These figures also give Q_1 as a function of τ . Four plots are generated for each case. The first and third plots for each case shows temperature and power generation, respectively, for a period extending from $\tau = 0 \rightarrow \tau \approx 2\tau_n$ where τ_n is the total time of fuel transfer. The second and fourth plots show the same quantities (i.e., temperature and power generation, respectively) over a longer period. The long-term plots are produced to show the temperature drop with time. Summarized results are given in Table 5.2.

Finally, computations are made to determine the time interval to boiling after all heat dissipation paths are lost. Computations are made for each case under the following two assumptions:

- o All cooling sources lost at the instant pool bulk temperature reaches the maximum value.
- o All cooling paths lost at the instant the heat dissipation power reaches its maximum value in the pool.

Results are summarized in Table 5.3. Table 5.3 gives the bulk boiling vaporization rate for all cases at the instant the boiling commences. This rate will decrease with time due to reduced heat generation in the fuel.



Table 5.2

MAXIMUM POOL BULK TEMPERATURE t , COINCIDENT TOTAL POWER Q_1 , AND
COINCIDENT SPECIFIC POWER FOR THE HOTTEST ASSEMBLY

Case No.	No. of Assemblies	Time to Transfer Fuel Into Pool, hrs	Maximum Pool Bulk Temp. °F	Coincident Time (After Initiation of Fuel Transfer), hrs	Coincident Specific Power, q , Btu/sec	$Q_1 \times 10^{-6}$ Btu/hour	Notes
1	76	19	140.0	36	55.339	21.8905	Normal condition*
2	96	24	147.3	40	54.498	24.9604	Normal condition**
3	193	48	174.3	61	51.572	42.5824	Full core offload*

* Discharge is assumed to be into a pool containing fuel from 15 previous discharges of 76 assemblies each at 18-month intervals.

** Discharge is assumed to be into a pool containing fuel from 12 previous discharges of 96 assemblies each at 24-month intervals.



Table 5.3

TIME (HRS) TO BOILING AND BOILING VAPORIZATION RATE FROM THE
INSTANT ALL COOLING IS LOST

Case No.	CONDITION 1		CONDITION 2	
	Loss of Cooling at Maximum Pool Bulk Temperature		Loss of Cooling at Maximum Power Discharge Rate	
	Time (Hrs)	Vap. Rate lb/hr	Time (Hrs)	Vap. Rate lb/hr
1	9	22145	10	22915
2	7	25329	8	26216
3	2.5	43676	2.75	44905



The radiological consequences of a spent fuel pool boiling event were evaluated and found acceptable, as discussed in Section 7.7.

5.2 THERMAL-HYDRAULIC ANALYSES FOR SPENT FUEL COOLING

This report section covers requirement III.1.5(3) of the NRC's "OT Position for Review and Acceptance of Spent Fuel Storage and Handling Applications," issued on April 14, 1978. Conservative methods have been used to calculate the maximum fuel cladding temperature as required therein. Also, it has been determined that nucleate boiling or voiding of coolant on the surface of the fuel rods occurs only at the locations where freshly discharged fuel assemblies are stored.

5.2.1 Basis

In order to determine an upper bound on the maximum fuel cladding temperature, a series of conservative assumptions are made. The most important assumptions are listed below:

- O As stated above, the fuel pool will contain spent fuel with varying time-after-shutdown (τ_s). Since the heat emission falls off rapidly with increasing τ_s , it is obviously conservative to assume that all fuel assemblies are fresh ($\tau_s = 100$ hours) and they all have had 4.5 years of operating time in the reactor for cases 1 and 3, and 4.0 years for case 2. The heat emission rate of each fuel assembly is assumed to be equal (Ref. 2).
- O As shown in Figure 2.1 in Section 2, the modules occupy an irregular floor space in the pool. For the hydrothermal analysis, a circle circumscribing the actual rack floor space is drawn. It is further assumed that the cylinder with this circle as its base is packed with fuel assemblies at the nominal pitch of 10.93 inches (see Figure 5.5).
- O The downcomer space around the rack module group varies, as shown in Figure 5.5. The nominal downcomer gap available in the pool is assumed to be the total gap available around the idealized cylindrical rack; thus, the maximum resistance to downward flow is incorporated into the analysis.



- 0 No downcomer flow is assumed to exist between the rack modules.

5.2.2 Model Description

In this manner, a conservative idealized model for the rack assemblage is obtained. The water flow is axisymmetric about the vertical axis of the circular rack assemblage, and thus, the flow is two-dimensional (axisymmetric three-dimensional). Figure 5.6 shows a typical "flow chimney" rendering of the thermal hydraulics model. The governing equation to characterize the flow field in the pool can now be written. The resulting integral equation can be solved for the lower plenum velocity field (in the radial direction) and axial velocity (in-cell velocity field), by using the method of collocation. It should be added that the hydrodynamic loss coefficients which enter into the formulation of the integral equation are also taken from well-recognized sources (Ref. 4) and wherever discrepancies in reported values exist, the conservative values are consistently used. Reference 5 gives the details of mathematical analysis used in this solution process..

After the axial velocity field is evaluated, it is a straightforward matter to compute the fuel assembly cladding temperature. The knowledge of the overall flow field enables pinpointing the storage location with the minimum axial flow (i.e., maximum water outlet temperature). This is called the most "choked" location. In order to find an upper bound on the temperature in a typical cell, it is assumed that it is located at the most choked location. Knowing the global plenum velocity field, the revised axial flow through this choked cell can be calculated by solving the Bernoulli's equation for the flow circuit through this cell. Thus, an absolute upper bound on the water exit temperature and maximum fuel cladding temperature is obtained. It is believed that, in view of the aforementioned assumptions, the temperatures calculated in this manner overestimate the temperature rise that will actually occur in the pool.



The maximum pool bulk temperature t is computed in Section 5.1.3 and reported in Table 5.2. The corresponding average power output from the hottest fuel assembly, q , is also reported in that table. The maximum radial peaking factor is 1.71 for the Diablo Canyon installation. Thus, it is conservative to assume that the maximum specific power of a fuel assembly is given by:

$$q_A = q \alpha_r \quad (5.2-1)$$

where:

$$\alpha_r = 1.71$$

The maximum temperature rise of pool water in the most disadvantageously placed fuel assembly is given in Table 5.4 for all loading cases. Having determined the maximum local water temperature in the pool, it is now possible to determine the maximum fuel cladding temperature. It is conservatively assumed that the total peaking factor α_T is 2.55 (includes 10% margin). Thus, a fuel rod can produce 2.55 times the average heat emission rate over a small length. The axial heat dissipation in a rod is known to reach a maximum in the central region, and taper off at its two extremities. For the sake of added conservatism it is assumed that the peak heat emission occurs at the top where the local water temperature also reaches its maximum. Furthermore, no credit is taken for axial conduction of heat along the rod. The highly conservative model thus constructed leads to simple algebraic equations which directly give the maximum local cladding temperature, t_c .

5.2.3 Results

Table 5.4 gives the maximum local cladding temperature, t_c , at the instant the pool bulk temperature has attained its maximum value. It is quite possible, however, that the peak cladding temperature occurs at the instant of maximum value of q_A , i.e.,



Table 5.4

MAXIMUM LOCAL POOL WATER TEMPERATURE AND LOCAL FUEL CLADDING
TEMPERATURE AT INSTANT OF MAXIMUM POOL BULK TEMPERATURE

Case No.	Maximum Water Temperature, °F	Local Temperature, °F	Maximum Coincident Pool Temperature, °F	Cladding Case Identified
1	188.0		225.0	76 assemblies
2	194.0		230.5	96 assemblies
3	219.5		254.3	193 assemblies



at the instant when the fuel assembly is first placed in a storage location. Table 5.5 gives the maximum local cladding temperature at $x = 0$. The local boiling temperature near the top of the fuel cladding is 240°F. However, the cladding temperature must be somewhat higher than the boiling temperature to initiate and sustain nucleate boiling. The above considerations indicate that a comfortable margin against the initiation of localized boiling exists in cases 1 and 2. For full core discharge (case 3) under the described assumptions, the maximum cladding temperature will give rise to localized nucleate boiling, but not to bulk pool boiling.



Table 5.5

POOL AND MAXIMUM CLADDING TEMPERATURE AT THE
INSTANT FUEL ASSEMBLY TRANSFER BEGINS

Case No.	Cladding Temperature, °F	Coincident Pool Temperature, °F	
		Bulk	Local
1	202.0	109.2	160.5
2	200.5	107.9	159.1
3	191.9	99.2	150.4



REFERENCES TO SECTION 5

1. NUREG-0800 U.S. Nuclear Regulatory Commission, Standard Review Plan, Branch Technical Position ASB 9-2, Rev. 2, July 1981.
2. FSAR, Diablo Canyon Power Plant.
3. Journal of Heat Transfer, Transactions of the ASME, August 1981, Vol. 103, "Some Fundamental Relationships for Tubular Heat Exchanger Thermal Performance," K.P. Singh.
4. General Electric Corporation, R&D Data Books, "Heat Transfer and Fluid Flow," 1974 and updates.
5. 4th National Congress of the ASME, "A Method for Computing the Maximum Water Temperature in a Fuel Pool Containing Spent Nuclear Fuel," paper 83-NE-7, Portland, Oregon (June 1983).



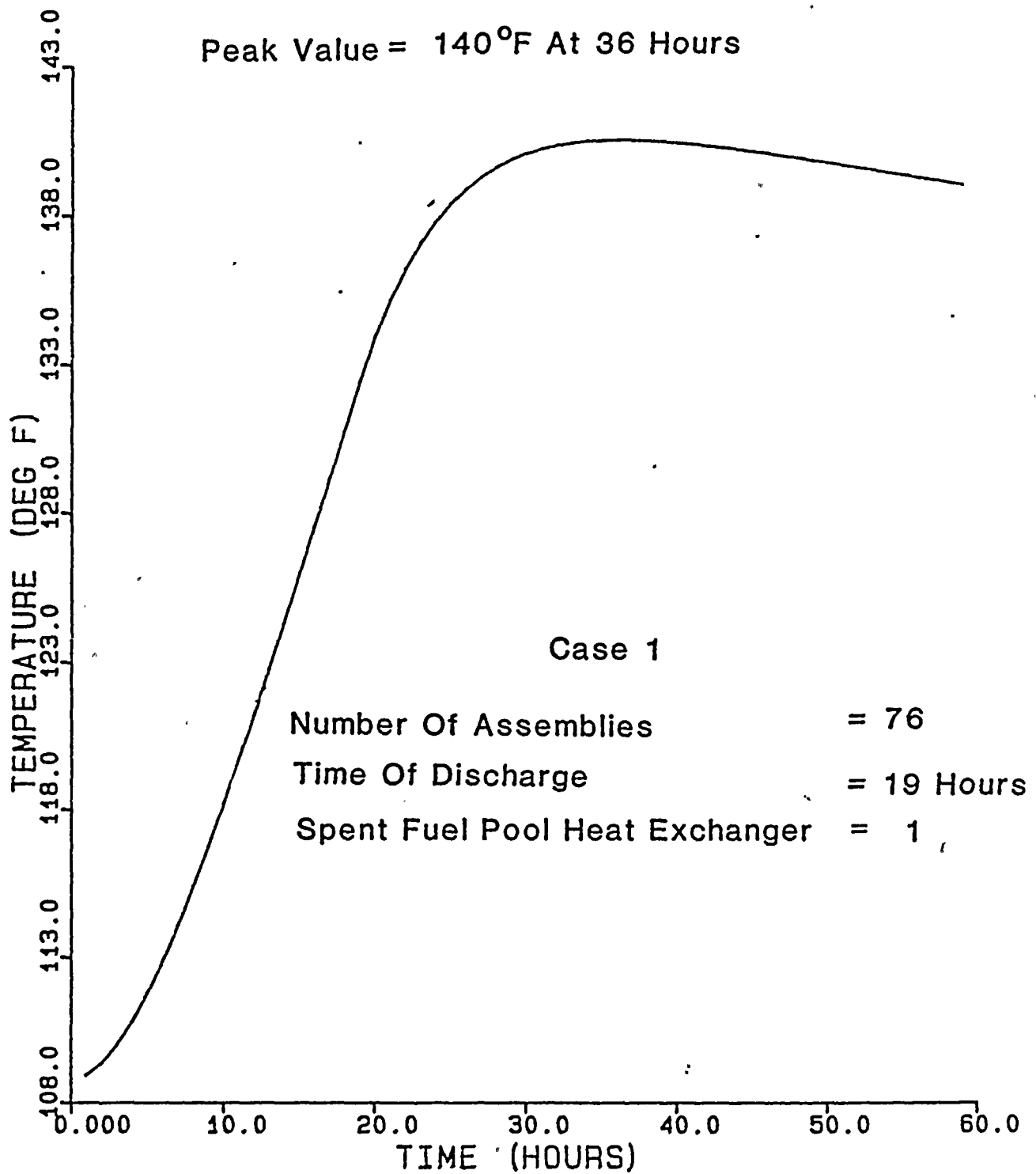


FIGURE 5.1a Pool Bulk Temperature



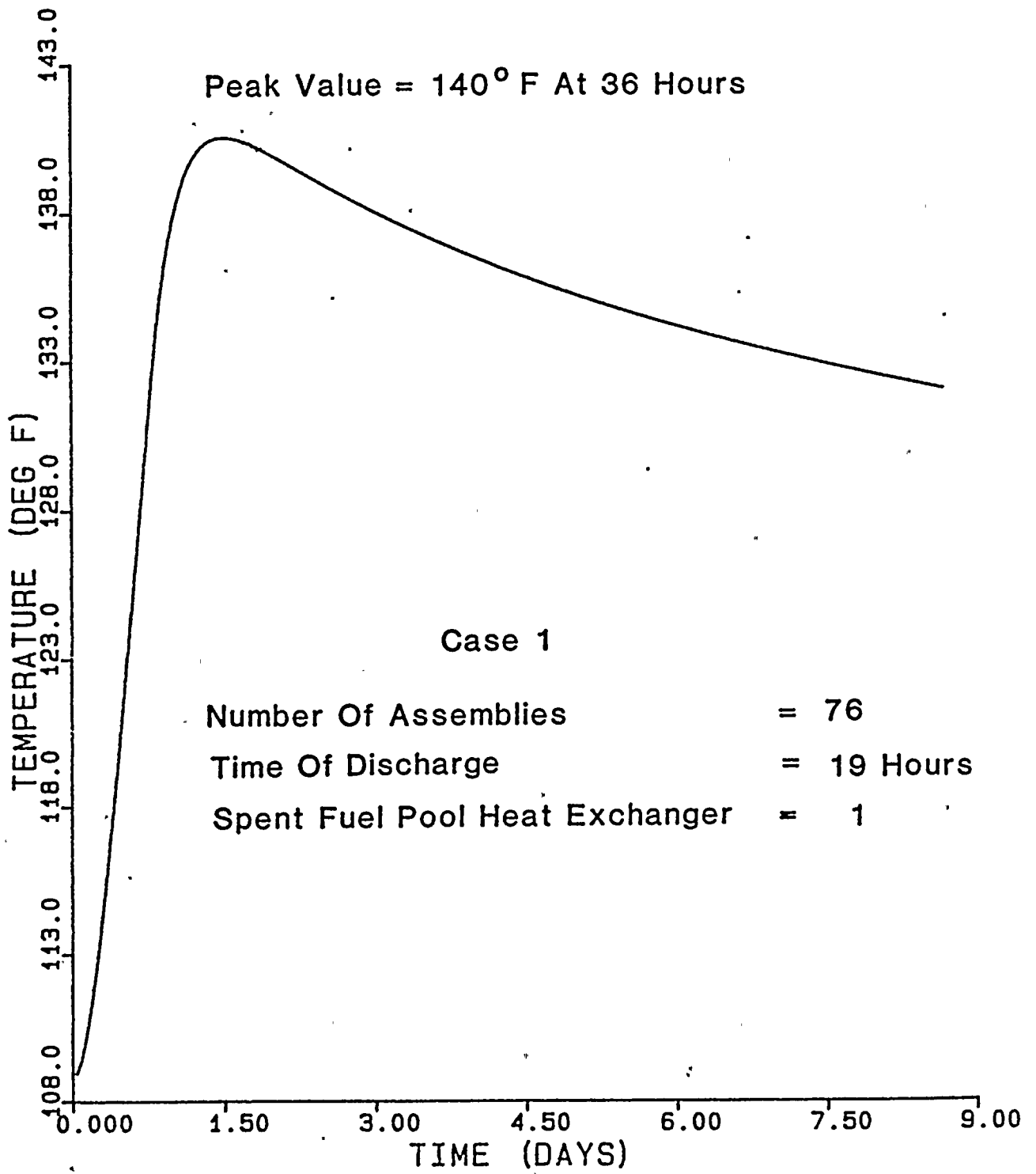


FIGURE 5.1b Pool Bulk Temperature



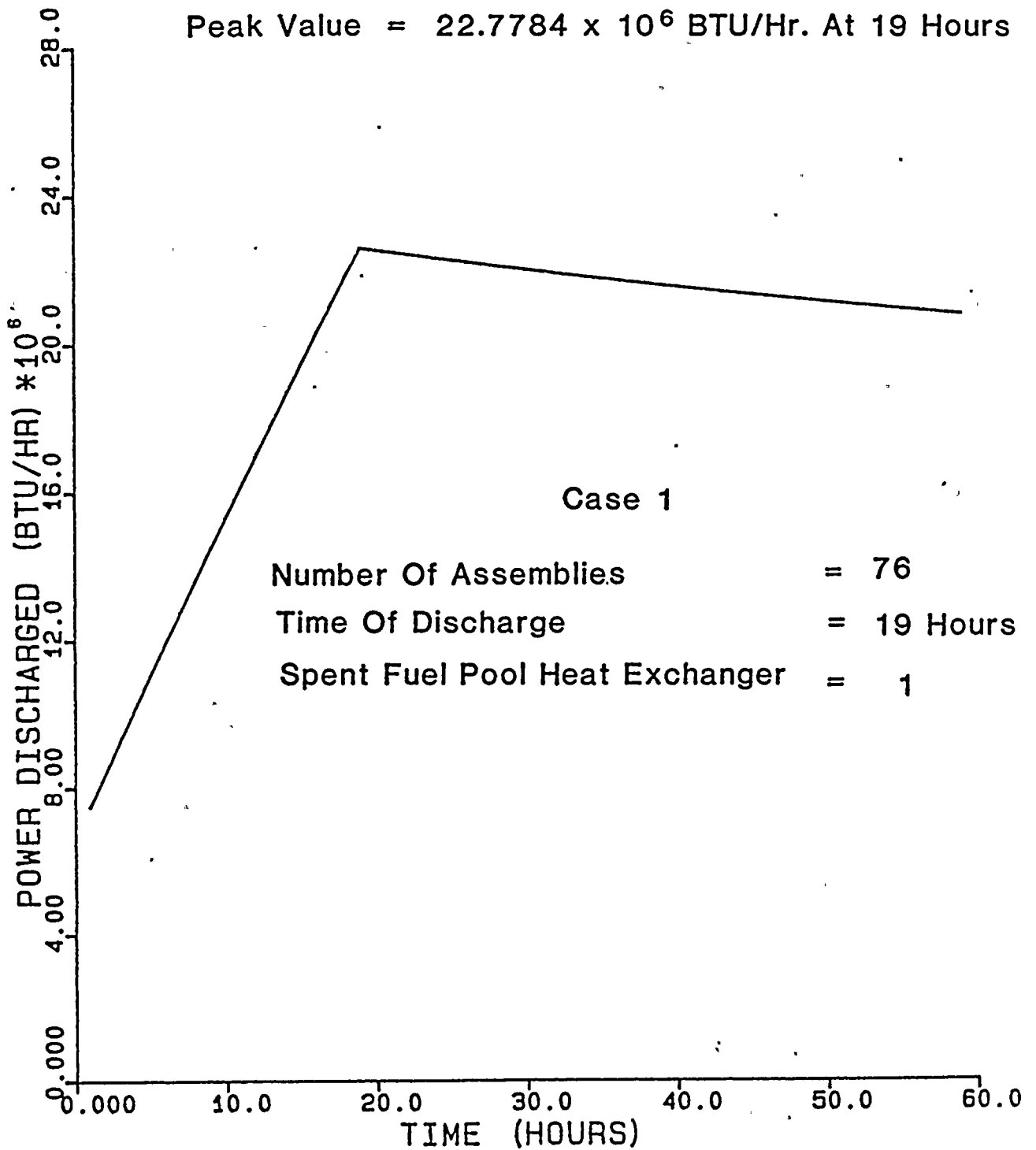


FIGURE 5.1c Power Discharged



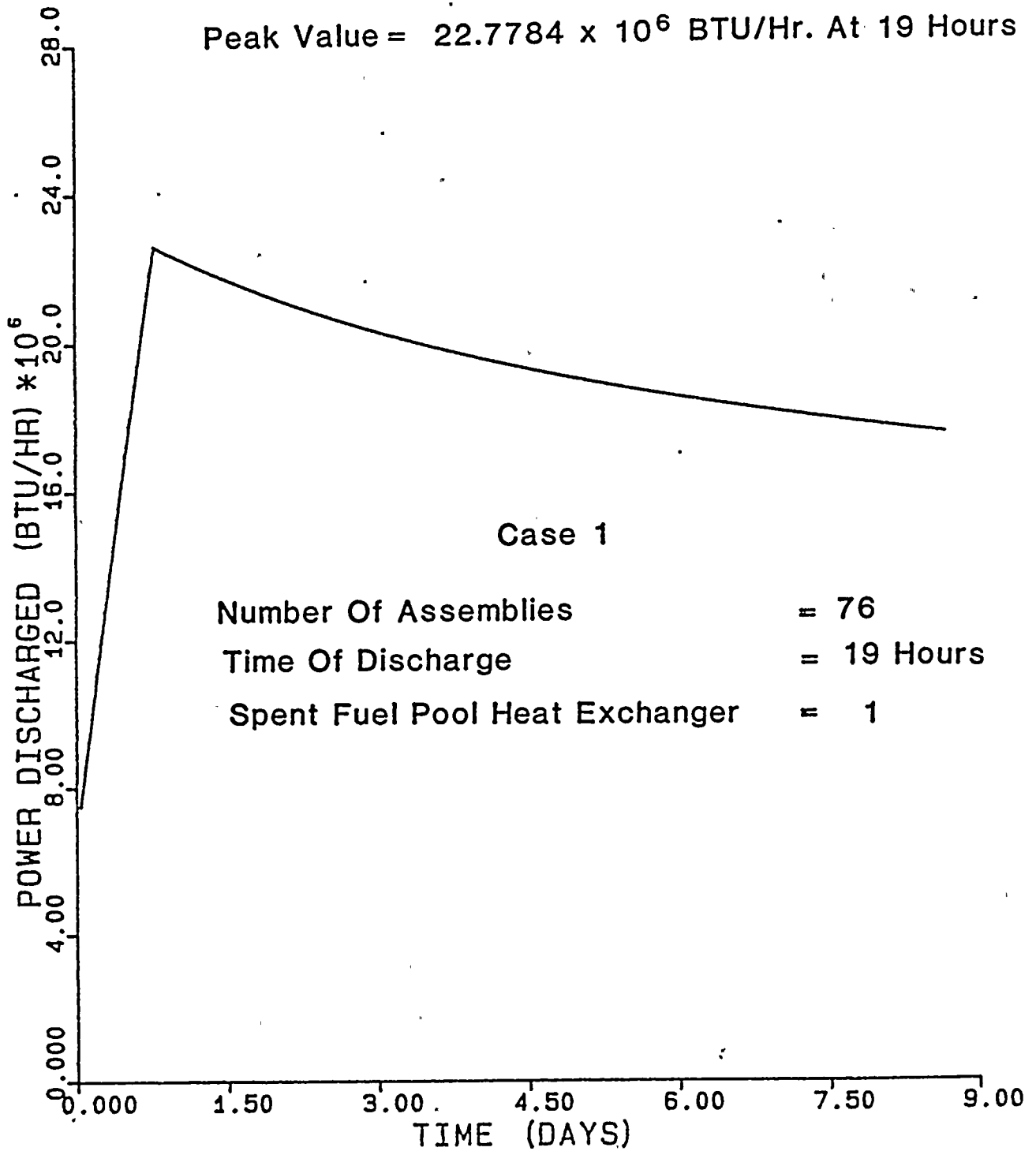


FIGURE 5.1d Power Discharged



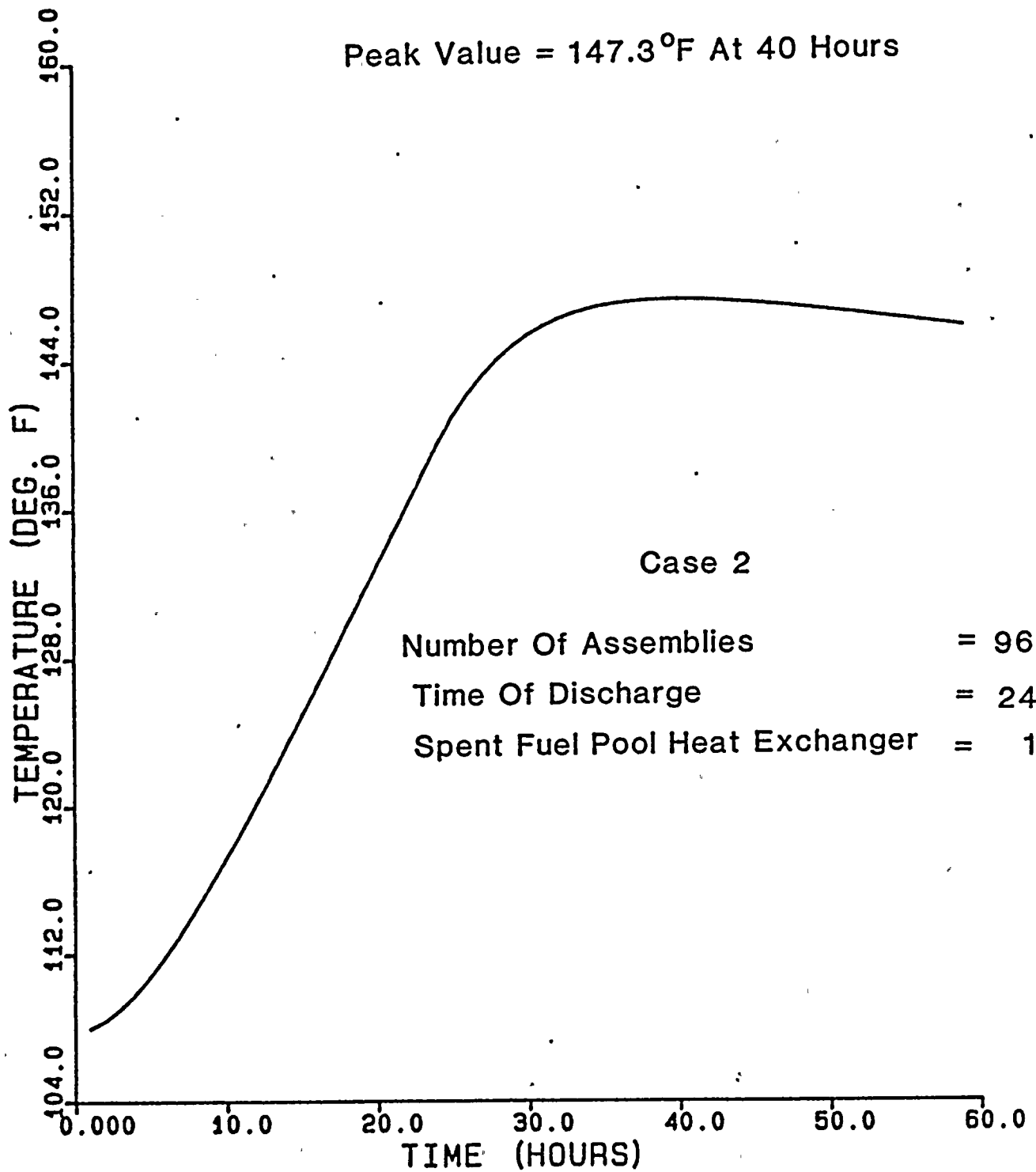


FIGURE 5.2a Pool Bulk Temperature



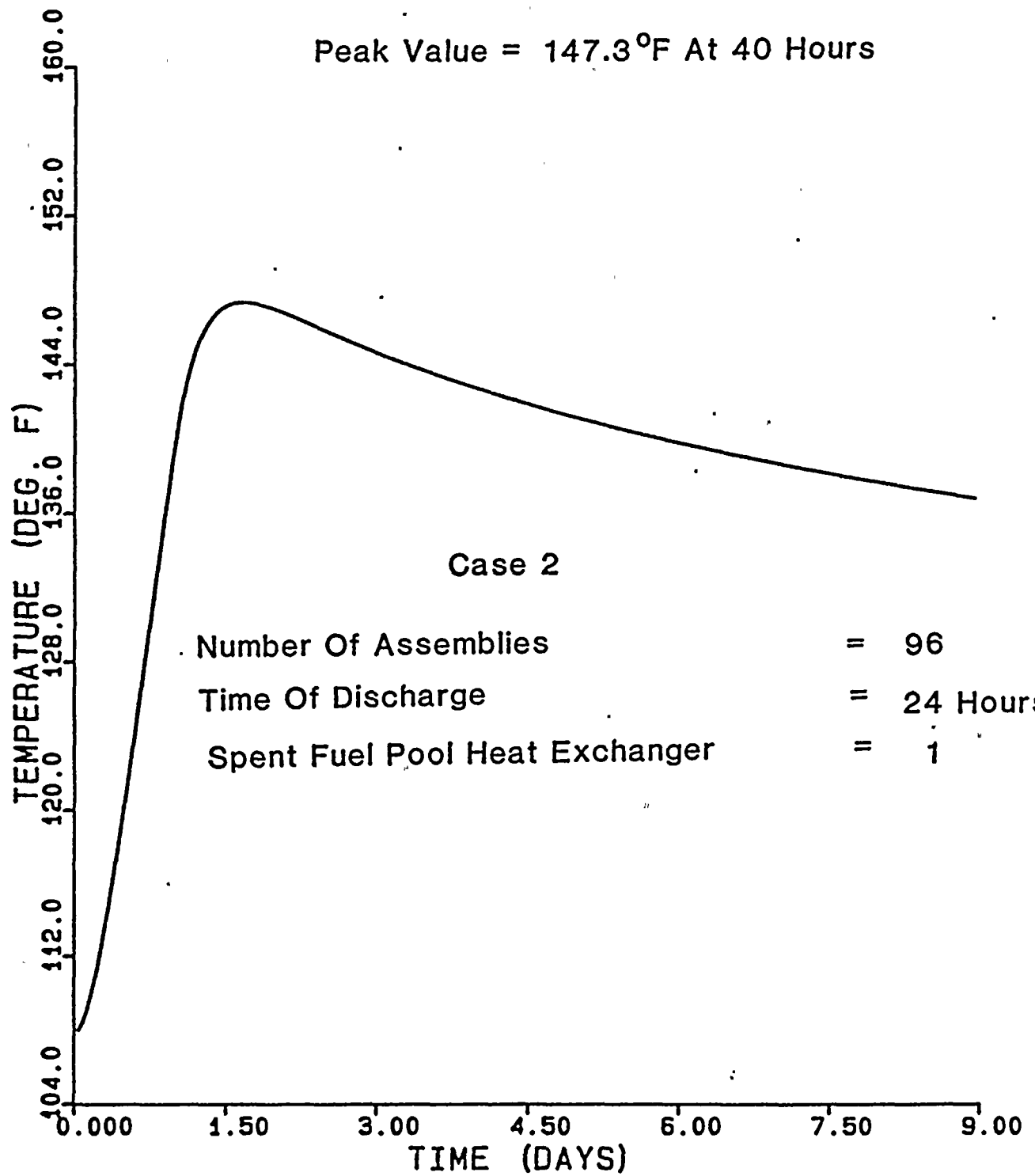


FIGURE 5.2b Pool Bulk Temperature



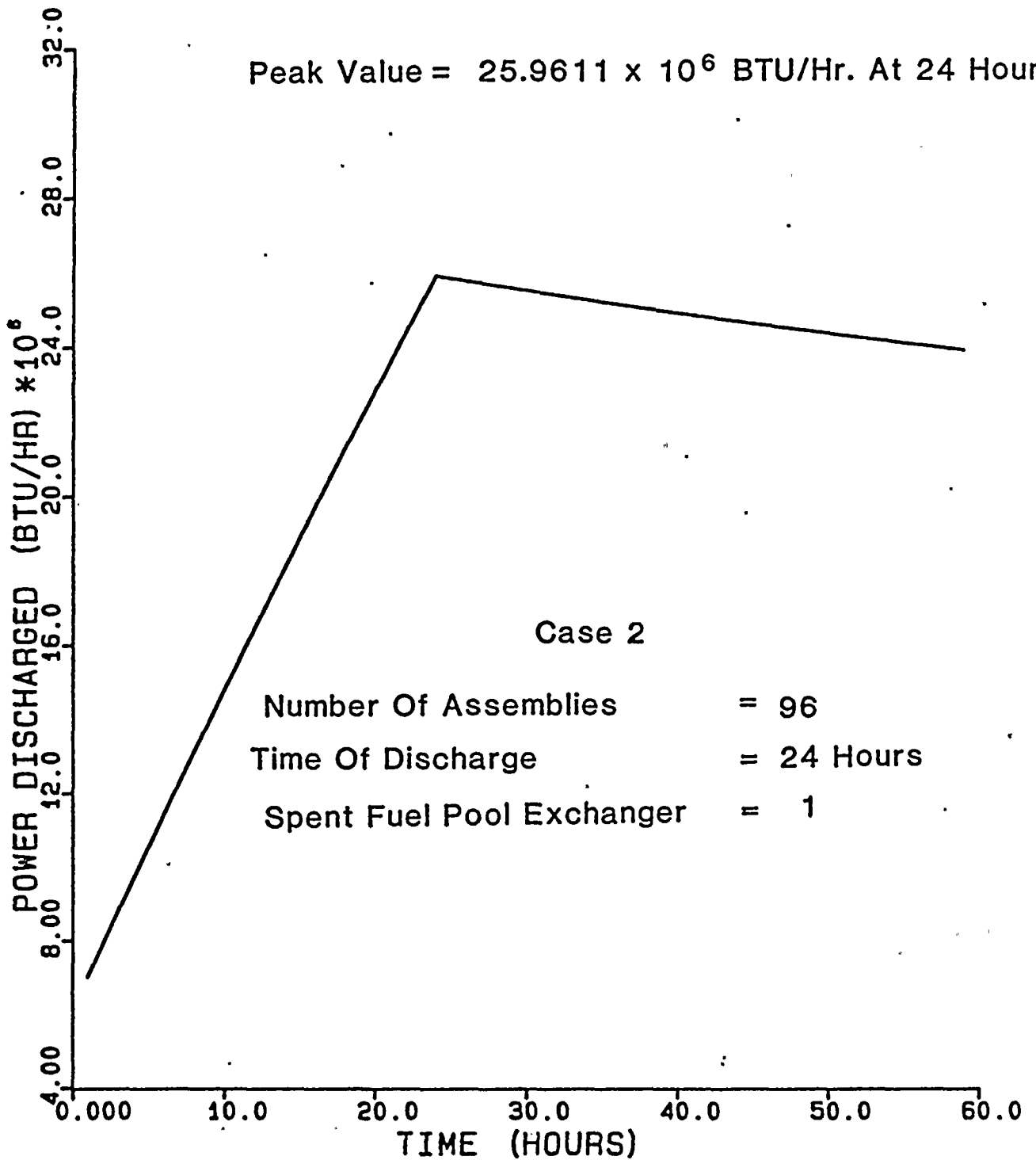


FIGURE 5.2c Power Discharged



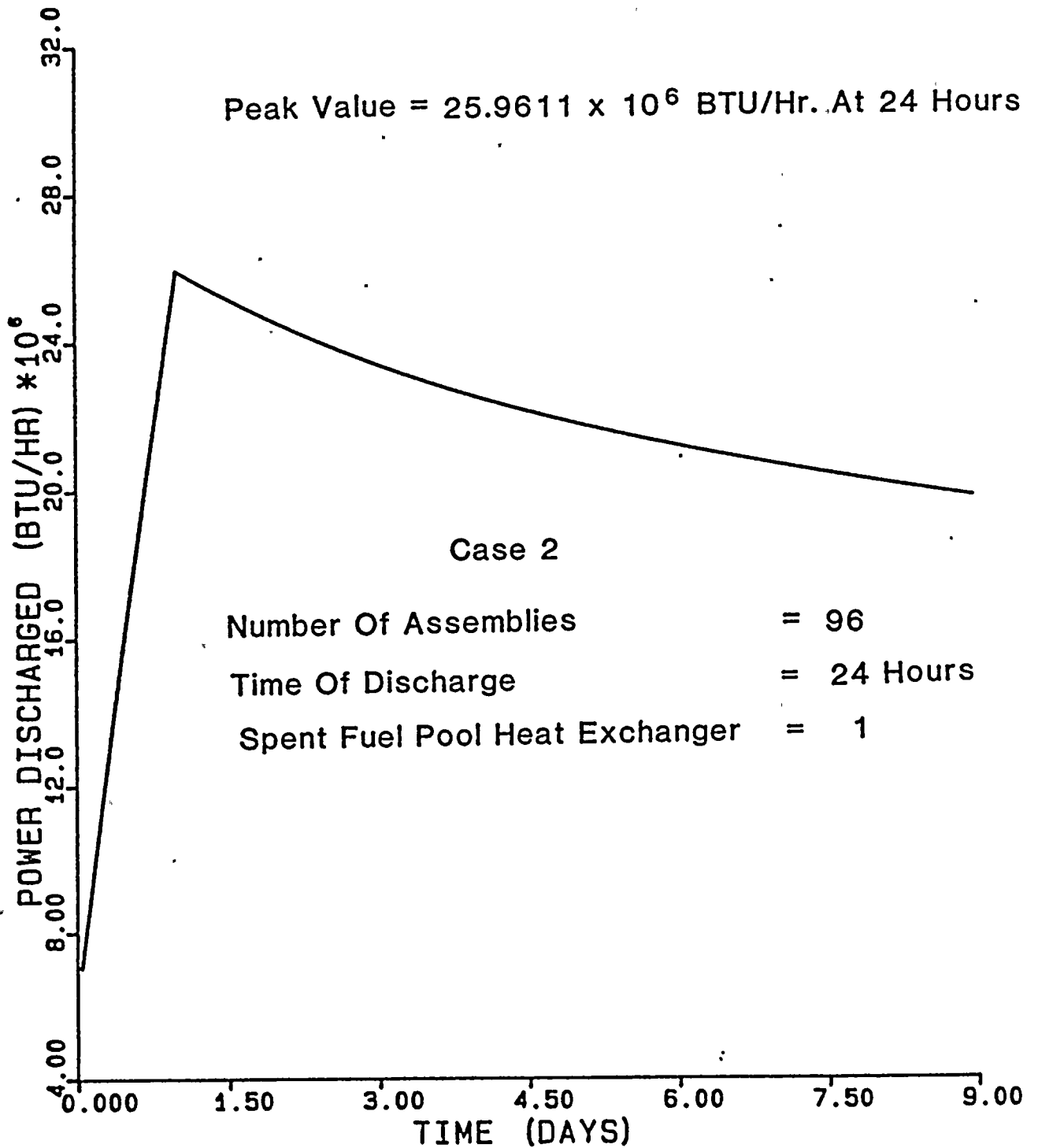


FIGURE 5.2d Power Discharged



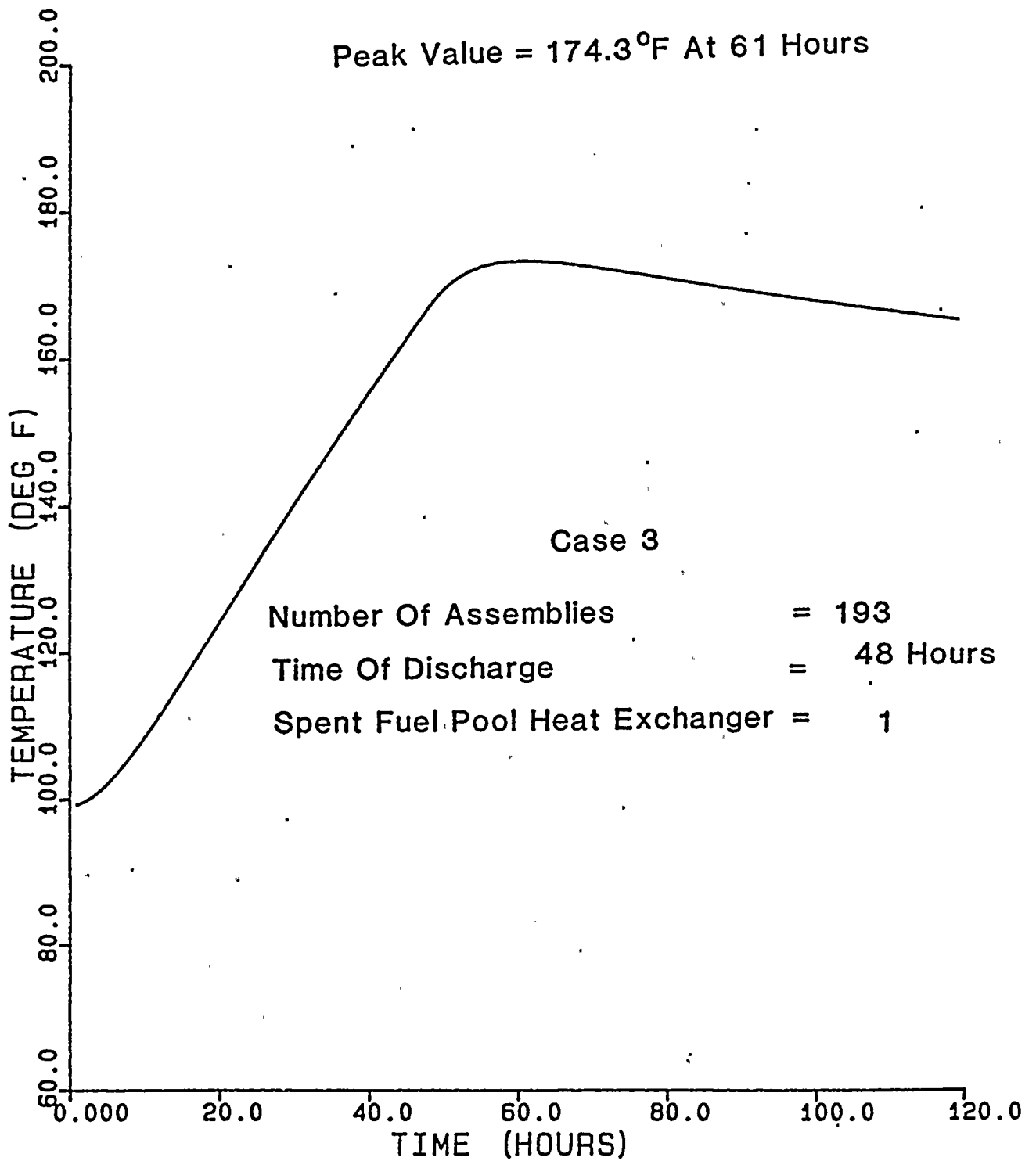


FIGURE 5.3a Pool Bulk Temperature; Full Core Discharge



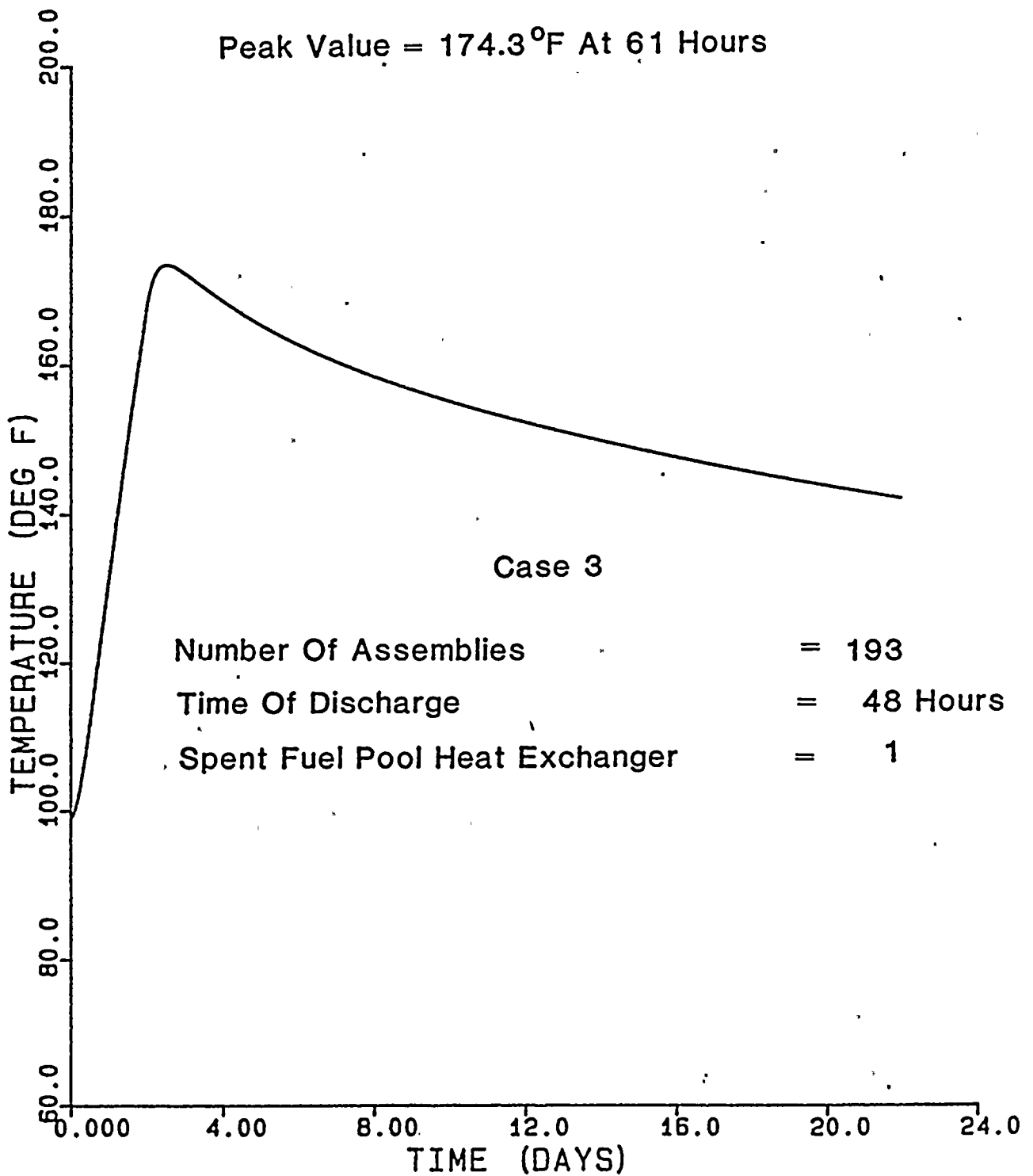


FIGURE 5.3b Pool Bulk Temperature; Full Core Discharge



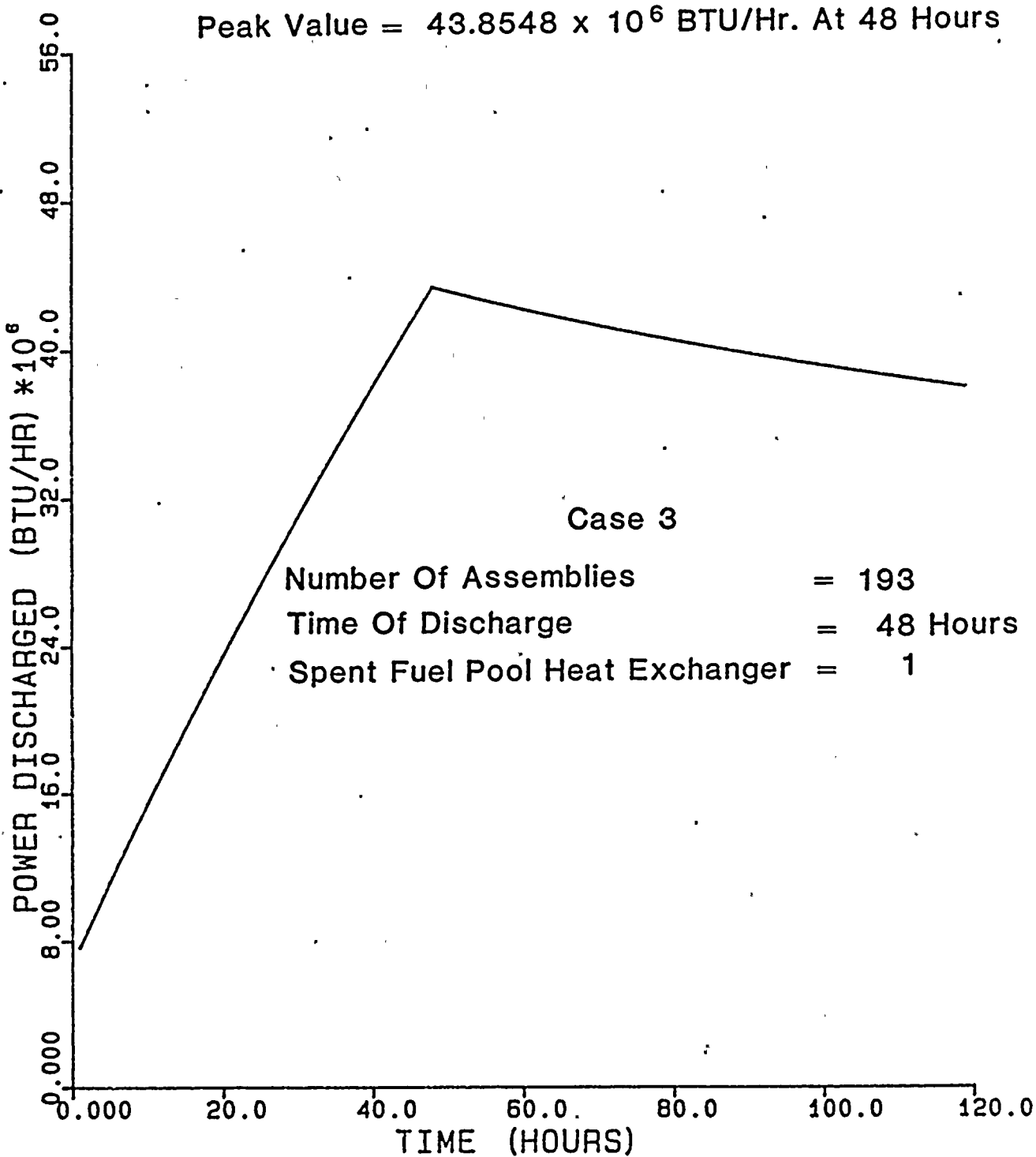


FIGURE 5.3c Power Discharged ; Full Core Discharge



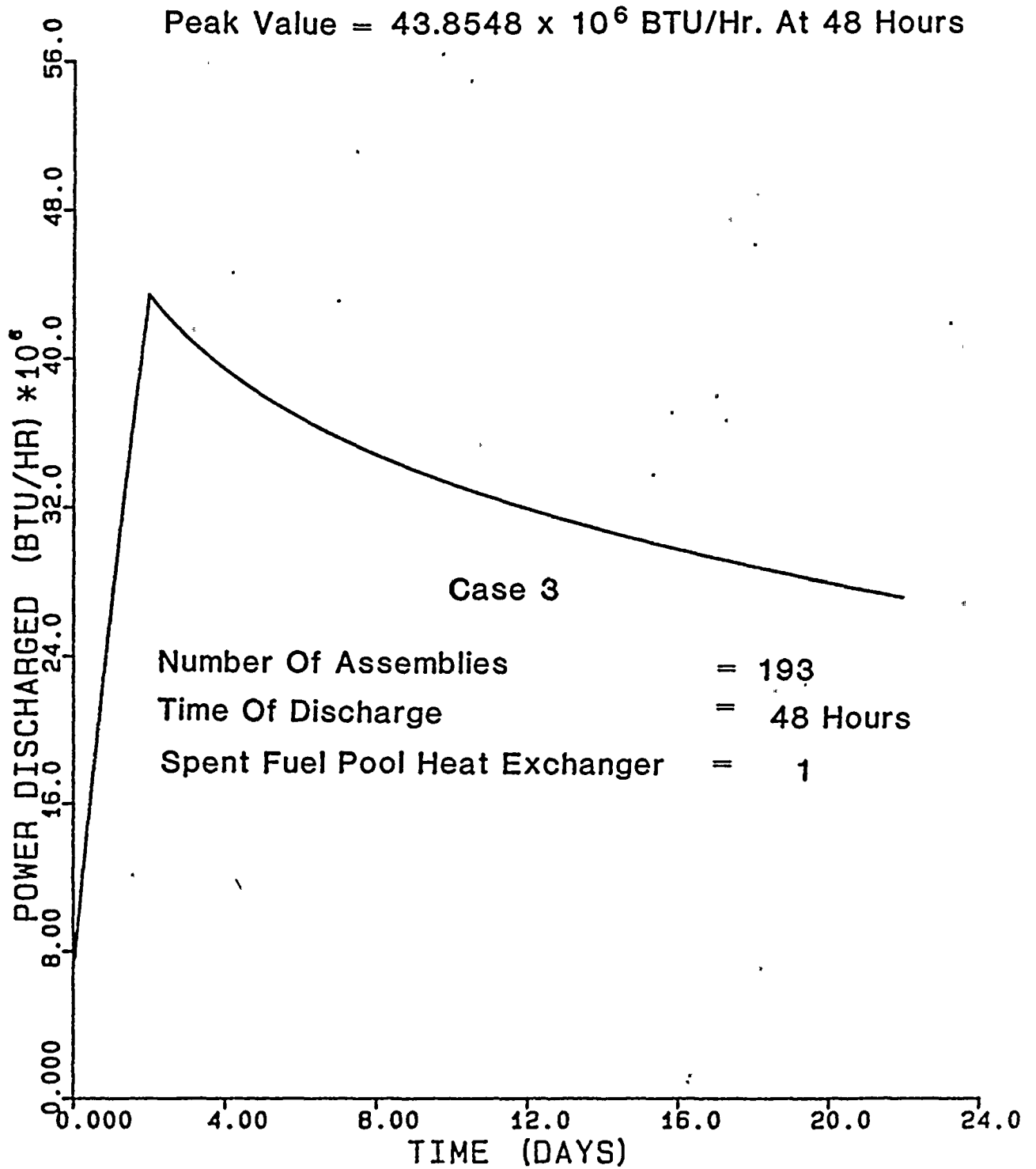


FIGURE 5.3d Power Discharged ; Full Core Discharge



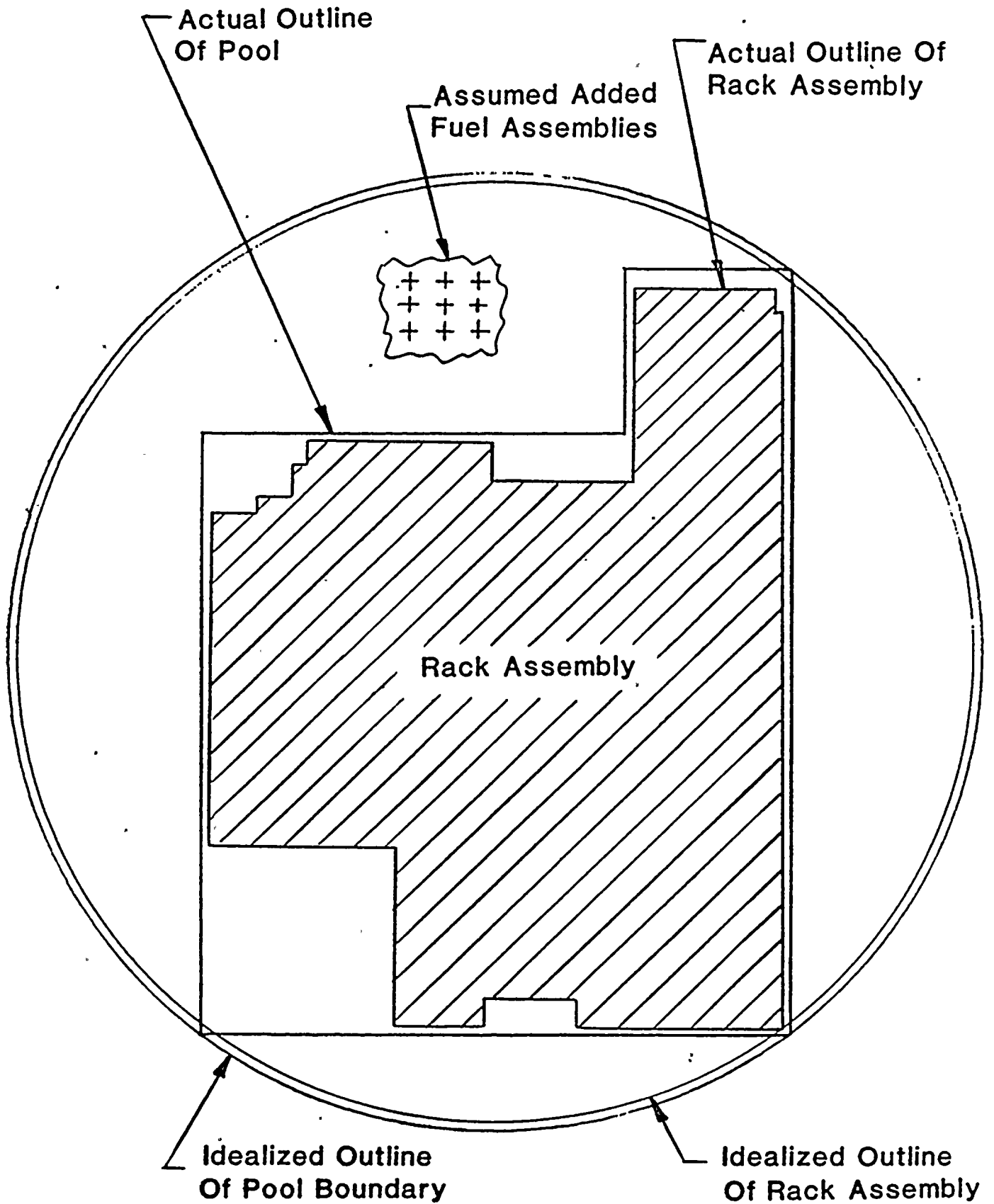


FIGURE 5.4 Idealization Of Rack Assembly



Water Assumed At The
Pool Bulk Temperature

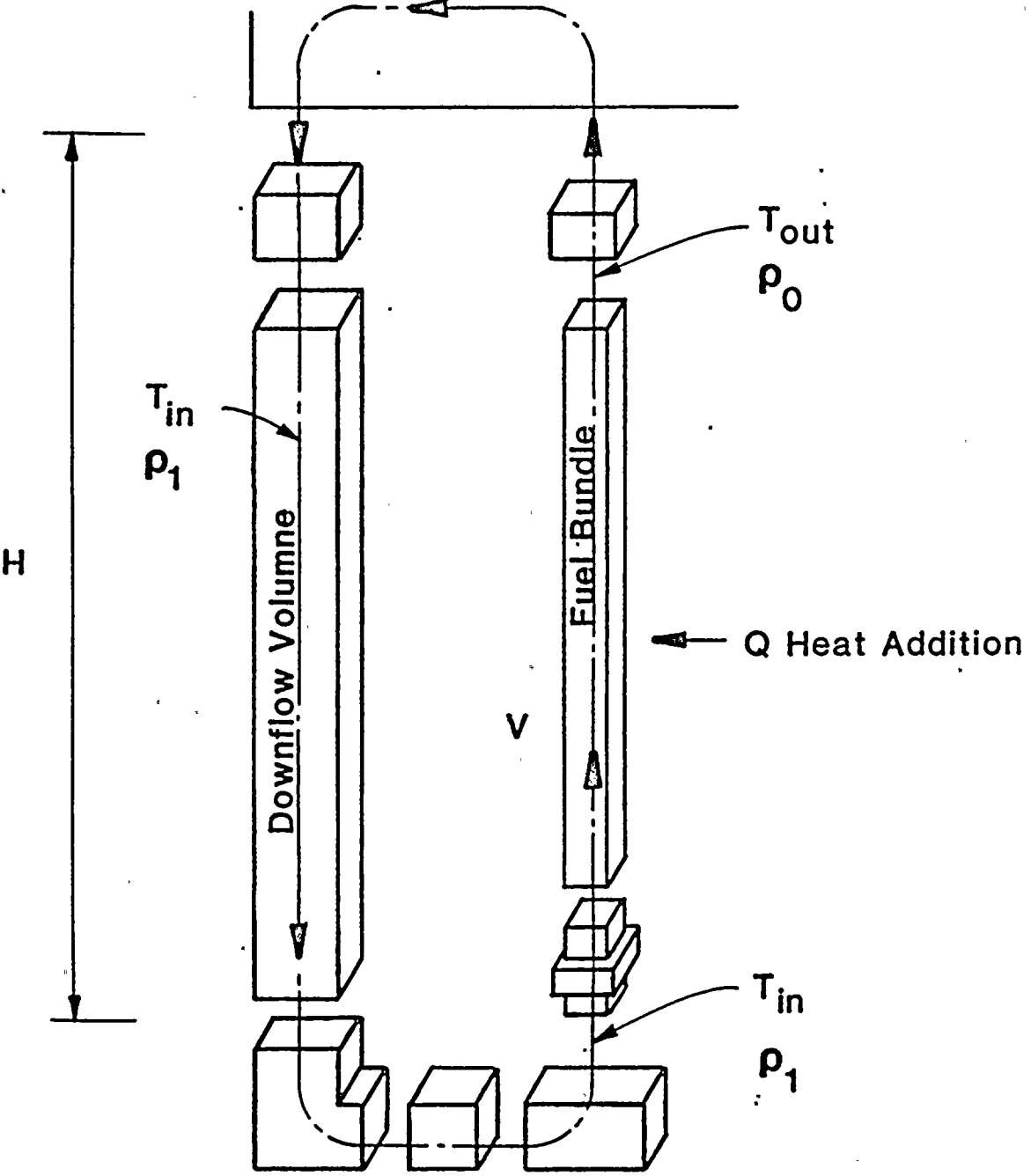


FIGURE 5.5 Thermal Chimney Flow Model



6. STRUCTURAL ANALYSIS

The purpose of this section is to demonstrate the structural adequacy of the spent fuel rack design under normal and accident loading conditions. The method of analysis presented herein uses a time-history integration method similar to that previously used in the Licensing Reports on High Density Fuel Racks for Fermi II (Docket No. 50-341), Quad Cities I and II (Docket Nos. 50-254 and 50-265), Rancho Seco (Docket No. 50-312), Grand Gulf Unit 1 (Docket No. 50-416), Oyster Creek (Docket No. 50-219), and V.C. Summer (Docket No. 50-395). The results show that the high density spent fuel racks are structurally adequate to resist the postulated stress combinations associated with level A, B, C, and D conditions as defined in References 1 and 2.

6.1 ANALYSIS OUTLINE

The spent fuel storage racks are Seismic Category I equipment. Thus, they are required to remain functional during and after an SSE (Safe Shutdown Earthquake) (Ref. 3). As noted previously, these racks are neither anchored to the pool floor nor attached to the side walls. The individual rack modules are not interconnected. Furthermore, a particular rack may be completely loaded with fuel assemblies (which corresponds to greatest rack inertia), or it may be completely empty. The coefficient of friction, μ , between the supports and pool floor is another indeterminate factor. According to Rabinowicz (Ref. 4) the results of 199 tests performed on austenitic stainless steel plates submerged in water show a mean value of μ to be 0.503 with a standard deviation of 0.125. The upper and lower bounds (based on twice the standard deviation) are thus 0.753 and 0.253, respectively. Two separate analyses are performed for the rack assemblies with values of the coefficient of friction equal to 0.2 (lower limit) and 0.8 (upper limit), respectively. The following analyses are performed for the geometrically limiting rack modules:



- O Fully loaded rack (all storage locations occupied),
 $\mu = 0.8; 0.2$ ($\mu =$ coefficient of friction)
- O Nearly empty rack $\mu = 0.8, 0.2$
- O Rack half full, $\mu = 0.8$

The method of analysis employed is the time-history method. The pool slab acceleration data were developed by the Pacific Gas and Electric Company, San Francisco, California.

The objective of the seismic analysis is to determine the structural response (stresses, deformation, rigid body motion, etc.) due to simultaneous application of the three orthogonal excitations. Thus, recourse to approximate statistical summation techniques such as the "Square-Root-of-the-Sum-of-the-Squares" method (Ref. 5) is avoided. For nonlinear analysis, the only practical method is simultaneous application.

Pool slab acceleration data are provided for three earthquakes: Design Earthquake (DE), Double Design Earthquake (DDE), and Hosgri Earthquake (HE). The rack specifications require design for conditions including the DE and using the more severe of DDE or HE. Studies performed on a typical rack module show that displacements and stresses are more severe using the Hosgri seismic event; therefore, all subsequent references herein refer to imposing the HE on the rack structures. The Hosgri seismic time-history has a peak "g" level that is much higher than the DDE condition. Figures 6.1.1-6 show the time-histories used for the analyses.

The seismic analysis is performed in three steps, namely:

1. Development of a nonlinear dynamic model consisting of inertial mass elements and gap and friction elements.



2. Generation of the equations of motion and inertial coupling and solution of the equations using the "component element time integration scheme" (References 6 and 7) to determine nodal forces and displacements
3. Computation of the detailed stress field in the rack (at the critical location) and in the support legs using the nodal forces calculated in the previous step. These stresses are checked against the design limits given in Section 6.5.

A brief description of the dynamic model follows.

6.2 FUEL RACK - FUEL ASSEMBLY MODEL

Since the racks are not anchored to the pool slab or attached to the pool walls or to each other, they can execute a wide variety of rigid body motions. For example, the rack may slide on the pool floor (so-called "sliding condition"); one or more legs may momentarily lose contact with the liner ("tipping condition"); or the rack may experience a combination of sliding and tipping conditions. The structural model should permit simulation of these kinematic events with inherent built-in conservatism. Since the Diablo Canyon racks are equipped with girdle bars to dissipate energy by inter-rack impact, it is also necessary to model the impact phenomena in a conservative manner. Similarly, the lift off of the support legs and subsequent impacts must be modelled using appropriate impact elements, and the Coulomb friction between the rack and the pool liner must be simulated by suitably piecewise linear springs. These special attributes of the rack dynamics require a strong emphasis on the modeling of the linear and nonlinear springs, dampers, and stop elements. The model outline in the remainder of this section, and the model description in the following section describe the detailed modeling technique to simulate these effects, with emphasis placed on the nonlinearity of the rack seismic response.



6.2.1 Outline of Model

- a. The fuel rack structure is a folded metal plate assemblage welded to a baseplate and supported on four legs. The rack structure itself is a very rigid structure. Dynamic analysis of typical multicell racks has shown that the motion of the structure is captured almost completely by the behavior of a six degrees-of-freedom structure; therefore, the movement of the rack cross-section at any height is described in terms of the six degrees-of-freedom of the rack base.
- b. The seismic motion of a fuel rack is characterized by random rattling of fuel assemblies in their individual storage locations. Assuming that all assemblies vibrate in phase obviously exaggerates the computed dynamic loading on the rack structure. This assumption, however, greatly reduces the required degree-of-freedom for modeling the fuel assemblies which are represented by two lumped masses. One mass is located at the top of the rack, while the second mass is at the rack base. The centroid of the fuel assembly mass can be located, relative to the rack structure centroid at that level, so as to simulate a partially loaded rack.
- c. The local flexibility of the rack-support interface is modeled conservatively in the analysis.
- d. The rack base support may slide or lift off the pool floor.
- e. The pool floor has a specified time-history of seismic accelerations along the three orthogonal directions.
- f. Fluid coupling between rack and assemblies, and between rack and adjacent racks, is simulated by introducing



appropriate inertial coupling into the system kinetic energy. Inclusion of these effects uses the methods of References 4 and 6 for rack/assembly coupling and for rack/rack coupling (see Section 6.2.3 of this report).

- g. Potential impacts between rack and assemblies are accounted for by appropriate "compression only" gap elements between masses involved.
- h. Fluid damping between rack and assemblies, and between rack and adjacent rack, is conservatively neglected.
- i. The supports are modeled as "compression only" elements for dynamic analysis. The bottom of a support leg is attached to a frictional spring as described in Section 6.2.2. The cross-section inertial properties of the support legs are computed and used in the final computations to determine support leg stresses.
- j. The effect of sloshing can be shown to be negligible at the bottom of a pool and is hence neglected.
- k. Inter-rack impact, if it occurs, is simulated by gap elements at the top and bottom of the rack in the two horizontal directions at the corners of the rack. The most conservative case of adjacent rack movement is assumed; each adjacent rack is assumed to move completely out of phase with the rack being analyzed.
- l. The form drag opposing the motion of the fuel assemblies in the storage locations is neglected in the results reported herein.
- m. The form drag opposing the motion of the fuel rack in the water is also conservatively neglected in the results reported herein.



- n. The rattling of the fuel assemblies inside the storage locations causes the "gap" between the fuel assemblies and the cell wall to change from a maximum of twice the nominal gap to a theoretical zero gap. However, the fluid coupling coefficients (Ref. 8) utilized are based on linear vibration theory (Ref. 9). Studies in the literature show that inclusion of the nonlinear effect (viz. vibration amplitude of the same order of magnitude as the gap) drastically lowers the equipment response (Ref. 10).

Figure 6.2.1 shows a schematic of the model. Six degrees-of-freedom are used to track the motion of the rack structure. Figures 6.2.2 and 6.2.3, respectively, show the inter-rack impact springs and fuel assembly/storage cell impact springs.

The fuel assemblies are modelled by two lumped masses. The lower mass is assumed to be attached to the baseplate and to move with the baseplate. The upper mass is located at the top of the rack and is free to move in a horizontal plane relative to the rack. Two degrees-of-freedom are used to track the motion of this mass.

6.2.2 Model Description (8 DOF Model)

The absolute degrees-of-freedom associated with each of the mass locations i , i^* are identified in Figure 6.2.1.



Table 6.2.1
DEGREES OF FREEDOM

Location (Node)	Displacement			Rotation		
	u_x	u_y	u_z	θ_x	θ_y	θ_z
1	p ₁	p ₂	p ₃	q ₄	q ₅	q ₆
1*	Point 1* is assumed fixed to base at $X_B, Y_B, Z=0$					
2	Point 2 is assumed attached to rigid rack at the top most point.					
2*	p ₇	p ₈				

$$p_i = q_i(t) + U_i(t)$$

$U_i(t)$ is the pool floor slab displacement seismic time-history. Thus, there are eight degrees-of-freedom in the system. Not shown in Fig. 6.2.1 are the gap elements used to model the support legs and the impacts with adjacent racks.

6.2.3 Fluid Coupling

An effect of some significance requiring careful modeling is the so-called "fluid coupling effect." If one body of mass (m_1) vibrates adjacent to another body (mass m_2), and both bodies are submerged in a frictionless fluid medium, then Newton's equations of motion for the two bodies have the form:

$$(m_1 + M_{11}) \ddot{X}_1 - M_{12} \ddot{X}_2 = \text{applied forces on mass } m_1$$

$$-M_{21} \ddot{X}_1 + (m_2 + M_{22}) \ddot{X}_2 = \text{applied forces on mass } m_2$$

\ddot{X}_1, \ddot{X}_2 denote absolute accelerations of mass m_1 and m_2 , respectively.

$M_{11}, M_{12}, M_{21},$ and M_{22} are fluid coupling coefficients which depend on the shape of the two bodies, their relative



disposition, etc. Fritz (Ref. 6) gives data for M_{ij} for various body shapes and arrangements. It is to be noted that the above equation indicates that the effect of the fluid is to add a certain amount of mass to the body (M_{11} to body 1), and an external force which is proportional to the acceleration of the adjacent body (mass m_2). Thus, the acceleration of one body affects the force field on another. This force is a strong function of the interbody gap, reaching large values for very small gaps. This inertial coupling is called fluid coupling. It has an important effect in rack dynamics. The lateral motion of a fuel assembly inside the storage location will encounter this effect. So will the motion of a rack adjacent to another rack. These effects are included in the equations of motion. The fluid coupling is between nodes 2 and 2* in Figure 6.2.1. Furthermore, the rack equations contain coupling terms which model the effect of fluid in the gaps between adjacent racks. The coupling terms modeling the effects of fluid flowing between adjacent racks are computed assuming that all adjacent racks are vibrating 180° out of phase from the rack being analyzed. Therefore, only one rack is considered surrounded by a hydrodynamic mass computed as if there were a plane of symmetry located in the middle of the gap region.

Finally, fluid virtual mass is included in the vertical direction vibration equations of the rack; virtual inertia is also added to the governing equation corresponding to the rotational degree-of-freedom, $q_6(t)$.

6.2.4 Damping

In reality, damping of the rack motion arises from material hysteresis (material damping), relative intercomponent motion in structures (structural damping), and fluid drag effects (fluid damping). In the analysis, a maximum of 4% structural damping is imposed on elements of the rack structure during HE seismic simulations. This is in accordance with the FSAR and NRC



guidelines (Ref. 11). Material and fluid damping are conservatively neglected. The dynamic model has the provision to incorporate fluid damping effects; however, no fluid damping has been used for this analysis.

6.2.5 Impact

The fuel assembly node 2* may impact the corresponding structural mass node 2. To simulate this impact, four compression-only gap elements around the upper fuel assembly node are provided (see Figure 6.2.3). As noted previously, fluid dampers may also be provided in parallel with the springs. The compressive loads developed in these springs provide the necessary data to evaluate the integrity of the cell wall structure and stored array during the seismic event. Figure 6.2.2 shows the location of the eight impact springs used to simulate any potential for inter-rack impacts. Section 6.4.1 gives more details on these additional impact springs.

6.3 ASSEMBLY OF THE DYNAMIC MODEL

The cartesian coordinate system associated with the rack has the following nomenclature:

- o x = Horizontal coordinate along the short direction of rack rectangular platform
- o y = Horizontal coordinate along the long direction of the rack rectangular platform
- o z = Vertically upward

As described in the preceding section, the rack, along with the base, supports, and stored fuel assemblies, is modeled for the general three-dimensional (3-D) motion simulation by an eight-



degree-of-freedom model. To simulate the impact and sliding phenomena expected, 24 nonlinear gap elements and 16 nonlinear friction elements are used. Gap and friction elements, with their connectivity and purpose, are presented in Table 6.3.1.

If the simulation model is restricted to two dimensions (one horizontal motion plus vertical motion, for example) for the purposes of model clarification only, then a descriptive model of the simulated structure which includes all necessary gap and friction elements is shown in Figure 6.3.1.

The impacts between fuel assemblies and rack show up in the gap elements, having local stiffness K_I , in Figure 6.3.1. In Table 6.3.1, these elements are gap elements 7 and 8. The support leg spring rates K_δ are modeled by elements 1 and 4 and 2 and 3 in Table 6.3.1 for the 2-D case. Note that the local compliance of the concrete floor may be included in K_δ . To simulate sliding potential, friction elements 2 plus 8 and 4 plus 6 (Table 6.2) are shown in Figure 6.3.1. The friction of the support/liner interface is modeled by a piecewise linear spring with a suitably large stiffness K_f up to the limiting lateral load, μN , where N is the current compression load at the interface between support and liner. At every time step during the transient analysis, the current value of N (either zero for liftoff condition, or a compressive finite value) is computed. Finally, the support rotational friction springs K_R reflect any rotational restraint that may be offered by the foundation. This spring rate is calculated using a modified Bousinesq equation (Ref. 4) and is included to simulate the resistive moment of the support to counteract rotation of the rack leg in a vertical plane. This rotation spring is also nonlinear, with a zero spring constant value assigned after a certain limiting condition of slab moment loading is reached.

The nonlinearity of these springs (friction elements 9 plus 15 and 11 plus 13 in Table 6.3.1) reflects the edging limitation imposed



Table 6.3.1

NUMBERING SYSTEM FOR GAP ELEMENTS AND FRICTION ELEMENTS

I. Nonlinear Springs (Gap Elements) (24 total)

<u>Number</u>	<u>Node Location</u>	<u>Description</u>
1	Support S1	Z compression only element
2	Support S2	Z compression only element
3	Support S3	Z compression only element
4	Support S4	Z compression only element
5	2,2*	X rack/fuel assembly impact element
6	2,2*	X rack/fuel assembly impact element
7	2,2*	Y rack/fuel assembly impact element
8	2,2*	Y rack/fuel assembly impact element
9	Top cross-section of rack (corners)	Inter-rack impact elements
10		Inter-rack impact elements
11		Inter-rack impact elements
12		Inter-rack impact elements
13		Inter-rack impact elements
14		Inter-rack impact elements
15		Inter-rack impact elements
16		Inter-rack impact elements
17	Bottom cross-section of rack (corners)	Inter-rack impact elements
18		Inter-rack impact elements
19		Inter-rack impact elements
20		Inter-rack impact elements
21		Inter-rack impact elements
22		Inter-rack impact elements
23		Inter-rack impact elements
24		Inter-rack impact elements

II. Friction Elements (16 total)

<u>Number</u>	<u>Node Location</u>	<u>Description</u>
1	Support S1	X direction support friction
2	Support S1	Y direction friction
3	Support S2	X direction friction
4	Support S2	Y direction friction
5	Support S3	X direction friction
6	Support S3	Y direction friction
7	Support S4	X direction friction
8	Support S4	Y direction friction
9	S1	X Slab moment
10	S1	Y Slab moment
11	S2	X Slab moment
12	S2	Y Slab moment
13	S3	X Slab moment
14	S3	Y Slab moment
15	S4	X Slab moment
16	S4	Y Slab moment



on the base of the rack support legs. In this analysis, this effect is neglected; any support leg bending, induced by liner/baseplate friction forces, is resisted by the leg acting as a beam cantilevered from the rack baseplate.

The spring rate K_δ modeling the effective compression stiffness of the structure in the vicinity of the support, is computed from the equation:

$$\frac{1}{K_\delta} = \frac{1}{K_1} + \frac{1}{K_2} + \frac{1}{K_3}$$

where:

K_1 = spring rate of the support leg treated as a tension-compression member = $E_{\text{SUPPORT}} A_{\text{SUPPORT}}/h$
(h = length of support leg)

K_2 = $1.05E_c B/(1-\nu^2)$ = local spring rate of pool slab
(E_c = Young's modulus of concrete, and B = length of bearing surface)

K_3 = spring rate of folded plate cell structure above support leg (same form as K_2 with E chosen to reflect the local stiffness of the honeycomb structure above the leg)

For the 3-D simulation, all support elements (listed in Table 6.3.1) are included in the model. Coupling between the two horizontal seismic motions is provided both by the offset of the fuel assembly group centroid which causes the rotation of the entire rack and by the possibility of liftoff of one or more support legs. The potential exists for the rack to be supported on one or more support legs or to liftoff completely during any instant of a complex 3-D seismic event. All of these potential events may be simulated during a 3-D motion and have been observed in the results.



6.4 TIME INTEGRATION OF THE EQUATIONS OF MOTION

6.4.1 Time-history Analysis Using 8 DOF Rack Model

Having assembled the structural model, the dynamic equations of motion corresponding to each degree-of-freedom can be written by using Newton's second law of motion; or by using Lagrange's equation. The system of equations can be represented in matrix notation as:

$$[M] \{q\} = [Q] + \{G\}$$

where the vector $[Q]$ is a function of nodal displacements and velocities, and $\{G\}$ depends on the coupling inertia and the ground acceleration. Premultiplying the above equations by $[M]^{-1}$ renders the resulting equation uncoupled in mass.

We have: $\{q\} = [M]^{-1} [Q] + [M]^{-1} \{G\}$

As noted earlier, in the numerical simulations run to verify structural integrity during a seismic event, all elements of the fuel assemblies are assumed to move in phase. This will provide maximum impact force level, and induce additional conservatism in the time-history analysis.

This equation set is mass uncoupled, displacement coupled, and is ideally suited for numerical solution using the central difference scheme. The computer program "DYNAHIS"* is utilized for this purpose.

* This code has been previously utilized in licensing of similar racks for Fermi II (Docket No. 50-341), Quad Cities I and II (Docket Nos. 50-254 and 265), Rancho Seco (Docket No. 50-312), Oyster Creek (Docket No. 50-219), and V.C. Summer (Docket No. 50-395).



Stresses in various portions of the structure are computed from known element forces at each instant of time.

Dynamic analysis of typical multicell racks has shown that the motion of the structure is captured almost completely by the behavior of a six-degree-of-freedom structure; therefore, in this analysis model, the movement of the rack cross-section at any height is described in terms of the rack base degrees-of-freedom ($q_1(t), \dots, q_6(t)$). The remaining degrees-of-freedom are associated with horizontal movements of the fuel assembly masses. In this dynamic model, a single lumped mass is used to represent fuel assembly movement. Therefore, the final dynamic model consists of six degrees-of-freedom for the rack plus two additional mass degrees-of-freedom for the one fuel mass. The single lumped mass, used to represent the fuel assembly vibrating mass, is located at the top of the rack to obtain the maximum moment during impacts. The effective mass of a single impacting body is chosen so as to yield the same angular momentum at the base of the rack as would be obtained by the continuous rod-like fuel assembly structure. The remaining portion of the fuel assembly mass is assumed to move with the rack base. Thus, the totality of fuel mass is included in the simulation.

6.4.2 Evaluation of Potential for Inter-rack Impact

Verification runs to establish the viability of the 8 DOF rack model and the representation of fuel assembly mass motion by 2 DOF have been carried out. The verification has been made by comparing the results with the output of a 32 DOF model. Verification is established by showing that the 8 DOF model gives the same level for critical displacements and stresses as does the 32 DOF model that includes rack elasticity and representation of fuel mass



motion by several vibrating masses. During these verification runs, it became apparent that due to the high level of slab acceleration associated with the Hosgri event, inter-rack impact could be anticipated to occur, especially for low values of the friction coefficient between the support and the pool liner. To account for this potential, yet still retain the simplicity of simulating only a single rack, gap elements were located at the corners of the rack at the top and at the baseplate. Figure 6.2.2 shows the location of these gap elements. Loads in these elements, computed during the dynamic analysis, are used to assess rack integrity if inter-rack impact occurs. The 8 DOF model is used to avoid possible numerical problems due to the large number of nonlinear elements that would be required to model inter-rack impact with the 32 DOF model.

6.5 STRUCTURAL ACCEPTANCE CRITERIA

There are two sets of criteria to be satisfied by the rack modules:

a. Kinematic Criterion

This criterion seeks to ensure that the rack is a physically stable structure. Diablo Canyon racks are designed to sustain certain inter-rack impact at designated locations in the rack modules. Therefore, physical stability of the rack is considered along with the localized inter-rack impacts. Localized permanent deformation of the module is permissible, so long as the minimum flux-trap gap in the active fuel region is not violated.



b. Stress Limits

The stress limits of the ASME Code, Section III, Subsection NF, 1983 Edition are used since this code provides the most appropriate and consistent set of limits for various stress types and various loading conditions. The following loading combinations are applicable (Ref. 1).

<u>Loading Combination</u>	<u>Stress Limit</u>
D	Level A service limits
D + T ₀	
D + T ₀ + E	
D + T _a + E	Level B service limits
D + T ₀ + P _f	
D + T _a + E'	Level D service limits The functional capability of the fuel racks should be demonstrated
D + F _d	

where:

- D = Dead weight-induced stresses (including fuel assembly weight)
- F_d = Force caused by the accidental drop of the heaviest load from the maximum possible height
- P_f = Upward force on the racks caused by postulated stuck fuel assembly
- E = Design Earthquake
- E' = Hosgri Earthquake
- T₀ = Differential temperature induced loads (normal or upset condition)
- T_a = Differential temperature induced loads. (abnormal design conditions)



The conditions T_a and T_o cause local thermal stresses to be produced. The worst situation will be obtained when an isolated storage location has a fuel assembly which is generating heat at the maximum postulated rate. The surrounding storage locations are assumed to contain no fuel. The heated water makes unobstructed contact with the inside of the storage walls, thereby producing the maximum possible temperature difference between the adjacent cells. The secondary stresses thus produced are limited to the body of the rack; that is, the support legs do not experience the secondary (thermal) stresses.

6.6 MATERIAL PROPERTIES

The data on the physical properties of the rack and support materials, obtained from the ASME Boiler & Pressure Vessel Code, Section III, appendices, and supplier's catalog, are listed in Tables 6.6.1 and 6.6.2. Since the maximum pool bulk temperature (except for the full core discharge case) is 140°-147°F, 150° is used as the reference design temperature for evaluation of material properties.

Table 6.6.1
RACK MATERIAL DATA

<u>Property</u>	<u>Young's Modulus E (psi)</u>	<u>Yield Strength S_y (psi)</u>	<u>Ultimate Strength S_u (psi)</u>
Value	27.9 x 10 ⁶	23150	68100
Section III Reference	Table I-6.0	Table I-2.2	Table I-3.2



Table 6.6.2

SUPPORT MATERIAL DATA

<u>Material</u>	<u>Young's Modulus</u>	<u>Yield Strength</u>	<u>Ultimate Strength</u>
1 ASTM 479-S21800 (top part of support)	27.9×10^6	44,900 psi	94,350 psi
2 SA564-630 (hardened at 1075°F) (bottom part of support)	27.9×10^6	101,040 psi	145,000 psi
Section III Reference	I-6.0	I-2.2	I-3.1

6.7 STRESS LIMITS FOR VARIOUS CONDITIONS

The following stress limits are derived from the guidelines of the ASME Code, Section III, Subsection NF, in conjunction with the material properties data of the preceding section.

6.7.1 Normal and Upset Conditions (Level A or Level B)

- a. Allowable stress in tension on a net section
 $= F_t = 0.6 S_y$ or
 $F_t = (0.6) (23,150) = 13,890$ psi (rack material)
 F_t = is equivalent to primary membrane stresses
 $F_t = (.6)(44,900) = 26,940$ psi for upper part of
support feet)
 $= (.6) (101040) = 60,624$ psi for lower part of
support feet
- b. On the gross section, allowable stress in shear is:
 $F_v = 0.4 S_y$
 $(0.4) (23,150) = 9,260$ psi (main rack body)
 $F_t = (.4)(44,900) = 17,960$ psi (for upper part of
support feet)
 $= (.4) (101040) = 40416$ psi



c. Allowable stress in compression, F_a :

$$F_a = \frac{[1 - (\frac{kl}{r})^2] 2C_c^2 S_y}{(\frac{5}{3}) + [3 (\frac{kl}{r})^2 8C_c] - [(\frac{kl}{r})^3 8C_c^3]}$$

where:

$$C_c = \left[\frac{(2\pi^2 E)}{S_y} \right]^{1/2}$$

kl/r for the main rack body is based on the full height and cross section of the honeycomb region. Substituting numbers, we obtain, for both support leg and honeycomb region:

$$\begin{aligned} F_a &= 13,890 \text{ psi (main rack body)} \\ F_a &= 26,940 \text{ psi (support legs - upper part)} \\ &= 60,624 \text{ psi (support legs - lower part)} \end{aligned}$$

d. Maximum allowable bending stress at the outermost fiber due to flexure about one plane of symmetry:

$$\begin{aligned} F_b &= 0.60 S_y = 13,890 \text{ psi (rack body)} \\ F_b &= 26,940 \text{ psi (support legs - upper part)} \\ &= 60,624 \text{ psi (support legs - lower part)} \end{aligned}$$

e. Combined flexure and compression:

$$\frac{f_a}{F_a} + \frac{C_{mx} f_{bx}}{D_x F_{bx}} + \frac{C_{my} f_{by}}{D_y F_{by}} < 1$$

where:

$$\begin{aligned} f_a &= \text{Direct compressive stress in the section} \\ f_{bx} &= \text{Maximum flexural stress along y-axis} \end{aligned}$$



f_{by} = Maximum flexural stress along y-axis

$$C_{mx} = C_{my} = 0.85$$

$$D_x = 1 - \frac{f_a}{F'_{ex}}$$

$$D_y = 1 - \frac{f_a}{F'_{ey}}$$

where:

$$F'_{ex,ey} = \frac{12\pi^2 E}{23 \left(\frac{kl_{bx,y}}{r_{bx,y}} \right)^2}$$

and the subscripts x,y reflect the particular bending plane of interest.

f. Combined flexure and compression (or tension):

$$\frac{f_a}{0.6 S_y} + \frac{f_{bx}}{F_{bx}} + \frac{f_{by}}{F_{by}} < 1.0$$

The above requirement should be met for both the direct tension or compression case.

6.7.2 Level D Service Limits

F-1370 (Section III, Appendix F), states that the limits for the Level D condition are the minimum of 1.2 (S_y/F_t) or ($0.7S_u/F_t$) times the corresponding limits for Level A condition. Since 1.2 S_y is less than 0.7 S_u for the rack material and for the upper part of the support feet, the multiplying factor is 2.0. For the lower part of the support feet, the multiplying factor is 1.67.



Instead of tabulating the results of these six different stresses as dimensioned values, they are presented in a dimensionless form. These so-called stress factors are defined as the ratio of the actual developed stress to its specified limiting value. With this definition, the limiting value of each stress factor is 1.0 for DE and 2.0 or 1.67 for the HE condition.

6.8 RESULTS

Figures 6.1.1, 6.1.2, and 6.1.3 show the pool slab motion in horizontal x, horizontal y, and vertical directions. This motion is for the Hosgri earthquake (HE). Figures 6.1.4, 6.1.5, and 6.1.6 show the corresponding motion for the DE seismic event.

Results are abstracted here for a 10x11 module (the largest module), and for a 6x11 configuration (which is a module with the largest aspect ratio).

A complete synopsis of the analysis of the 6x11 module subject to the Hosgri earthquake motions is presented in a summary table labelled as Table 6.8.1. Table 6.8.1 gives the maximum values of stress factors R_i ($i = 1, 2, 3, 4, 5, 6$). The values given in the tables are the maximum values in time and space (all sections of the rack). Table 6.8.2 gives typical results for a 10x11 rack. The stress factors are defined as:

R_1 = Ratio of direct tensile or compressive stress on a net section to its allowable value (note support feet only support compression)

R_2 = Ratio of gross shear on a net section to its allowable value

R_3 = Ratio of maximum bending stress due to bending about the x-axis to its allowable value for the section



R_4 = Ratio of maximum bending stress due to bending about the y-axis to its allowable value

R_5 = Combined flexure and compressive factor (as defined in 6.7.1e above)

R_6 = Combined flexure and tension (or compression) factor (as defined in 6.7.1f above)

As stated before, the allowable value of R_i ($i = 1, 2, 3, 4, 5, 6$) is 1 for the DE condition and 2 or 1.67 for the HE earthquake.

It is found that the results corresponding to HE are most critical vis-a-vis the corresponding allowable limits. The results given herein are for the Hosgri earthquake. The maximum stress factors (R_i) are below the limiting value for the HE condition for all sections. It is noted that the critical load factors reported for the support feet are all for the upper segment of the foot and are to be compared with the limiting value of 2.0.

Tables 6.8.1 and 6.8.2 also present results which are used to show that significant margins of safety exist against local deformation of the fuel storage cell due to rattling impact of fuel assemblies and against local overstress of impact bars due to inter-rack impact.

Analyses (not included here) have also been carried out for the DE earthquake to demonstrate that load factors are below 1.0. Results obtained for all rack sizes and shapes are enveloped by the data presented herein. Overturning has also been considered for the cases where racks are adjacent to open areas. The tabular results shown assume that the rack metal thicknesses are based on a total metal thickness of 0.08 inch in the cell structure area (Region I configuration). The racks with cell wall metal thicknesses = 0.09 inch will be slightly heavier but will not significantly affect the safety margins since the rack weight is a small fraction of the total dead weight of a fully loaded unit.



Table 6.8.1

SUMMARY OF RESULTS - RACK TYPE 6x11

Run No.	Remarks	Rack/ Rack Impact	Impact Loads (lb)		Load Factors R_i for Rack Base* and for Supports					
			Between Storage Cell/Fuel Assembly	Between Rack to Rack	R_1	R_2	R_3	R_4	R_5	R_6
ee01	Hosgri quake COF = .8, full	Yes	1.360x10 ⁵	0.565x10 ⁵	.091	.114	.185	.126	.258	.291
			5.30x10 ^{5**}	1.75x10 ^{5**}	.198	.233	.640	.342	.844	.962
ee02	Hosgri quake COF = .2, full	Yes	0.991x10 ⁵	0.619x10 ⁵	.053	.023	.092	.064	.146	.164
					.092	.033	.094	.080	.184	.199
ee03	Hosgri quake COF = .2, 11 cells (simulates near empty rack)	Yes	1.66x10 ⁴	3.77x10 ⁴	.084	.035	.173	.119	.212	.238
					.146	.052	.143	.124	.271	.293
ee04	Hosgri quake COF = .8, 11 cells (simulates near empty rack)	Yes	2.300x10 ⁴	3.950x10 ⁴	.057	.059	.064	.076	.212	.239
					.143	.151	.415	.244	.705	.800

* Upper set of values in each column are load factors for rack base (1.0 allowable); lower set of values are similar maximum load factors for support feet (2.0 allowable). (The upper part of the support feet have the more critical load levels; the lower support feet locations have much lower load factors which meet the required 1.67 HE level limit with significant margin.)

** Allowable impact value with a factor of safety of 2 over the load which would initiate plastic action.



Table 6.8.1 (continued)

SUMMARY OF RESULTS - RACK TYPE 6x11

Run No.	Remarks	Rack/ Rack Impact	Impact Loads (lb)		Load Factors R_i for Rack Base* and for Supports					
			Between Storage Cell/Fuel Assembly	Between Rack to Rack	R_1	R_2	R_3	R_4	R_5	R_6
ee05	Hosgri quake COF = .8 half full in positive Y half	Yes	6.0×10^4	5.210×10^4	.069	.097	.167	.087	.243	.273
					.163	.229	.524	.629	.876	1.00



Table 6.8.2

SUMMARY OF RESULTS - RACK TYPE 10x11

Run No.	Remarks	Rack/ Rack Impact	Impact Loads (lb)		Load Factors R_i for Rack Base* and for Supports					
			Between Storage Cell/Fuel Assembly	Between Rack to Rack	R_1	R_2	R_3	R_4	R_5	R_6
aa001	Hosgri EQ COF = .8 Full fuel load	Yes	2.494×10^5	$.714 \times 10^5$.119	.092	.146	.136	.232	.263
			$8.830 \times 10^{5**}$	$1.75 \times 10^{5**}$.262	.277	.659	.687	1.30	1.48
aa002	Hosgri EQ COF = .2 Full fuel load	Yes	2.426×10^5	6.770×10^4	.053	.022	.072	.057	.148	.164
					.140	.051	.141	.112	.300	.327
acorn 10	Hosgri EQ Corner rack COF = .8 Full fuel load	Yes	2.497×10^5	7.630×10^4	.122	.156	.231	.134	.323	.364
					.342	.389	1.07	.731	1.47	1.66
acorn 12	Hosgri EQ Corner rack COF = .2 Full fuel load	Yes	2.127×10^5	2.737×10^4	.051	.023	.081	.065	.147	.164
				max. movement 2.79 in. toward wall	.149	.051	.141	.120	.314	.343

* Upper set of values in each row are load factors for rack base (1.0 allowable); lower set of values are similar maximum load factors for support feet (2.0 allowable). (The upper part of the support feet have the more critical load levels; the lower support feet locations have much lower load factors which meet the limiting HE load factor of 1.67 with significant margin.)

** Allowable impact value with a factor of safety of 2 over the load which would initiate plastic action.





6.9 IMPACT ANALYSES

6.9.1 Impact Loading Between Fuel Assembly and Cell Wall

The local stress in a cell wall is estimated from peak impact loads obtained from the dynamic simulations. Plastic analysis is used to obtain the limiting impact load that can be tolerated. Including a safety margin of 2.0, we find that the total limit load for the number of cells (NC) is:

<u>NC</u>	<u>Limit Load (lb)</u>
66	530100
110	883501

From the results of the dynamic analyses, we find the actual impact loads do not exceed 251,000 lb for NC = 110 and do not exceed 136,000 lb for NC = 66.

6.9.2 Impacts Between Adjacent Racks

All of the dynamic analyses assume, conservatively, that adjacent racks move completely out of phase. Thus, the highest potential for inter-rack impact is achieved. Based on the dynamic loads obtained in the gap elements simulating adjacent racks, we can study rack integrity in the vicinity of the impact point. The use of high-yield stress framing material around the top of the rack allows us to permit impact loads of up to 175,000 lb. The maximum reported value in the tables in this report is 71,400 lb. Thus, impacts between racks can be accommodated without violating rack integrity. We also study the case where the corner of one rack impacts an adjacent rack away from a corner. We show, under such a condition, that the stress levels remain below the yield value.



6.10 WELD STRESSES

The critical weld locations under seismic loading are at the connection of the rack to the baseplate and in the support leg welds. For the rack welds, the allowable weld stress is the ASME Code value of 18,520 psi. For the support legs, the allowable weld stress is 80% of the yield strength (HE conditions) \approx 35,200 psi. The welds at the rack base are fillet welds. Accounting for skip welding in this location, the maximum principal stress is 7151 psi. The support leg weld stress is found to be 27,494 psi under HE conditions, which is less than the allowable value.

Weld stresses due to heating of an isolated hot cell are also computed. The assumption used is that a single cell is heated, over its entire length, to a temperature above the value associated with all surrounding cells. No thermal gradient in the vertical direction is assumed so that the results are conservative. Using the temperatures associated with this unit, we show that the spot welds along the entire cell length do not exceed the allowable value for a thermal loading condition. The maximum computed shear stress in the spot welds, at the most critical location, is less than 6,400 psi under the HE condition.

6.11 SUMMARY OF MECHANICAL ANALYSES

The mathematical model constructed to determine the impact velocity of falling objects is based on several conservative assumptions, such as:

1. The virtual mass of the body is conservatively assumed to be equal to its displaced fluid mass. Evidence in the literature (Ref. 12), indicates that the virtual mass can be many times higher.
2. The minimum frontal area is used for evaluating the drag coefficient.



3. The drag coefficients utilized in the analysis are the lower bound values reported in the literature (Ref. 13). In particular, at the beginning of the fall when the velocity of the body is small, the corresponding Reynolds number is low, resulting in a large drag coefficient.
4. The falling bodies are assumed to be rigid for the purposes of impact stress calculation on the rack. The solution of the immersed body motion problem is found analytically. The impact velocity thus computed is used to determine the maximum stress generated due to stress wave propagation.

With this model, the following analyses are performed:

- a. Dropped Fuel Accident I

A fuel assembly (weight = 1616 pounds with control rod assembly) is dropped from 36 inches above the module and impacts the base. The final velocity of the dropped fuel assembly (just prior to impact) is calculated and, thus, the total energy at impact is known. To study baseplate integrity, we assume that this energy is all directed toward punching of the baseplate in shear and thus transformed into work done by the supporting shear stresses. It is determined that shearing deformation of the baseplate is less than the thickness of the baseplate so that we conclude that local piercing of the baseplate will not occur. Direct impact with the pool liner does not occur. The subcriticality of the adjacent fuel assemblies is not violated.



b. Dropped Fuel Accident II

One fuel assembly drops from 36 inches above the rack and hits the top of the rack. Permanent deformation of the rack is found to be limited to the top region such that the rack cross-sectional geometry at the level of the top of the active fuel (and below) is not altered. The region of local permanent deformation does not extend below 6 inches from the rack top. An energy balance approach is used here to obtain the results.

c. Jammed Fuel-handling Equipment and Horizontal Force

A 4400-pound uplift force and an 1100-pound horizontal force are applied at the top of the rack at the "weakest" storage location; the force is assumed to be applied on one wall of the storage cell boundary as an upward shear force. The plastic deformation is found to be limited to the region well above the top of the active fuel.

These analyses prove that the rack modules are engineered to provide maximum safety against all postulated abnormal and accident conditions.

6.12 Evaluation of Spent Fuel Pool Structure

The spent fuel storage pool for each unit is located on the eastern side of the auxiliary building. The pools are reinforced concrete structures with seam-welded, stainless steel liners. All the walls are 6 feet thick except the one adjacent to the fuel transfer canal which is 5 feet thick. The floor slab is a 5-foot-thick concrete mat founded on bedrock.

The auxiliary building, which includes the pool structures, has been seismically qualified using the criteria outlined in Chapter 3



of the Diablo Canyon FSAR Update. The new high density racks are designed as free-standing with no connection to the walls or the floor slab. Rack reaction loads are applied only to the floor liner and concrete mat via the rack support legs as vertical bearing and horizontal shear loads. The horizontal loads are transferred to bedrock through frictional resistance between the rack support legs and the liner and floor slab; the vertical loads are transferred to bedrock by bearing.

The floor slab and liner have been evaluated and found to be adequate to support and transfer the rack reaction loads. Stresses in the liner plate and the floor slab are within the bearing and shear allowable values. In addition, stresses in the bedrock are within the allowable bearing pressure.

6.13 Definition of Terms Used in Section 6

S1, S2, S3, S4	Support designations
P_i	Absolute degree-of-freedom number i
q_i	Relative degree-of-freedom number i
μ	Coefficient of friction
U_i	Pool floor slab displacement time history in the i -th direction
x, y coordinates	horizontal direction
z coordinate	vertical direction
K_I	Impact spring between fuel assemblies and cell
K_f	Linear component of friction spring
K_δ	Axial spring of support leg locations
N	Compression load in a support foot
K_R	Rotational spring provided by the pool slab
Subscript i	When used with U or X indicates direction ($i = 1$ x-direction, $i = 2$ y-direction, $i = 3$ z-direction)



REFERENCES TO SECTION 6

1. USNRC Standard Review Plan, NUREG-0800 (1981).
2. ASME Boiler & Pressure Vessel Code, Section III, Subsection NF (1983).
3. USNRC Regulatory Guide 1.29, "Seismic Design Classification," Rev. 3, 1978.
4. "Friction Coefficients of Water Lubricated Stainless Steels for a Spent Fuel Rack Facility," Prof. Ernest Rabinowicz, MIT, a report for Boston Edison Company, 1976.
5. USNRC Regulatory Guide 1.92, "Combining Modal Responses and Spatial Components in Seismic Response Analysis," Rev. 1, February 1976.
6. "The Component Element Method in Dynamics with Application to Earthquake and Vehicle Engineering," S. Levy and J.P.D. Wilkinson, McGraw Hill, 1976.
7. "Dynamics of Structures," R.W. Clough and J. Penzien, McGraw Hill (1975).
8. "Mechanical Design of Heat Exchangers and Pressure Vessel Components," Chapter 16, K.P. Singh and A.I. Soler, Arcturus Publishers, Inc., 1984.
9. R.J. Fritz, "The Effects of Liquids on the Dynamic Motions of Immersed Solids," Journal of Engineering for Industry, Trans. of the ASME, February 1972, pp 167-172.
10. "Dynamic Coupling in a Closely Spaced Two-Body System Vibrating in Liquid Medium: The Case of Fuel Racks," K.P. Singh and A.I. Soler, 3rd International Conference on Nuclear Power Safety, Keswick, England, May 1982.
11. USNRC Regulatory Guide 1.61, "Damping Values for Seismic Design of Nuclear Power Plants," 1973.
12. "Flow Induced Vibration," R.D. Blevins, VonNostrant (1977).
13. "Fluid Mechanics," M.C. Potter and J.F. Foss, Ronald Press, p 459 (1975).



6-33

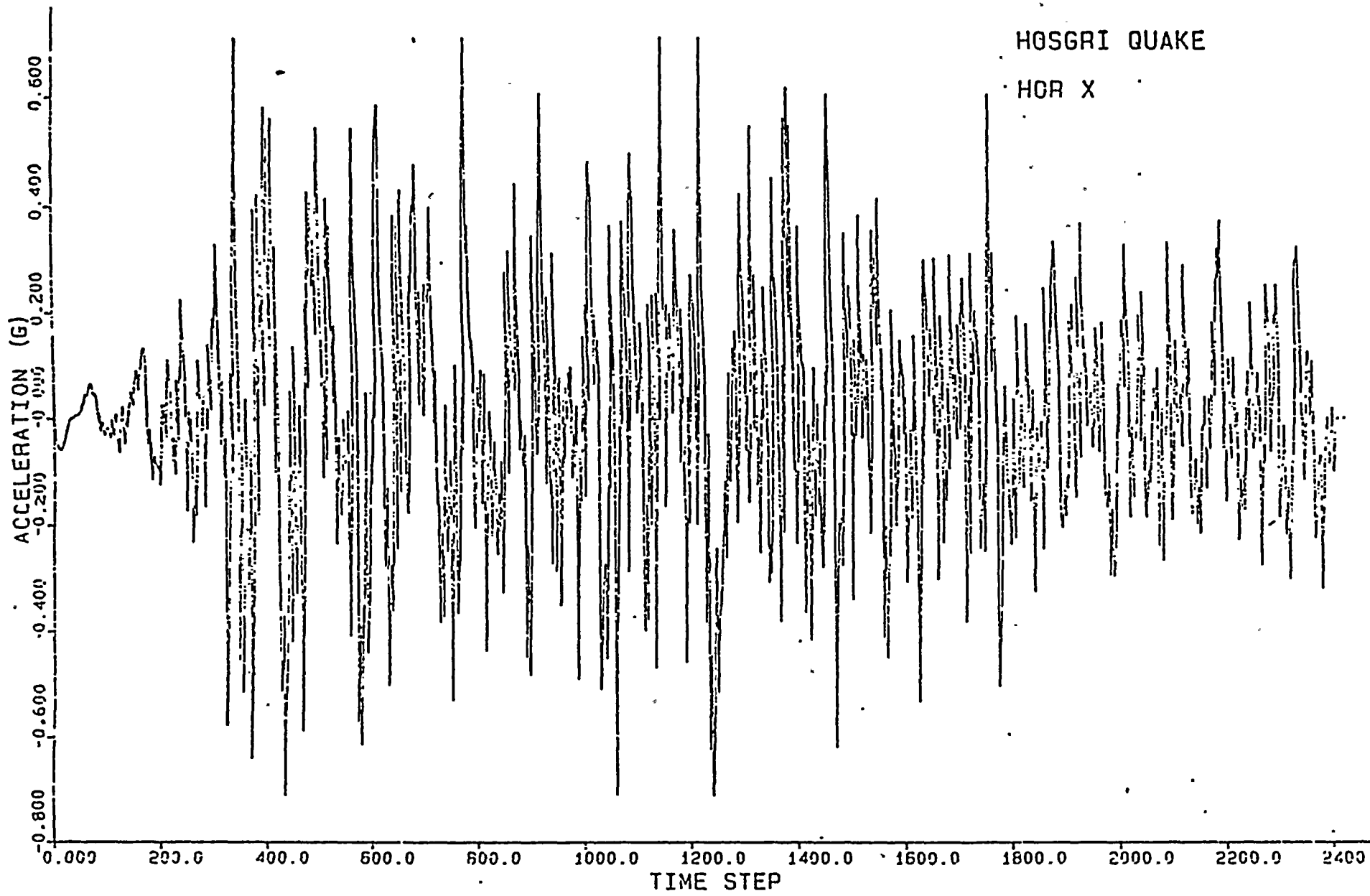


FIGURE 6.1.1



6-34

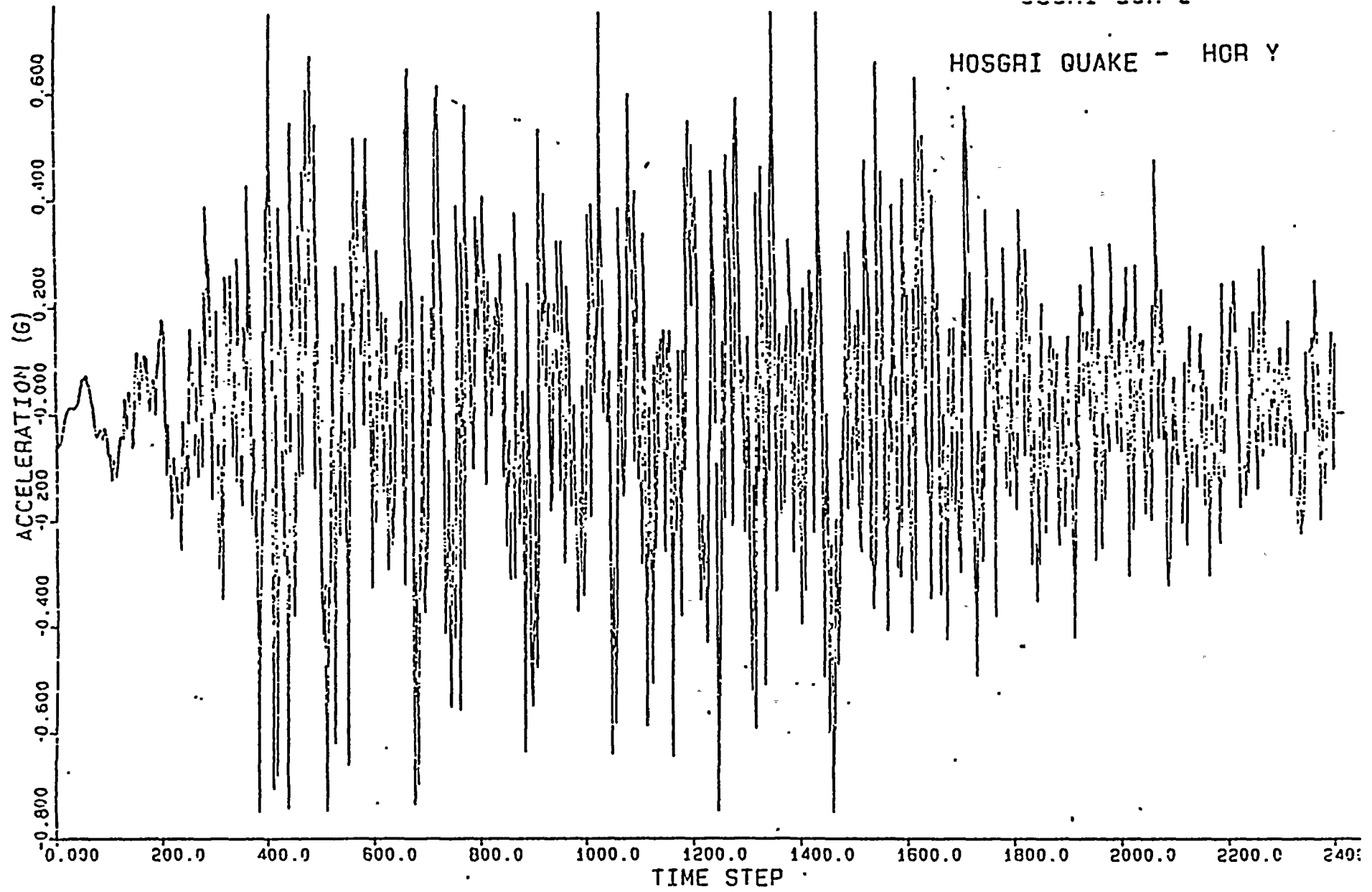


FIGURE 6.1.2



SE-9

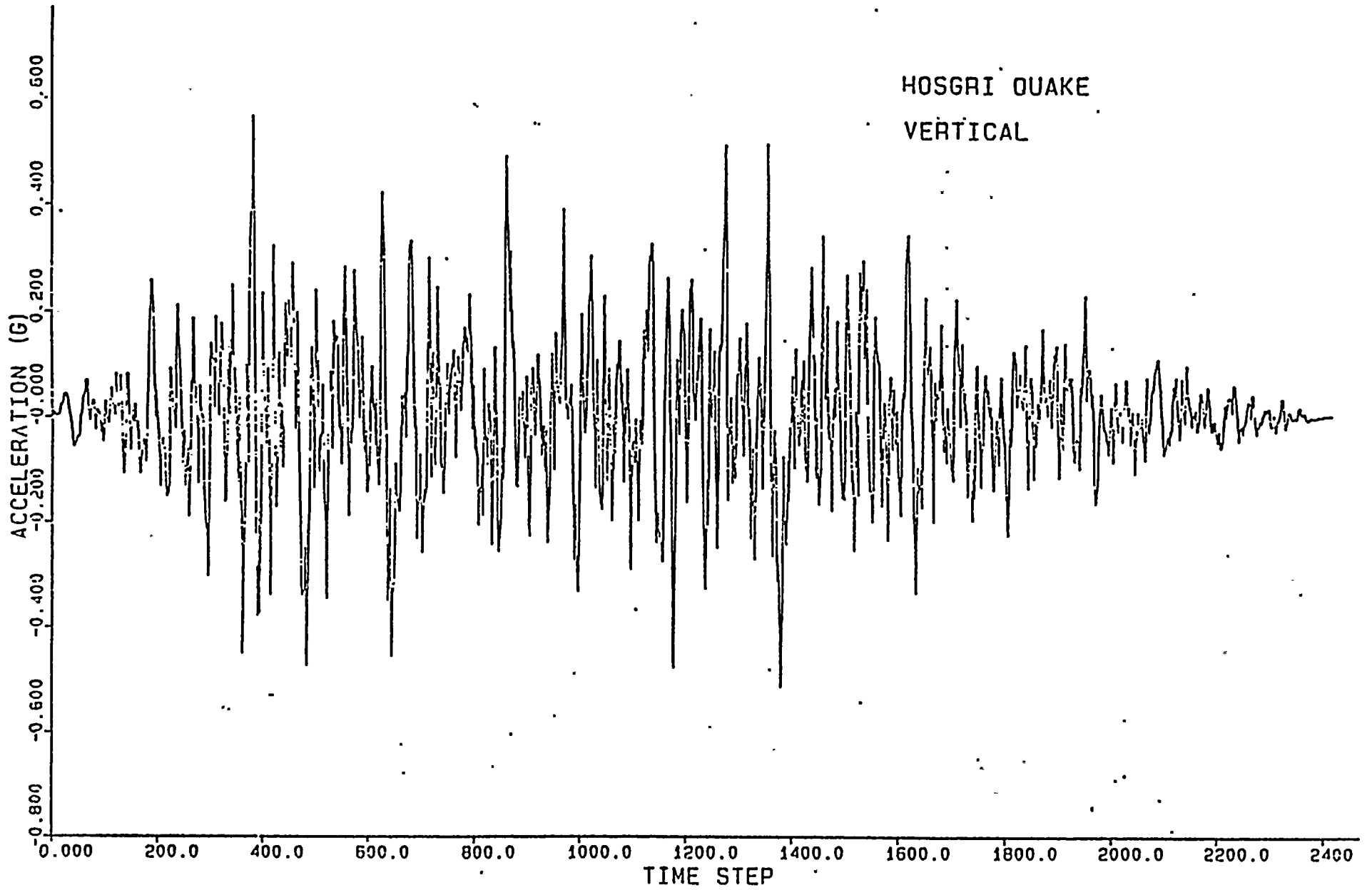


FIGURE 6.1.3



OBE QUAKE

HOR X

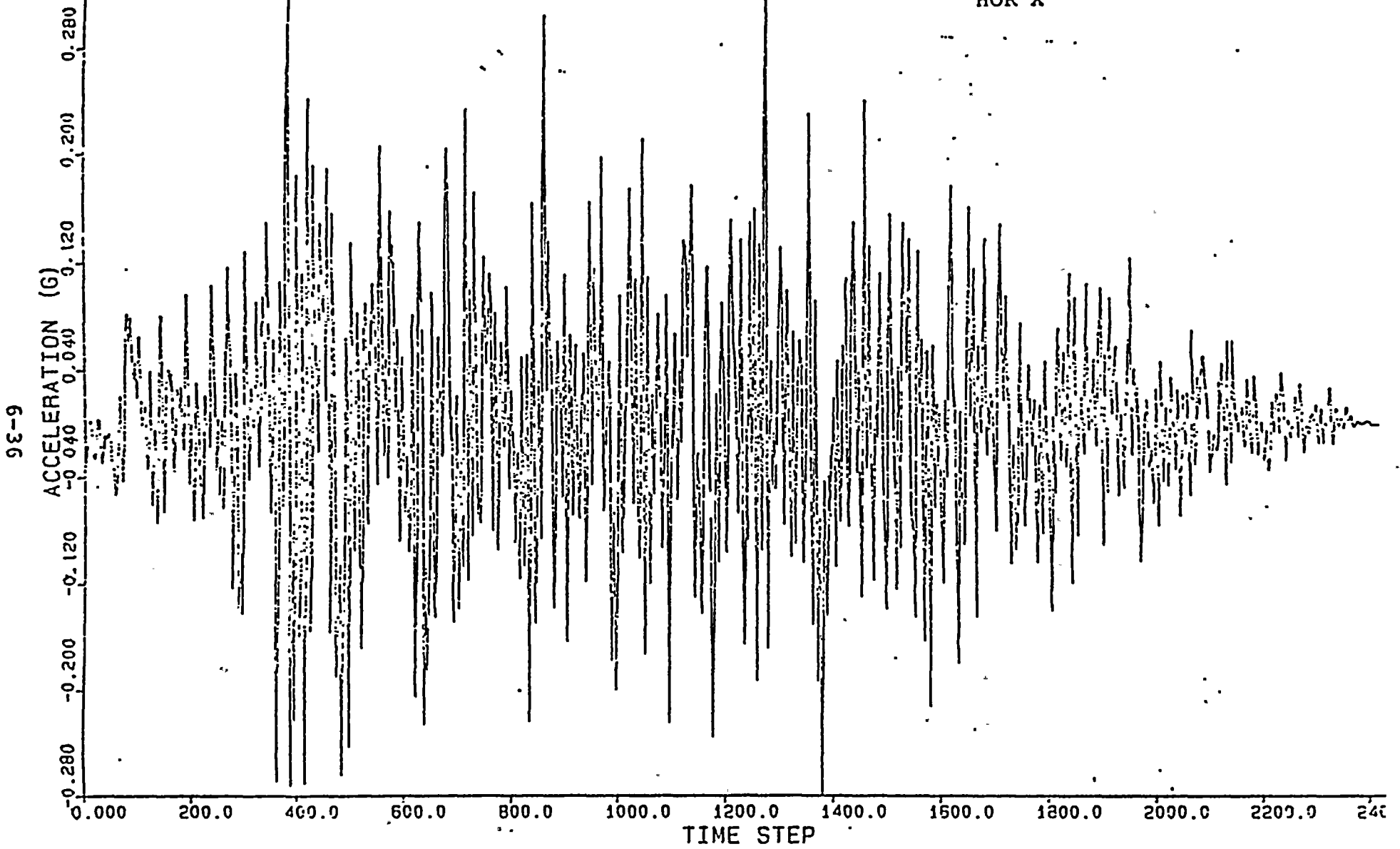


FIGURE 6.1.4



6-37

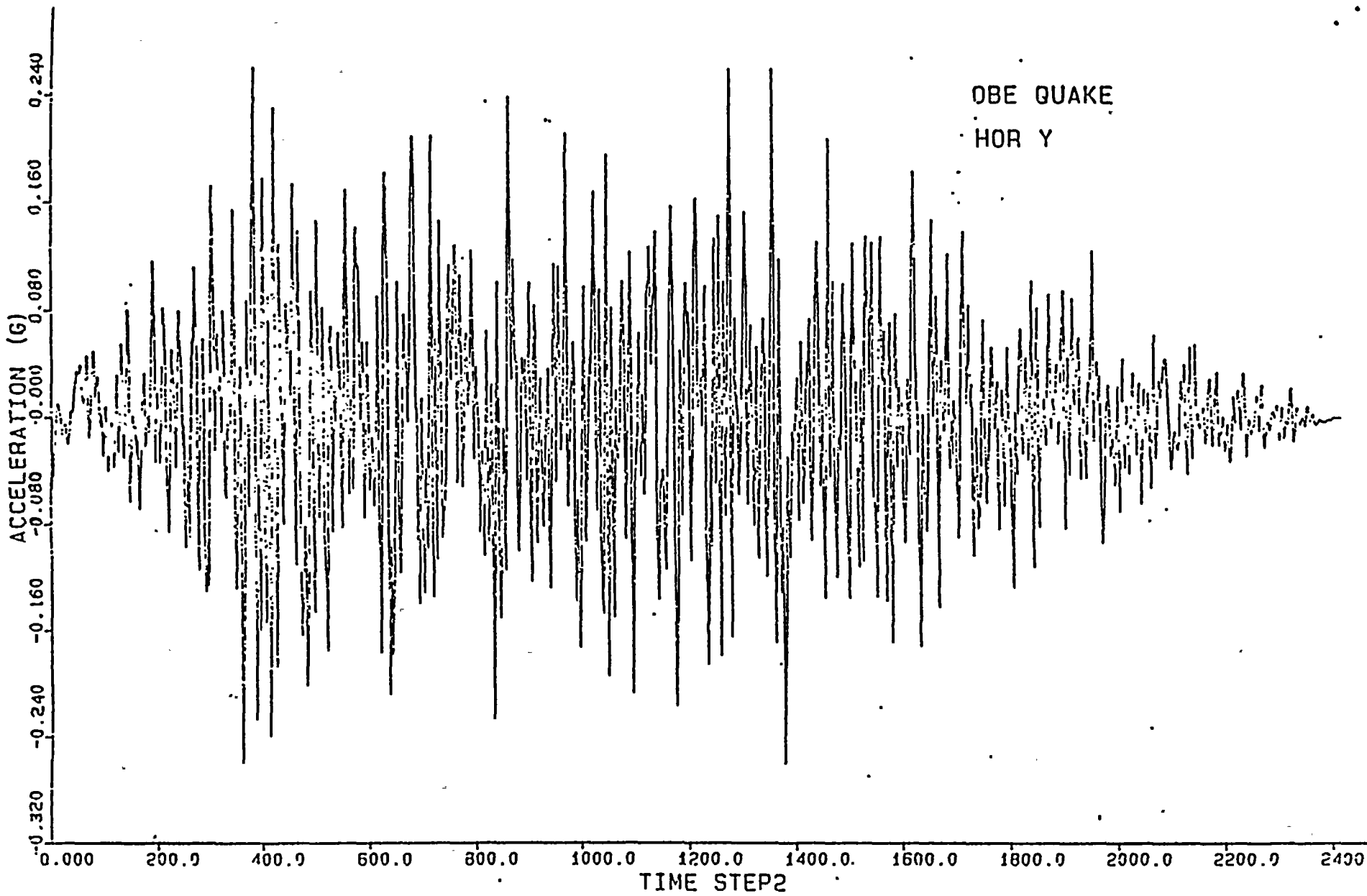


FIGURE 6.1.5



68-9

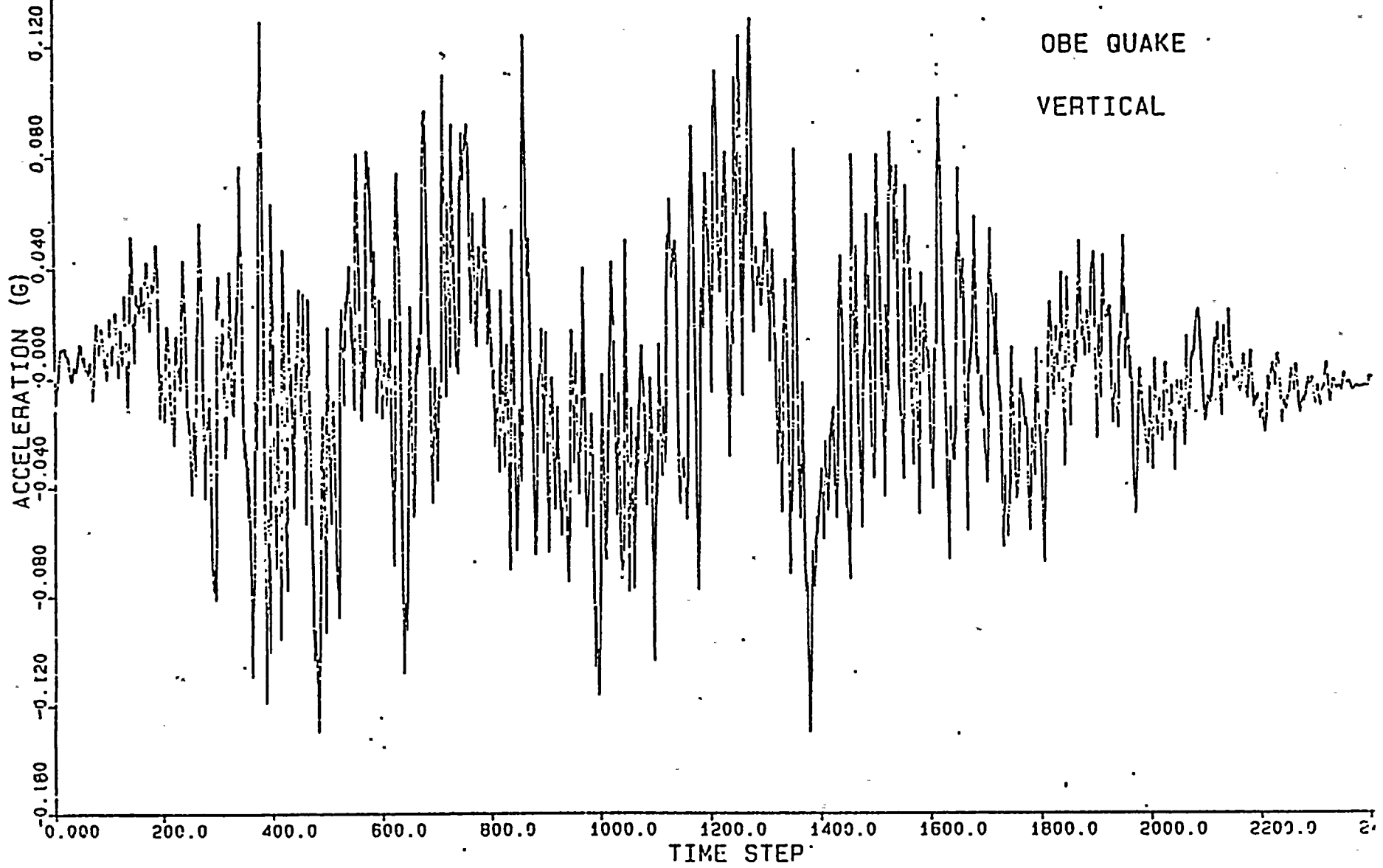


FIGURE 6.1.6





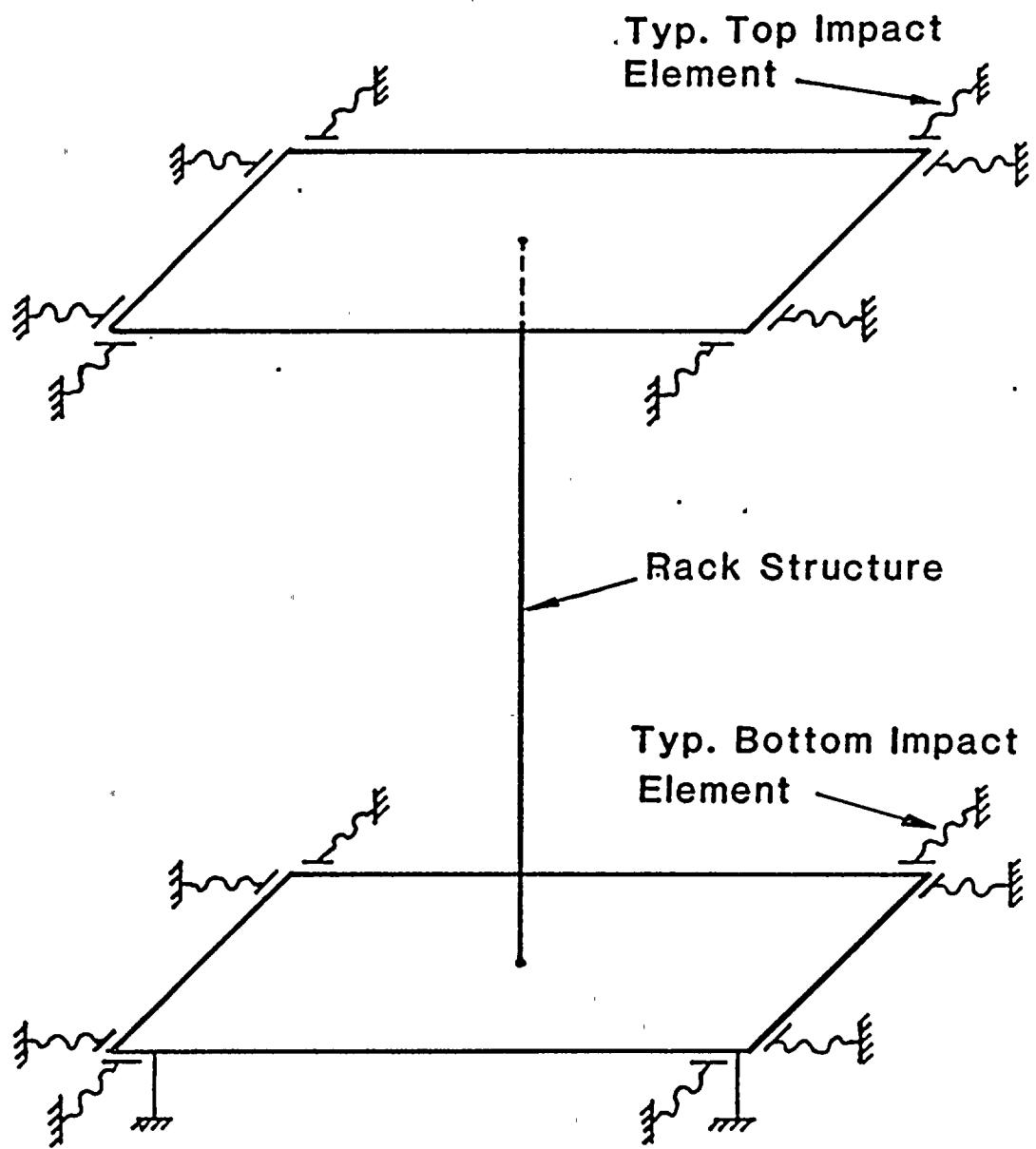


FIGURE 6.2.2 Gap Elements To Simulate Inter-rack Impacts



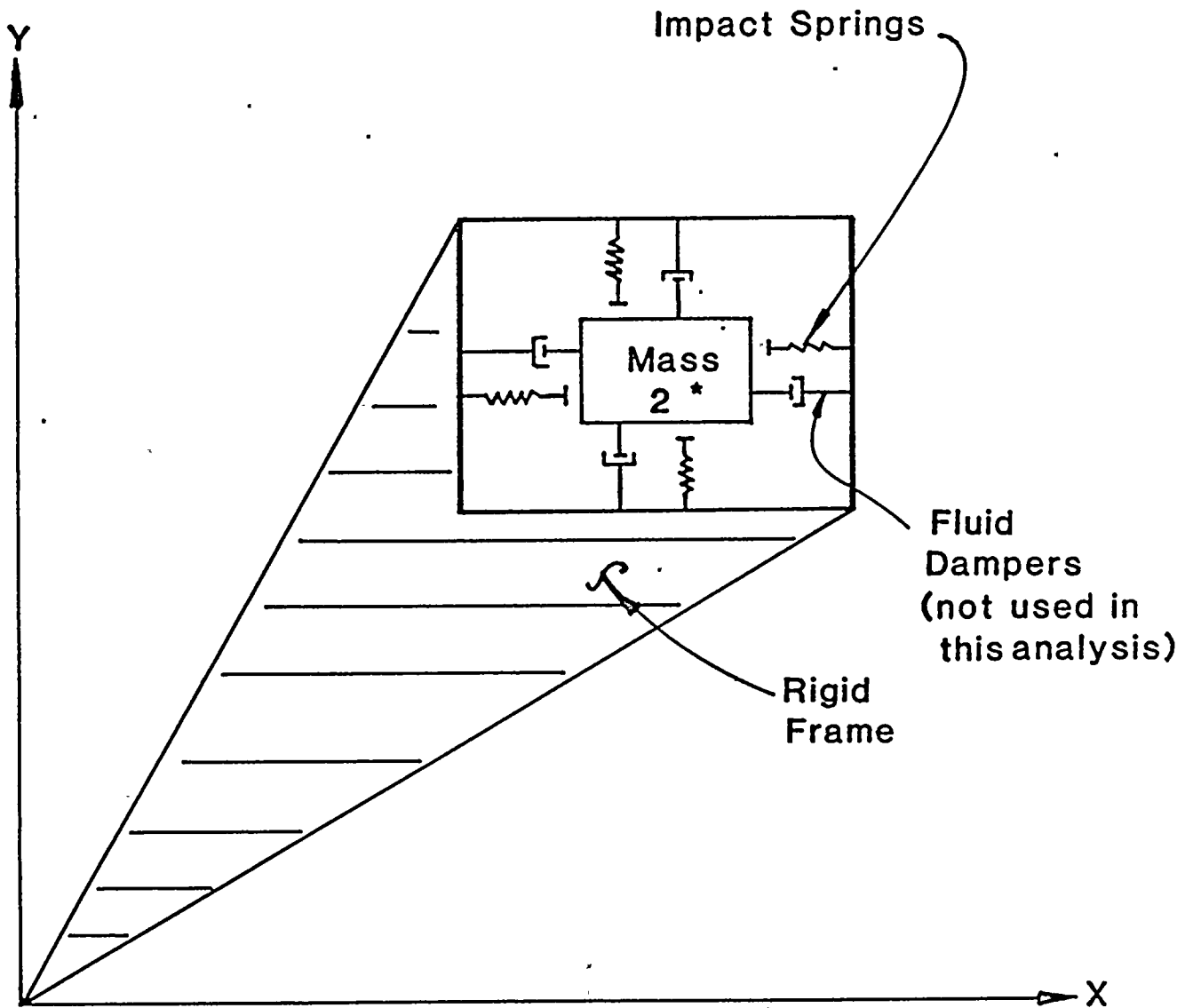


FIGURE 6.2.3 Impact Springs And Fluid Dampers



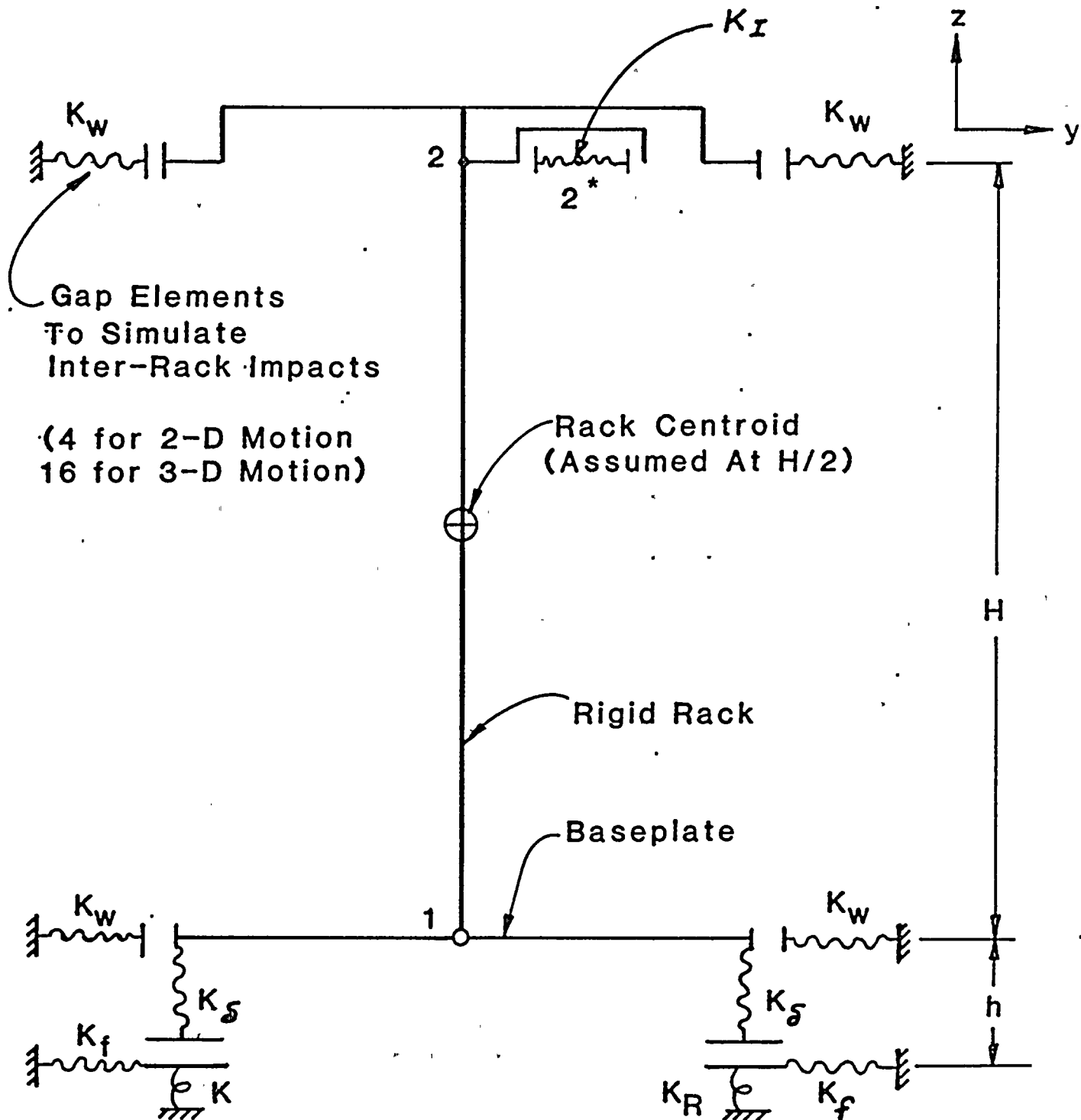


FIGURE 6.3.1 Spring Mass Simulation For Two-Dimensional Motion



7. ENVIRONMENTAL EVALUATION

7.1 SUMMARY

Installation of high density spent fuel storage racks at the Diablo Canyon Power Plant will increase the licensed storage capacity of the spent fuel pools from 270 to a maximum of 1324 assemblies for each unit. Radiological consequences of expanding the capacity have been evaluated with the objective of determining if there is a significant additional onsite or offsite radiological impact relative to that previously reviewed and evaluated (Ref. 1). In addition, radiological impact to operating personnel has been evaluated to ensure that exposures remain as low as is reasonably achievable (ALARA).

The decay heat loading and the radiological burden to the spent fuel pool water are determined almost entirely by refueling operations. The frequency of refueling operations and the conduct of refueling are independent of the increased capacity of the storage pool, except that the increased capacity should reduce fuel movement and allow continued normal operation. Since the fuel assemblies which will utilize the bulk of the storage capacity (and will ultimately fill all incremental capacity above that of the existing design) are aged, their contribution to either the peak decay-heat load or the increased radiological impact, in terms of increased dose, is negligible. A study performed by the NRC (Ref. 2) supports this conclusion. Consequently, the increase in the storage capacity of the spent fuel pool will neither significantly alter the operating characteristics of the current pool nor result in a measurable change in impact on the environment.

7.2 CHARACTERISTICS OF STORED FUEL

Because of radioactive decay, the heat generation rate and the intensity of gamma radiation from the spent fuel assemblies



decreases substantially with decay time. After a cooling time of about 4 years (Ref. 3), the decay heat generation rate is less than 2% of the rate at 7 days -- the nominal time at which depleted fuel assemblies are transferred to the spent fuel pool. The intensity of gamma radiation is very nearly proportional to the decay heat and decreases with cooling time in a similar manner.

The bulk of the heat load is due to freshly discharged fuel; aged fuel contributes relatively little to the total heat load. Therefore, this expansion will not significantly increase the thermal dissipation to the environment. Since the intensity of gamma radiation follows the decline in decay heat generation rate, it is similarly concluded that there will be no significant increase in gamma radiation due to the expanded storage.

It is important to note that the aged fuel in the expanded storage capacity will not contain significant amounts of radioactive iodine or short-lived gaseous fission products, since these would have decayed during the refueling period. The Krypton-85 which might escape from defective fuel assemblies has been shown to do so quickly (Ref. 2) (i.e., within a short time after discharge from the core). Further, the residual Krypton-85 will be contained within the fuel pellet matrix and hence any leakage would occur at very low rates (Ref. 2). Cesium 134/137 (Ref. 2) is strongly bound within the fuel pellet matrix and its dissolution rate in water is extremely small. Any Cesium dissolved in the pool water is easily controllable in the cleanup system (demineralizer-ion exchanger resin bed) (Ref. 2). Thus, the planned storage expansion will not significantly increase the release of gaseous radionuclides.

7.3 RELATED INDUSTRY EXPERIENCE

Experience with storing spent fuel underwater has been substantial (Refs. 2, 3, and 4). These references show that the



pool water activity, normally low, experiences a small increase during refueling periods, which then decays rapidly with time. Typical concentrations (Ref. 5) of radionuclides in spent fuel pool water range from 10^{-4} $\mu\text{Ci/ml}$ to 10^{-3} $\mu\text{Ci/ml}$, with the higher value associated with refueling operations. References 2 and 5 also state that the increase in pool water activity during refueling can be attributed to:

- O Dislodging (sloughing off) of corrosion products on the fuel assembly during transfer and handling operations
- O The possible short-term exposure of fuel pellets to pool water via a cladding defect
- O Mixing of the spent fuel pool water with the higher activity reactor coolant. Upon cessation of the refueling operations, the fuel pool water and the reactor coolant system would be isolated from each other, thereby terminating transports of corrosion products from the reactor coolant system. Thus, deposition of crud is a function of refueling operations and is not impacted by the expanded storage.
- O Furthermore, it has been shown (Ref. 6) that release of fission products from failed fuel decreases rapidly after shutdown to essentially negligible levels. The dissolution of exposed fuel pellets (made of UO_2) is very slow in water at fuel pool temperatures and the corrosion of the cladding (Zircaloy 4) at spent fuel pool water temperatures is virtually nil (Refs. 2 and 5). Another mechanism available for the release of the gaseous fission products is diffusion through the UO_2 pellet. It has been shown that at low water temperatures ($<150^\circ\text{F}$), the diffusion coefficient is extremely small (Ref.7). Therefore, the small increase in activity of the spent fuel pool water is due to either crud transport, fission products release, or cross-flow from the reactor coolant system, and is only a function of refueling operations. It is reasonable to assume that the increased capacity of the spent fuel pool will reduce fuel handling operations, thereby reducing the probability of increased pool water activity due to crud dislodging. Thus, the expansion of fuel pool storage capacity will not cause a significant increase in dose either onsite or offsite.
The corrosion properties of irradiated Zircaloy cladding have been reviewed in References 2 and 4 and the



conclusion is drawn that the corrosion of the cladding in spent fuel pool water is negligible. The minor incremental heating of pool water, due to the expansion of storage capacity, is far too small to materially affect the corrosion properties of Zircaloy cladding.

7.4 DIABLO CANYON POWER PLANT EXPERIENCE

At present there are no stored spent fuel assemblies in the Diablo Canyon fuel pools.

7.5 SPENT FUEL POOL COOLING AND CLEANUP SYSTEM (FPCC)

It has been shown previously (Section 5 and Diablo Canyon FSAR Update) that the cooling system at Diablo Canyon is adequate to handle the expected heat loads and maintain the temperature peaks within acceptable limits. It has been shown in Section 5 that the small increase in heat load due to the storage capacity expansion will neither significantly increase the thermal dissipation to the environment nor increase the propensity for corrosion of the cladding.

It has also been shown that the crud deposition in the spent fuel pool water occurs during refueling outages and that the planned expansion will not increase long-term crud deposition. The fuel pool cleanup system (filter and demineralizer) is designed to maintain fuel pool water clarity and is operated and maintained in accordance with the Diablo Canyon operating procedures. The cleanup system takes a surface skim from the fuel pool and cleans it through a process of filtration and demineralization to prevent crud buildup on the fuel pool walls at the water-to-air interface.

The spent fuel pool water is sampled and analyzed periodically to confirm proper operation of the pool cleanup system. The frequency of filter and resin replacement is determined primarily by requirements for water clarity rather than the loading of fission product radionuclides.



The spent fuel pool modification will not result in a significantly higher quantity of solid radwaste.

7.6 FUEL POOL RADIATION SHIELDING

7.6.1 Source Terms

The spent fuel gamma source terms used for the fuel pool shielding evaluation were generated using the point reactor fission product inventory code ORIGEN-2. The following assumptions were used in the analysis:

- O Initial fuel enrichment = 4.5%
- O Reactor power level = 3411 MWt
- O Average assembly discharge burnup = 55,000 MWd/MTU
- O Power level for average assembly = 17.67 MWt
- O Power level for peak power assembly = 27.39 MWt
(peaking factor of 1.55)
- O Burnup for peak power assembly = 30,000 MWd/MTU
(18-month cycle at maximum power)
- O Decay time after shutdown = 100 hours

The peaking factor of 1.55 and burnup for peak power assembly of 30,000 MWd/MTU for one cycle were chosen to produce the highest possible gamma source term attainable under operational conditions. The average assembly burnup and power level were chosen to represent a conservative gamma source term for the spent fuel. The 100-hour decay time is the minimum permitted period before refueling can begin.

The photon energy production rates of an average assembly and of a peak power spent fuel assembly are given in Tables 7.1 and 7.2, respectively.



Table 7.1

PHOTON ENERGY PRODUCTION RATES OF
AN AVERAGE SPENT FUEL ASSEMBLY

<u>Photon Energy (MeV)</u>	<u>Photon Energy Production Rate (MeV/sec)</u>
1.50E-002	3.16E+015
2.50E-002	8.27E+014
3.75E-002	1.47E+015
5.75E-002	1.49E+015
8.50E-002	3.73E+015
1.25E-001	1.20E+016
2.25E-001	1.47E+016
3.75E-001	1.02E+016
5.75E-001	4.61E+016
8.50E-001	7.30E+016
1.25E+000	1.12E+016
1.75E+000	4.21E+016
2.25E+000	3.45E+015
2.75E+000	2.44E+015
3.50E+000	2.67E+013
5.00E+000	1.92E+008
7.00E+000	3.09E+007
1.10E+001	5.59E+006
TOTAL	2.26E+017



Table 7.2

PHOTON ENERGY PRODUCTION RATES OF
PEAK SPENT FUEL ASSEMBLY

<u>Photon Energy</u> (MeV)	<u>Photon Energy Production Rate</u> (MeV/sec)
1.50E-002	3.98E+015
2.50E-002	1.17E+015
3.75E-002	2.10E+015
5.75E-002	1.88E+015
8.50E-002	4.84E+015
1.25E-001	1.56E+016
2.25E-001	1.86E+016
3.75E-001	1.44E+016
5.75E-001	5.77E+016
8.50E-001	1.11E+017
1.25E+000	1.01E+016
1.75E+000	6.66E+016
2.25E+000	2.94E+015
2.75E+000	3.94E+015
3.50E+000	4.18E+013
5.00E+000	1.75E+007
7.00E+000	2.82E+006
1.10E+001	<u>5.11E+005</u>
TOTAL	3.15E+017



7.6.2 Radiation Shine Due to Spent Fuel Storage

During partial core discharge, 76 fuel assemblies will be discharged into the pool beginning 100 hours after reactor shutdown, at a rate of up to 4 assemblies per hour. For the case of a full core discharge (FCD), 193 assemblies are discharged, although this is a short term condition since the usable assemblies are placed back into the reactor for startup.

To evaluate the adequacy of the bulk shielding of the pool walls, the radiation shine from 100 freshly discharged fuel assemblies arranged in a 10 x 10 array placed next to the spent fuel pool wall is calculated. The results of this 10 x 10 array envelope the FCD case because of the self-shielding effect of the fuel assemblies and the geometry of the fuel storage locations. The photon production rates used are given in Table 7.1.

The perimeter walls of the spent fuel pool are 6 feet thick with the exception of the wall between the refueling canal and the pool which is 5 feet thick. These walls, together with the design water gap between the pool wall and the high density racks, are used to calculate the dose rates in the adjacent areas. The results are provided in Table 7.3.

Table 7.3 shows the maximum calculated dose rate is 0.13 mrem/hr for areas around the pool at floor elevation 115 feet, 0 inches. This dose rate is below the currently designated radiation level limit of 1 mrem/hr for the same areas. Note that the top of the spent fuel rack is approximately at elevation 113 feet. The dose rates for areas adjacent to the pool at floor elevation 100 feet, 0 inches are somewhat higher but will not result in any significant personnel exposure problem for the following reasons:

- 0 The dose rate in areas adjacent to the east and north walls at floor elevation 110 feet, 0 inches is calculated as 2.3 mrem/hr which will allow an occupancy of 40 hours per week and still not exceed the 10 CFR 20 exposure limits.



Table 7.3

CALCULATED DOSE RATES IN AREAS ADJACENT
TO THE SPENT FUEL POOL (UNIT 1, TYPICAL)

Location	High Density Rack Dose Rate (mrem/hr)
Floor el. 115 ft, 0 in., areas adjacent to the east, north, and south walls*	0.13
Floor el. 110 ft, 0 in., areas adjacent to the east and north walls **	2.3
Floor el. 110 ft, 0 in., stairway 2J adjacent to the south wall*	6.2
Floor el. 110 ft, 0 in., spent fuel pool heat exchanger area*	8.1
Fuel transfer canal	74

* A design water gap of 4-1/8 inches between the high density rack and the wall is used.

** A design water gap of 9 inches between the high density rack and the wall is used.

- O The dose rate for stairway 2J at floor elevation 110 feet, 0 inches is calculated as 6.2 mrem/hr. This stairway, however, is usually accessed with low frequency. Therefore, the increased radiation level will not result in significantly increased plant man-rem exposures.
- O The spent fuel pool heat exchanger area is not normally accessed, thus the calculated radiation level of 8.1 mrem/hr for this area will not cause any exposure problem.
- O The above dose rates provided are an upper limit since they are calculated for freshly discharged fuel. The radiation will decrease with time due to decay of the spent fuel. It is estimated that the above dose rates will reduce by a factor of three 1 month after the fuel is discharged into the pool.



The dose rate in the refueling canal is calculated to be 74 mrem/hr which is consistent with the currently designated radiation level of Zone IV (>15 mrem/hr).

The above discussion indicates that the spent fuel pool shielding is adequate for installation of the high density racks.

7.6.3 Radiation Shine Due to the Fuel Transfer Operation

The radiation levels at or above the pool water surface due to the transfer of a peak power fuel assembly are also calculated. The photon energy production rates for this peak fuel assembly are given in Table 7.2.

The minimum water level above the active fuel is 10 feet. This height is used to determine the dose rates at the pool surface and at locations above the pool surface. The results are provided in Table 7.4.

Table 7.4

CALCULATED DOSE RATE AT OR ABOVE POOL WATER SURFACE DUE TO TRANSFER OF A PEAK POWER FUEL ASSEMBLY

Location	Dose Rate (mrem/hr)
Pool water surface:	6.90
10 ft above surface	1.80
20 ft above surface	0.80
30 ft above surface	0.45
40 ft above surface	0.29
50 ft above surface	0.20
Floor el. 115 ft, 0 in., areas adjacent to the east, north, and south walls*	2.50

* A design water gap of 4-1/8 inches between the peak power fuel assembly and the 6-foot-thick pool wall is used.



Table 7.4 shows that the dose rate is 6.9 mrem/hr at the pool water surface during transfer of a peak power fuel assembly. The radiation level decreases to 1.8 mrem/hr at 10 feet above the pool surface. Since the fuel transfer operation normally lasts less than a day (76 assemblies at 4 assemblies per hour), the above radiation field does not create excessive operator exposure.

Table 7.4 also indicates that the maximum calculated dose rate of 2.5 mrem/hr for areas around the pool at floor elevation 115 feet, 0 inches during the transfer of a peak power fuel assembly. This dose rate will allow an occupancy of 40 hours per week and is, therefore, acceptable.

7.7 RADIOLOGICAL CONSEQUENCES

As stated earlier (Refs. 2, 4-6, 8, and 9), it can be shown that there will be no significant increase in activity due to Krypton-85, Cesium 134/137, or crud buildup on pool walls. It is concluded that the incremental impact from the release of either volatile fission products or crud with the expanded capacity of the spent fuel pool for normal conditions will be negligible.

A conservative analysis has been performed to determine the radiological consequences of a postulated spent fuel pool boiling event. This analysis is consistent with the methodology and assumptions utilized in a similar pool boiling calculation performed for the Limerick Generating Station (Ref. 10). The Limerick pool boiling analysis was reviewed by the NRC and found acceptable (Ref. 11).

The following assumptions were used to calculate the heat generation and boiling rates in the spent fuel pool:



- O The spent fuel pool contains the maximum inventory of 1324 fuel assemblies in high density racks. The full core offload is the last addition to the spent fuel pool prior to loss of cooling and has been decayed for 148 hours. The previous single region refuelings have been decayed for 100 hours.
- O The decay heat is calculated by using the decay heat equations presented in NRC Branch Technical Position APCS 9-2. The decay heat generation rate for the spent fuel pool for various times after the postulated loss of cooling is given in Table 7.5.
- O All the heat generated by the fuel is assumed to be absorbed by the water. No heat is assumed to be lost to the surroundings by conduction through the concrete and steel or by evaporation.

Table 7.5

DECAY HEAT AND EVAPORATION RATES

Time After Loss of Pool Cooling (hrs)	Decay Heat ($\times 10^7$ Btu/hr)	Evaporation Rate (ft ³ /hr)
0	4.35	0.00
2	4.33	3.10*
8	4.27	704.11
24	4.12	680.58
96	3.68	607.55
360	3.65	602.53
480	2.71	446.86
600	2.54	418.66
720	2.40	395.92

* Evaporation due to air moving over spent fuel pool



The following assumptions were used to calculate the offsite doses for the loss of cooling to the spent fuel pool:

- O The saturation noble gas and iodine inventories in the core are based on a power level of 3411 MWt with a maximum initial enrichment of 4.5 percent by weight and a maximum discharge burnup of 50,000 MWd/MTU.
- O The spent fuel pool cooling system fails following the full-core offload of 193 assemblies decayed for 148 hours.
- O Pool boiling occurs 3 hours after loss of spent fuel pool cooling.
- O 1% of the fuel rods in the core are defective.
- O The gap activity consists of 10% of the total noble gases except Kr-85, 30% of the Kr-85 activity, and 10% of the total radioactive iodine contained in the fuel rods.
- O Prior to boiling, activity in the spent fuel pool is assumed to be released via evaporation due to air moving above the pool.
- O Noble gases released from the fuel are assumed to be instantaneously released from the spent fuel pool.
- O The iodine and noble gas leakage rates from the fuel rods are $1.3 \times 10^{-8} \text{ sec}^{-1}$ and $6.5 \times 10^{-8} \text{ sec}^{-1}$, respectively (Ref. 12). These are the full power design fuel leak rates.
- O A constant spike factor of 50 was applied to the leakage rate from the fuel to account for the potential spiking effects during the temperature transient. The leakage rate returns to the normal full power unspiked rate when boiling begins, since the fuel should now be close to its new steady-state temperature. Although the analysis was performed for a release spike factor of 50, there are presently no data to support the spiking phenomena in the spent fuel pool boiling situation. Spikes have been observed for the large, rapid temperature and pressure changes associated with shutdowns and startups, but such significant spiking effects would not be expected during the long, slow temperature change that would be associated with a loss of cooling.
- O Radioactive iodine activity released from the fuel is uniformly mixed in the spent fuel pool water volume.



- O The activity release rate from the pool depends on the evaporation rate. Prior to boiling, evaporation is assumed to be due to air moving over the spent fuel pool; after boiling, evaporation is due to the heat generation from the spent fuel, as given in Table 7.5.
- O The iodine partition factor at the pool surface is 0.1.
- O No credit is taken for iodine plateout on walls and equipment or for washout by condensing water vapor in the refueling area.
- O It is assumed that all activity in the steam released to the air in the refueling area is instantaneously released to the atmosphere without filtration or condensation in the ventilation system.
- O The atmospheric dispersion factors for dilution of the radioactive releases are the same as those used in Chapter 15 of the FSAR Update. These 5 percentile ground level \bar{X}/q_s are given in Table 7.6. Time "0" is assumed to be the start of the accident when pool cooling is lost.
- O The thyroid dose models and breathing rates given in Regulatory Guide 1.4 are used.

Table 7.6

ATMOSPHERIC DISPERSION FACTORS

Time	Boundary	\bar{X}/q (sec/M ³)
0 - 2 hr	EAB	5.3×10^{-4}
0 - 8 hr	LPZ	2.4×10^{-5}
8 - 24 hr	LPZ	4.8×10^{-6}
1 - 4 days	LPZ	1.5×10^{-6}
4 - 30 days	LPZ	3.4×10^{-7}

As shown in Table 7.7, the offsite dose consequences of a postulated pool boiling event are a small fraction of 10 CFR 100 limits and they are, therefore, acceptable.



Table 7.7

RESULTS OF SPENT FUEL POOL BOILING ANALYSIS

<u>Site Boundary 2-Hour Dose (Rem)</u>	
Thyroid	8.44×10^{-4}
Whole body	9.84×10^{-3}
<u>LPZ 30-Day Dose (Rem)</u>	
Thyroid	1.51×10^{-1}
Whole body	7.16×10^{-4}

The design basis fuel handling accident (dropped assembly) in the fuel handling building in Section 15.5.22 of the FSAR was reviewed for possible effects on radiological dose consequences. The review determined that the conclusions in the FSAR were still valid, and that offsite radiological dose consequences were well within 10CFR100 limits.

7.8 RERACKING OPERATION

Installation of the fuel racks will include removal of the existing racks, making minor pool modifications, and cleaning and installing the new racks. The existing racks are bolted to the pool floor. After removal of the racks, any anchor bolts that may interfere with the new racks will be removed. Other pool modifications, including removing some brackets and moving the storage location for the spent fuel handling tool, will be done to eliminate interferences with the high density racks.

The new racks will first be cleaned outside of the fuel handling building and then brought in for installation. The fuel handling building overhead crane and, possibly, a temporary crane will be used to place the racks in the pool. This effort is scheduled to be performed prior to the first refueling for each unit, which will allow a "dry" installation with no water or spent fuel in



the pools. In this case, the existing fuel racks will not have been exposed to spent fuel and will only be nominally contaminated, if at all. Therefore, doses to individuals involved in the reracking will be negligible.

If there is a delay in installing the high density racks until after the first refueling, then a "wet" installation will be required. All pool modifications that can be completed prior to filling the pool with water will be done to minimize underwater work. Although divers may be needed for some tasks, all of the work associated with the installation will be sequenced to minimize potential radiation exposure of personnel due to the spent fuel located in the pool. ALARA considerations will be fully incorporated in the installation procedures for this condition. If the fuel handling building overhead crane is used over the pool, electrical interlocks will be adjusted on the crane to preclude carrying racks over any stored fuel assemblies.

Exact disposition of the existing racks has not been determined. They will be decontaminated and/or packaged and disposed of in accordance with the applicable Federal and State regulations.

7.9 CONCLUSIONS

Based upon the industry experience and evaluations discussed in previous sections, the following conclusions are made:

- Minor increases in radiological burden to the pool water, if any, can be adequately handled by the fuel pool cleanup system (filter and demineralizer), thereby maintaining the radionuclide concentration in the water at an acceptably low level.
- No appreciable increase in solid radioactive wastes (i.e., filter media and demineralizer resin) is anticipated.
- No increase in release of radioactive gases is expected since any long-lived inert radioactive gas potentially available for release (i.e., KR-85) will have leaked from the fuel either in the reactor core during operation or during the first few months of residence in the pool. Further, Vol. 1, Ref. 3 (pp. 4-16) has shown



airborne activity to be considerably lower than that allowable by Table 1 of 10 CFR Part 20, Appendix B. Therefore, the planned expansion will not significantly increase the release of radioactive gases.

- O The existing spent fuel pool cooling system will keep the pool water temperature at an acceptable level (See Section 5, Thermal-Hydraulic Considerations).
- O The existing radiation protection monitoring systems and program are adequate to detect and to warn of any unexpected abnormal increases in radiation level. This provides sufficient assurance that personnel exposures can be maintained as low as is reasonably achievable.
- O For a dry reracking operation, radiation exposures will be extremely low. If the reracking occurs after the first refueling, procedural controls and necessary precautions will be taken to reduce radiation exposure to as low as is reasonably achievable, and hence, radiological impact will be minimized.
- O Expanding the storage capacity of the spent fuel pool will not significantly increase the onsite or offsite radiological impact above that of the currently authorized storage capacity, nor is any significant increase in environmental radiological or nonradiological impact anticipated.



REFERENCES TO SECTION 7

1. FSAR, Diablo Canyon Power Plant, Docket Nos. 50-275 and 50-323.
2. NUREG-0575, "Handling and Storage of Spent Light Water Power Reactor Fuel," Vol. 1, Executive Summary and Text, USNRC, August 1979.
3. NUREG-0800, USNRC Standard Review Plan, Branch Technical Position ASB9-2, Rev. 2, July 1981.
4. J. R. Weeks, "Corrosion of Materials in Spent Fuel Storage Pools," BNL-NUREG-2021, July 1977.
5. A. B. Johnson, Jr., "Behavior of Spent Nuclear Fuel in Water Pool Storage," BNWL-2256, September 1977.
6. J. M. Wright, "Expected Air and Water Activities in the Fuel Storage Canal," WAPD-PWR-CP 1723 (with Addendum), undated.
7. ANS 5.4 Proposed Standard, "Method for Calculating the Fractional Release of Volatile Fission Products from Oxide Fuel," American Nuclear Society, issued for review, 1981.
8. "Licensing Report on High Density Spent Fuel Racks for Quad Cities, Units 1 and 2," Docket Nos. 50-254 and 50-265, Commonwealth Edison Company, June 1981.
9. "Licensing Report for High Density Spent Fuel Storage Racks," Rancho Seco Nuclear Generating Station, Sacramento Municipal Utilities District, Docket No. 50-312, June 1982.
10. Final Safety Analysis Report, Limerick Generating Station Units 1 and 2, Section 9.1
11. Safety Evaluation Report Related to the Operation of Limerick Generating Station Units 1 and 2, NUREG-0991, August 1983.
12. Source Term Data for Westinghouse Pressurized Water Reactors, WCAP-8253, July 1975.



8. IN-SERVICE SURVEILLANCE PROGRAM FOR BORAFLEX
NEUTRON ABSORBING MATERIAL

8.1 PROGRAM INTENT

A sampling program to verify the integrity of the neutron absorber material employed in the high density fuel racks in the long-term environment is described in this section.

The program is conducted in a manner which allows access to the representative absorber material samples without disrupting the integrity of the entire fuel storage system. The program is tailored to evaluate the material in normal use mode and to forecast future changes using the data base developed.

8.2 DESCRIPTION OF SPECIMENS

The absorber material used in the surveillance program, henceforth referred to as poison, is representative of the material used within the storage system. It is of the same composition, produced by the same method, and certified to the same criteria as the production lot poison. The sample coupon is of similar thickness as the poison used within the storage system and not less than 4 by 2 inches on a side. Figure 8.1 shows a typical coupon. Each poison specimen is encased in a stainless steel jacket of an identical alloy to that used in the storage system, formed so as to encase the poison material and fix it in a position and with tolerances similar to the design used for the storage system. The jacket has to be closed by tack welding in such a manner as to retain its form throughout the test period and still allow rapid and easy opening without causing mechanical damage to the poison specimen contained within. The jacket should permit wetting and venting of the specimen similar to the actual rack environment.



8.3 SPECIMEN EVALUATION

After the removal of the jacketed poison specimen from the cell at a designated time, a careful evaluation of that specimen should be made to determine its actual condition as well as its apparent durability for continued function. Separation of the poison from the stainless steel specimen jacket must be performed carefully to avoid mechanical damage to the poison specimen. Immediately after the removal, the specimen and jacket section should be visually examined for any effects of environmental exposure. Specific attention should be directed to the examination of the stainless steel jacket for any evidence of physical degradation. Functional evaluation of the poison material can be accomplished by the following measurements:

- O A neutron radiograph of the poison specimen aids in the determination of the maintenance of uniformity of the boron distribution.
- O Neutron attenuation measurements will allow evaluation of the continued nuclear effectiveness of the poison. Consideration must be given in the analysis of the attenuation measurements for the level of accuracy of such measurements, as indicated by the degree of repeatability normally observed by the testing agency.
- O A measurement of the hardness of the poison material will establish the continuance of physical and structural durability. The hardness acceptability criterion requires that the specimen hardness will not exceed the hardness listed in the qualifying test document for laboratory test specimen irradiated to 10^{11} rads. The actual hardness measurement should be made after the specimen has been withdrawn from the pool and allowed to air dry for not less than 48 hours to allow for a meaningful correlation with the pre-irradiated sample.
- O Measurement of the length, the width, and the average thickness and comparison with the preexposure data will indicate dimensional stability within the variation range reported in the Boraflex laboratory test reports.

A procedure will be prepared for execution of the test procedure and interpretation of the test data.



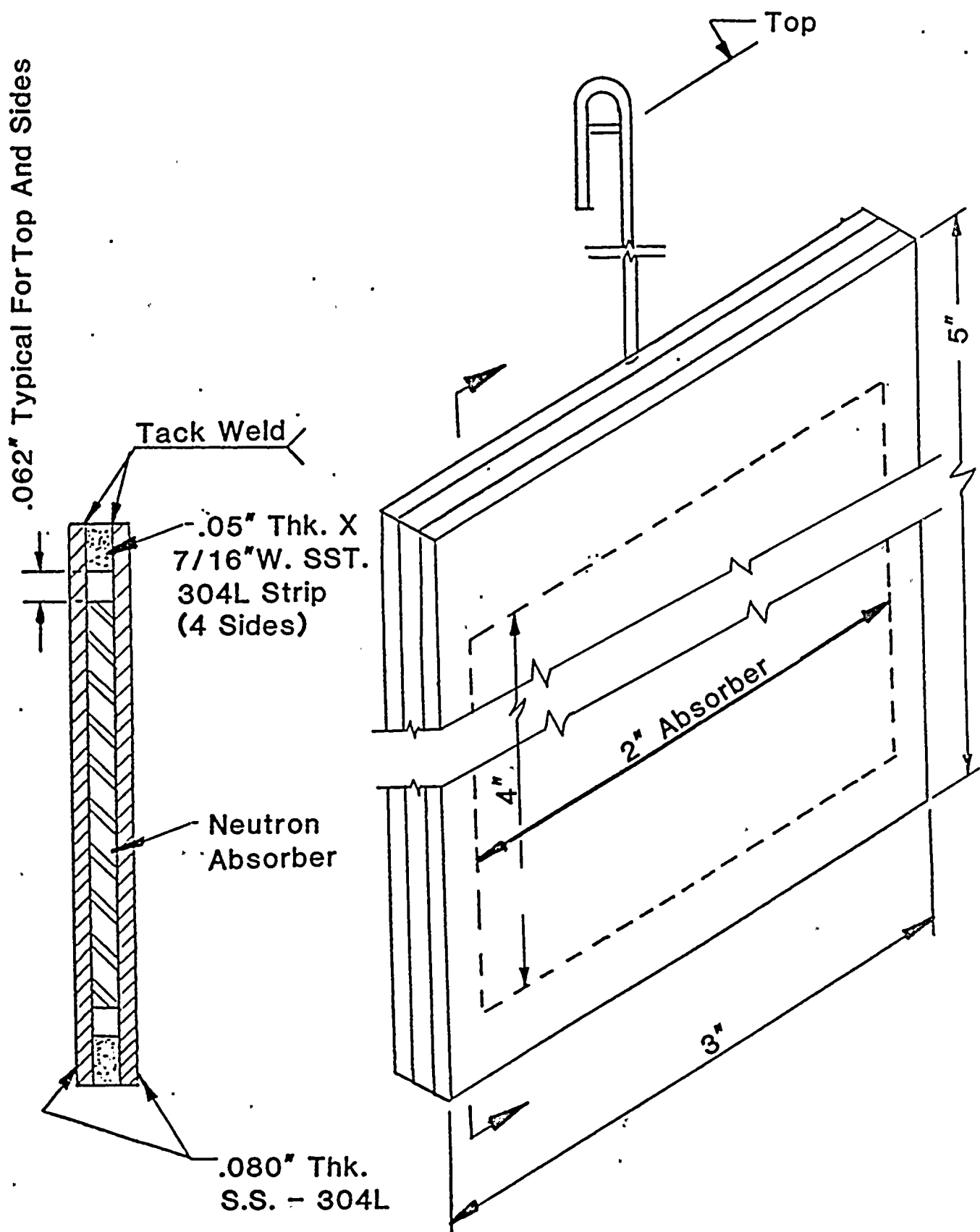


FIGURE 8.1 Test Coupon



9. COST/BENEFIT ASSESSMENT

A cost/benefit assessment has been prepared in accordance with the requirements of Reference 1, Section V - Part 1. The assessment demonstrates that the installation of high density spent fuel storage racks is the most advantageous means of handling spent fuel.

The material is presented to satisfy the NRC's need for information. It is PGandE's position that no environmental impact statement need be prepared in support of the request because there will be no significant impact on the environment. NRC precedent establishes that alternatives and economic costs need not be discussed when there is no significant environmental impact. However, for completeness, alternatives to reracking for additional spent fuel storage capacity are discussed in Section 9.3.

9.1 SPECIFIC NEEDS FOR SPENT FUEL STORAGE

Disposal of Diablo Canyon nuclear fuel is scheduled to be carried out by the Department of Energy in or after 1998 in accordance with Public Law 97-425, Nuclear Waste Policy Act of 1982. As Diablo Canyon spent fuel may not be accorded a high priority under the DOE Program, PGandE is seeking to provide a spent fuel storage capacity to support approximately 20 years of nominal operation. No other contractual arrangements exist for the interim storage or reprocessing of spent fuel from Diablo Canyon Power Plant. Therefore, increased storage capacity in the Diablo Canyon fuel pools is the only viable option under consideration. Table 1.1, the Fuel Discharge Schedule, indicates that with the high density spent fuel racks, loss of full core discharge capability (FCDC) will occur in 2007.



9.2 COST OF SPENT FUEL STORAGE

The design and manufacture of the spent fuel storage racks will be undertaken by the organizations described in Section 1. It is expected that the total project cost will be between \$13.5 and \$14 million for both units.

9.3 ALTERNATIVES TO SPENT FUEL STORAGE

PGandE has considered the various alternatives to the proposed onsite spent fuel storage. These alternatives are discussed below:

a. Shipment of Fuel to a Reprocessing or Independent Spent Fuel Storage/Disposal Facility

No commercial spent fuel reprocessing facilities are presently operating in the United States. PGandE has made contractual arrangements whereby spent nuclear fuel and/or high level nuclear waste will be accepted and disposed of by the U.S. Department of Energy. However, such services are not expected to be available before 1998. The existing Diablo Canyon spent fuel storage capacity will not provide full core discharge capability beyond 1988. Spent fuel acceptance and disposal by the Department of Energy is not, therefore, an alternative to increased onsite pool storage capacity.

b. Shipment of Fuel to Another Reactor Site

Shipment of Diablo Canyon fuel to another reactor site could provide short-term relief to the storage capacity problem. However, transshipment of spent fuel merely serves to transfer the problem to another site and does not result in any additional net long-term storage capacity. Accordingly, PGandE does not consider the transshipment of spent fuel to be an appropriate alternative to high density spent fuel storage at the site.

c. Not Operating the Plant after the Current Spent Fuel Storage Capacity is Exhausted

As indicated in NUREG-0575, "Final Environmental Impact Statement on Handling and Storage of Spent Light Water Power Reactor Fuel," (Ref.2) the replacement of



nuclear power by coal generating capacity would cause excess mortality to rise from 0.59 - 1.70 to 15 - 120 per year for 0.8 GWY(e). Based on these facts, not operating the plant or shutting down the plant after exhaustion of spent fuel discharge capacity is not a viable alternative to high density storage in the spent fuel pool. The prospective 1985 expenditure of approximately \$3.75 million for the high density racks is small compared to the estimated value of replacement power equivalent to the plant's energy output: approximately \$80.2 million per month in 1986 and \$114.5 million per month in 1990.

The subject of the comparative economics associated with various spent fuel options is the subject of Chapter 6 of NUREG-0575 (Ref. 2). Although the material presented is generic, it is of value in comparing the costs of the various options. Of the options presented in that chapter, high density spent fuel storage at the site is the most economic option at \$18 per KgU. The price of away from reactor (AFR) fuel storage, if available, would be \$115 per KgU. This corresponds to 0.5 mill/Kwh from a 1000 MWe power reactor for AFR storage. The marginal cost per KgU of high density spent fuel racks for Diablo Canyon Power Plant is less than \$12.

9.4 RESOURCE COMMITMENTS

The expansion of the Diablo Canyon Power Plant spent fuel storage capacity will require the following primary resources:

- O Stainless steel - 284,815 lb/unit
- O Boraflex neutron absorber - 3,950 lb/unit of which 1,832 lb is boron carbide (B₄C) powder

The requirement for stainless steel represents a small fraction of the total domestic production for 1985 (Ref. 3). Although the fraction of domestic production of B₄C required for the fabrication is somewhat higher than that for stainless steel, it



is unlikely that the commitment of B₄C to this project will affect other alternatives. Experience has shown that the production of B₄C is highly variable and depends on need but could easily be expanded to accommodate additional domestic needs.



REFERENCES TO SECTION 9

1. B. K. Grimes, "OT Position for Review and Acceptance of Spent Fuel Storages and Handling Applications," April 14, 1978.
2. NUREG-0575, "Final Environmental Impact Statement on Handling and Storage of Spent Light Water Power Reactor Fuel," Vols. 1-3, USNRC, August 1979.
3. "Mineral Facts and Problems," Bureau of Mines Bulletin 671, 1980.



10. QUALITY ASSURANCE PROGRAM

10.1 INTRODUCTION

This chapter provides a general description of the quality assurance program that is implemented to assure that the quality objectives of the contract specification are met.

10.2 GENERAL

The quality assurance program used on this project is based upon the system described in Oat's Nuclear Quality Assurance Manual. This system is designed to provide a flexible but highly controlled system for the design, manufacture, and testing of customized components in accordance with various codes, specifications, and regulatory requirements. The Oat Nuclear Quality Assurance Program has been accepted by ASME and has been approved by the PG&E Quality Assurance Department and placed on PG&E's Qualified Suppliers List.

The philosophy behind Oat's Quality Assurance System is that it shall provide for all controls necessary to fulfill the contract requirements with sufficient simplicity to make it functional on a day-to-day basis. The system readily adapts to different designs and component configurations, making possible the construction of many varied forms of equipment. The following paragraphs provide an overview of the system and how it has been applied to PG&E's specifications.

10.3 SYSTEM HIGHLIGHTS

The design control is organized to provide for careful review of all contract requirements to extract each individual design and



quality criterion. These criteria are translated into design and quality control documents customized to the contract requirement and completely reviewed and approved by responsible and qualified personnel.

The system for control of purchased material includes generating detailed descriptions of each individual item of material along with specifications for any special requirements such as impact testing, corrosion testing, monitoring or witnessing of chemical analysis, provision of over-check specimens, special treatments or conditioning of material, source inspection, and provision of performance documentation on any of the above.

Material receipt inspection includes a complete check of all material and its documentation. Upon acceptance, each item of material is individually listed on a control sheet issued once a week to assure that only accepted material goes into fabrication.

The fabrication control system provides that a shop traveller is prepared for each subassembly and assembly in each contract. The traveller is generated specifically to provide step-by-step instructions for fabrication, inspection, testing, cleaning, packaging, etc., which address all standard and special requirements of the contract specifications. Special attention is given to deployment of fabrication sequence and inspection steps to preclude the possibility of missing pages or incorrect sheets (incorrect B¹⁰ loading). All nondestructive examination procedures and test procedures are custom written to apply to PG&E's requirements.

The system provides for qualification and written certification of personnel performing quality-related activities including nondestructive examination and fabrication inspection, welding, engineering, production supervision, and auditing.



Other PG&E requirements are fully covered in the Quality Assurance Program, including document control, control of measuring and test equipment, control of nonconforming material and parts, corrective action auditing, and other areas as specified by PG&E.

10.4 SUMMARY

Oat's quality assurance system provides the full measure of quality assurance required by the contract. All special requirements of the specifications are covered, including source inspection of material and witnessing of material testing by the engineer, furnishing of material certifications and test reports within 5 days of shipment, and obtaining verification of qualification testing of poison materials.

